

Volume 15, No. 4

October, 1963

SOVIET ATOMIC ENERGY

**АТОМНАЯ ЭНЕРГИЯ
(ATOMNAYA ÉNERGIYA)**

TRANSLATED FROM RUSSIAN



CONSULTANTS BUREAU



ADVANCES IN TRACER METHODOLOGY

Volume 1

Edited by Dr. Seymour Rothchild,
Technical Director, New England Nuclear Corporation

Proceedings of the Fifth Annual Symposium on Advances in Tracer Methodology, held October 20, 1961, in Washington, D. C., and selected and up-dated papers from the first four Symposia held from 1957-1960, sponsored by the New England Nuclear Corporation in collaboration with Packard Instrument Co., Inc.

The interest in tritium as a tracer isotope, which has developed to major proportions in recent years, is reflected in the first two symposia, concerned solely with tritium, and in succeeding symposia, which contain a large number of papers on **tritium**. Of special interest are:

- Liquid Scintillation Counting of Tritium
- Gas Counting of Tritium
- Tritium in Biochemical Studies
- Tritium Recoil Labeling of Linseed Oil
- Some Aspects of Stereoselectivity in the Introduction of Tritium into Steroids.

Among the other aspects of tracer methodology described, special attention has been devoted to **recent developments in the synthesis of labeled compounds:**

- The Gas Exposure Technique for Tritium Labeling
- Experiences with Tritiated Compounds Prepared by Exposure to Tritium Gas
- Reaction of Unsaturated Organic Compounds with Tritium Gas
- Preparation of Tritium Labeled Paromomycin (Humatin)
by Biosynthesis in a Medium Containing Tritiated Water,

to tracer applications and methods:

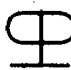
- Use of Radioisotopes in Steroid Methodology
- Metabolism of DL-Epinephrine-7- H^3 D-Bitartrate
- Application of Tritium in the Determination of Gibberellins
- The Efficiency of Autoradiographic Stripping-Film Applied to
Tissue Sections Containing Tritiated Thymidine
- Application of Whole-Body Liquid Scintillation Counters
to Pharmacological Studies,

and to radioisotope analysis methodology:

- Monitoring Gas Chromatography for H^3 - and C^{14} -Labeled
Compounds by Liquid Scintillation Counting
- Determination of Radioactive Sulfur in Biological Materials
- Scintillation Counting of C^{14} -Labeled Paper Chromatograms
- Liquid Scintillation Counting of $C^{14}O_2$ in Aqueous Carbonate Solutions
- Parr Bomb Combustion of Tissues for Carbon-14 and Tritium Analyses
- Determination of Tritium and Carbon-14 in Biological
Samples by Rapid Combustion Techniques

• 50 reports • fully illustrated • indexed • literature references • 343 pages, \$12.00

Contents on request

 **PLENUM PRESS** 227W. 17th St., New York, N. Y. 10011

A. I. Alikhanov	A. I. Leipunskii
A. A. Bochvar	M. G. Meshcheryakov
N. A. Dollezhal'	M. D. Millionshchikov
K. E. Erglis	(<i>Editor-in-Chief</i>)
V. S. Fursov	I. I. Novikov
I. N. Golovin	V. B. Shevchenko
V. F. Kalinin	A. P. Vinogradov
N. A. Kolokol'tsov	N. A. Vlasov
(<i>Assistant Editor</i>)	(<i>Assistant Editor</i>)
A. K. Krasin	M. V. Yakutovich
I. F. Kvartskhava	A. P. Zefirov
A. V. Lebedinskii	

SOVIET ATOMIC ENERGY

A translation of **ATOMNAYA ÉNERGIYA**

A publication of the Academy of Sciences of the USSR

© 1964 CONSULTANTS BUREAU ENTERPRISES, INC.
227 West 17th Street, New York 11, N. Y.

Vol. 15, No. 4

October, 1963

CONTENTS

	P A G E	
	ENG.	RUSS.
The Use of High Frequency Electromagnetic Fields to Contain and Stabilize a Plasma—S. M. Osovets	997	283
Calculation of the Thermodynamic Properties of Cesium Vapor up to 1500° K and a Pressure of 22 bars—N. I. Agapova, B. L. Paskar' and L. R. Fokin	1007	292
Enlarged Radiochemical Equipment Using the Radiation from Spent Nuclear Reactor Fuel Elements—V. L. Karpov, A. Kh. Breger, M. E. Eroshov, V. E. Drozdov, G. N. Lisov, S. G. Stoenko, D. M. Torgovitskii, B. I. Vainshtein and N. P. Syrkus	1018	302
A Radiochemical Investigation of the Yields of Rare-Earth Elements from U ²³⁸ Photofission—K. A. Petrzhak and R. V. Sedletskii	1025	308
The Effect of the Iron Minerals in Ores on Oxidation of Uranium in Acid—G. M. Alkhazashvili, G. M. Nesmeyanova and L. N. Kuz'mina	1031	313
LETTERS TO THE EDITOR		
Study of the Motion of Individual Charged Particles in Corrugated Magnetic Fields—V. M. Balebanov, V. B. Glasko, A. L. Groshev, V. V. Kuznetsov, A. G. Sveshnikov and N. N. Semashko	1036	318
The Over-All Kinetic Energy of U ²³³ and Th ²³² Fragments—S. S. Kovalenko, K. A. Petrzhak and V. M. Adamov	1039	320
Delayed Neutrons from Fission of U ²³³ by 15-MeV Neutrons—B. P. Maksyutenko	1042	321
Determination of the Partial Alpha-Decay Period of Pu ²⁴¹ —R. B. Ivanov, A. S. Krivokhatskii, L. M. Krizhanskii, V. G. Nedovesov and M. I. Yakunin	1043	322
The Fast-Neutron Capture Cross Sections of Copper and Zirconium—Yu. Ya. Stavisskii and A. V. Shapar'	1045	323
Use of Large Area Semiconducting Detectors in α -Spectrometry—V. F. Kushniruk, É. Z. Ryndina, S. M. Solov'ev and I. I. Chuburkova	1047	324
The Attenuation of a High-Energy Neutron Flux in Shielding—M. M. Komochkov and B. S. Sychev	1049	325
The Effect of Reflectors Made of Various Materials on the Increase in the Number of Neutron Captures in the Uranium Carbide Blanket of a Fast Reactor—V. I. Golubev, A. V. Zvonarev, M. N. Nikolaev and M. Yu. Orlov	1053	327
Calculation of the Spectral and Angular Distribution of Scattered γ -Quanta from a Point Monodirectional Cs ¹³⁷ Source in Iron—L. R. Kimel', A. M. Panchenko and V. P. Terent'ev	1055	328

(continued)

Annual Subscription: \$95

Single Issue: \$30

Single Article: \$15

All rights reserved. No article contained herein may be reproduced for any purpose whatsoever without permission of the publisher. Permission may be obtained from Consultants Bureau Enterprises, Inc., 227 West 17th Street, New York City, United States of America.

CONTENTS (continued)

	P A G E	
	ENG.	RUSS.
The Effect of Shield Shape on the Attenuation of γ -Rays from Volume Sources—D. P. Osanov.	1059	331
Measurement of the Frequency Characteristics of an IRT-1000 Reactor by the Oscillation Method—L. V. Konstantinov, A. I. Efanov and V. V. Postnikov.	1060	332
Photoneutron Method for Beryllium Determination in the Laboratory—V. N. Smirnov and D. V. Tokareva	1063	334
Displacement of Uranium from Chloride Melts by Zinc—I. F. Nichkov, S. P. Rasponin and A. F. Tsarenko.	1066	336
A New Type of Porous Bed Model for Neutron Logging—N. K. Kukharenko, Ya. N. Basin, Yu. P. Bal'vas and Yu. V. Tyukaev.	1069	338
Secondary Dust Component of Radioactive Contamination in the Surface Layer of the Atmosphere—B. I. Styro, Ch. A. Garbalyauskas, V. I. Luyanas, V. P. Matulyavichus, T. N. Nedvetskaite and I. S. Tomkus	1072	339
NEWS OF SCIENCE AND TECHNOLOGY		
Conference on Electrostatic Generators and Direct-Voltage Accelerators—G. M. Osetinskii.	1075	342
International Conference on Sector-Focused Cyclotrons and Meson Factories—P. Lapostol.	1078	343
IAEA Symposium on Thermodynamics of Nuclear Materials—V. V. Akhachinskii.	1082	346
The Use of Gamma-Ray Sources in Nondestructive Testing at the Csepel Metallurgical Combine (Hungary)—E. Fényvéssy, K. Scserbak and K. Vara	1090	351
BIBLIOGRAPHY		
New Literature	1093	354

THE USE OF HIGH FREQUENCY ELECTROMAGNETIC FIELDS
TO CONTAIN AND STABILIZE A PLASMA

S. M. Osovets

Translated from *Atomnaya Energiya*, Vol. 15, No. 4,
pp. 283-292, October, 1963
Original article submitted February 26, 1963

This paper discusses the basic proposals that have been made up to the present time by Soviet and foreign scientists relating to the interaction of a plasma with high frequency electromagnetic fields. These proposals deal with the problem of controlled thermonuclear reactions, and are in the direction of overcoming the difficulties that arise in containment and stabilization of a plasma. The paper sets forth the ideas forming the basis of these proposals, and the important equations and diagrams are given, which illustrate the principles on which they operate.

Introduction

Studies on the magnetic containment and thermal insulation of a hot plasma are being carried out along several lines in connection with the problem of controlled thermonuclear synthesis. What is characteristic of each of these lines of work is the way in which the magnetic field acting on the plasma varies with time. From this point of view, the important directions of study may be classified in the following way:

1. Methods in which the plasma is contained by means of stationary magnetic fields. The devices based on these methods are called traps, and the function of the magnetic field is simply to hold the plasma inside the trap.
2. Quasistationary methods, in which the magnetic fields used vary slowly with time. In this case, the rates of change of the field are small in comparison with the velocities determining the processes in the plasma—the velocities of the ions, the velocities of propagation of the magnetohydrodynamic waves, and the rates at which instabilities of magnetohydrodynamic type develop. What is characteristic of these methods is that induced currents are produced which flow in the plasma, and these are used both to contain the plasma and to heat it by Joule heat.
3. One-shot pulse methods involving the use of rapidly varying magnetic fields, changing at rates comparable with the rates of the processes occurring in the plasma, the principal ones of which have been recounted above. In this method, the plasma is heated either by a shock wave or by adiabatic compression of the plasma.
4. Methods using high frequency magnetic and electric fields. This paper is devoted to a discussion of these methods.

Before we begin presenting what methods of this last type consist of, we shall give a brief discussion of the reasons which have made it necessary to look for new methods of investigation in the containment of a hot plasma. With the exception of one-shot pulse methods, all the other lines of work involve producing magnetic fields of a configuration such that the plasma as a whole is in an equilibrium state, where the equilibrium is stable to magnetohydrodynamic perturbations. It is further necessary not to have large particle losses in any definite directions. The stability equations are no less important than the plasma containment itself. For an equilibrium plasma formation to be stable to perturbations of the surface or changes of shape the magnetic field intensity must increase everywhere from the center of the chamber holding the plasma to the periphery.

Building devices using quasistationary or stationary magnetic fields with a configuration approximating the ideal trap, and at the same time satisfying the stability conditions, is fraught with considerable difficulties. The difficulties are due to the fact that the charged particles move freely along the lines of force in the field; and if the lines of force go beyond the trap, the particles are in no way hindered from striking the walls of the chamber. Accordingly, an effort is made to produce a magnetic field such that either the lines of magnetic force are closed inside the chamber, or the particles will find it difficult to get to the points where the lines of force leave the trap.

The simplest configuration in which the lines of force are closed inside the chamber is the toroidal system, in which the magnetic field is directed along the large circumference of a torus. However, this system is not an

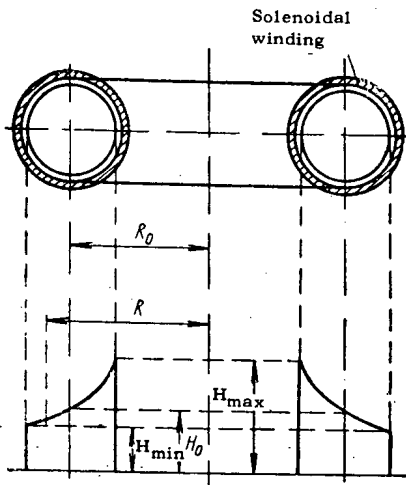


Fig. 1. Distribution of longitudinal magnetic field intensity in the "Tokamak" systems.

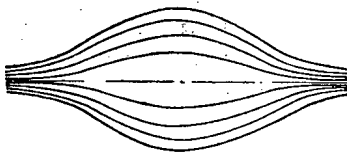


Fig. 2. Configuration of the lines of force in the magnetic field in an adiabatic trap.

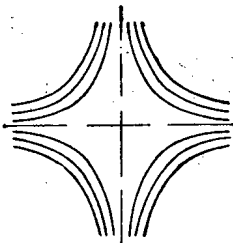


Fig. 3. Configuration of the lines of force in the magnetic field of a trap with sharp point geometry.

the losses from particles flowing out along the magnetic field lines to allowable values. However, the shape of the magnetic field is here such that the field intensity is everywhere dropping from the axis of the trap toward the periphery. It is well known that a plasma in a field of this sort develops instability of convective type, as a result of which the plasma moves comparatively rapidly across the magnetic field to the walls of the chamber. To produce conditions in a trap such that the plasma remains stable to perturbations of this type, the field intensity must everywhere increase from the center toward the periphery. To this end, traps have been proposed with a sharp point magnetic field geometry, having lines of force of the shape shown in Fig. 3. The field intensity at the center of such traps is equal to zero, and increases toward the walls. However, here, instead of the holes characteristic of an adiabatic trap, there is a circular "gap" through which it is easy for the particles to get out of the vessel. Accordingly, although a trap of this sort gives better conditions for stability than the adiabatic trap, it is still less "ideal" in the sense of particle loss through the gap. Thus, in all the types of traps best known at the present time, there are conflicts between the plasma containment conditions and the stability conditions. The need to produce magnetic field

ideal trap, since the field intensity drops from the inner circumference to the outer circumference of the torus (Fig. 1). As a result of this there is a difference in magnetic pressures, and the plasma goes out of equilibrium (the so-called toroidal effect). To compensate for this effect in systems of "Tokamak" type, an induced current is produced in the plasma in the same direction as the lines of force in the magnetic field. The interaction between this current and the image current in the metallic wall of the chamber produces a quasiequilibrium configuration for a time of the order of the field penetration time through the metal wall. Thus, having the induced current present makes it possible to produce conditions approximating the conditions in an ideal trap. However, as the induced current flows through the plasma, it can lead to the development of other forms of instability.

The first form is current instability of magnetohydrodynamic type. The current thread is unstable to perturbations that change its shape. To suppress this type of instability, the "Tokamak" systems use a strong longitudinal magnetic field, which, while compensating for the magnetohydrodynamic instabilities of the lower modes with $m=0$ (lateral displacements), and $m=1$ (bending), can lead to instabilities in the higher modes. Further, an induced current flowing in a strong magnetic field produces a large distortion in the electron velocity distribution function. A group of strongly accelerated electrons is formed with energies of many kiloelectron-volts. Having a large number of electrons with energies greatly in excess of the thermal value produces kinetic instabilities, which in turn increase the transfer coefficients. Using rotational transformation of the magnetic field lines as in systems of stellarator type would seem to make it possible to avoid toroidal drift, and in this way get closer to the conditions for an ideal trap, where the magnetic field lines close inside the chamber. However, the experiments made so far do not provide the basis for drawing any definite conclusions, since they have only been made with an induced current present. Under these conditions, no essential difference can be seen between the stellarator and the "Tokamak".

In traps where the magnetic field lines leave the chamber, there are "holes" through which the particles can escape from the effective volume. The conditions under which the particles escape are determined by the configuration of the magnetic field. In traps of adiabatic type (the shape of the magnetic force lines is shown in Fig. 2) it seems to be possible, under certain conditions, to reduce

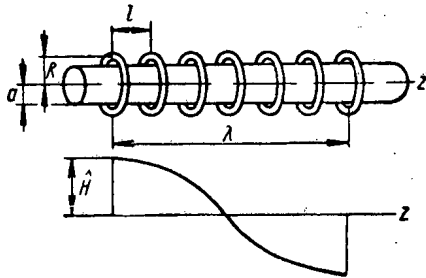


Fig. 4. Arrangement of windings, and instantaneous magnetic field intensity distribution in a traveling wave system.

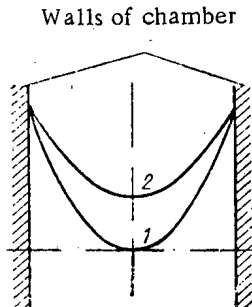


Fig. 5. Magnetic field distribution over the cross section of the discharge chamber in a system with sharp point geometry (1), and in a traveling wave system (2).

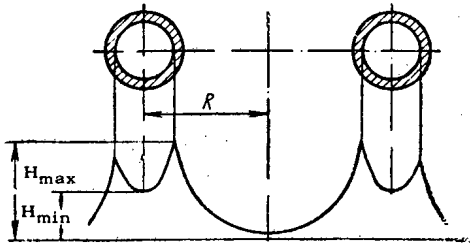


Fig. 6. Magnetic field intensity distribution in a toroidal traveling wave system.

functions of the high frequency fields are limited solely to maintaining stability in the system. The plasma is contained by fields that do not change with time, or else change quite slowly. The methods in which stability is achieved by high frequency fields acting on an equilibrium plasma we shall give the name of dynamic stabilization methods.

This classification is what determines the direction of study. As far as the methods of causing the high frequency fields to act on the plasma are concerned, there are also two ways that need to be distinguished:

1) acting on the plasma with fields of comparatively low frequency, where the characteristic dimensions of the system are much less than the wavelength in vacuum. In this case, the plasma is acted upon solely by the magnetic field, since the electric field E_{\sim} is small in comparison with the magnetic field (in the ratio $E_{\sim} \cong (l/\lambda)H_{\sim}$);

2) the plasma is placed in a system of endovibrator type, and is acted upon by an electromagnetic wave with $E_{\sim} = H_{\sim}$. The first method may be given the name lumped constant method (inductance L and capacity C), while the second may be called the distributed constant method.

configurations such as to satisfy the stability conditions with respect to even the most dangerous types of perturbations leads to a worsening of the conditions under which the particles are contained in a given volume. However, the effort to approximate the conditions in an ideal trap may lead to worsening of the stability conditions. This forces us to look for new solutions, where the conflicting requirements do not exist. One of the ways offering new possibilities involves using high frequency magnetic fields to contain and stabilize the plasma. Up to the present time, several proposals have been made for using high frequency fields both to construct traps and to stabilize the instabilities. The theoretical assumptions on which these proposals are based allow some systematization to be made of the directions being followed by existing studies involving the use of high frequency fields. As far as experiments are concerned, since the first proposals for using high frequency fields were only made in the Soviet Union in 1957, it is natural that less has been done along this than along other familiar lines, the more so since building high powered high frequency equipment involves great engineering difficulties (some of the existing experimental results are given below).

The purpose of the present paper is to systematize the fundamental work that has been done on the interaction of a plasma with high frequency fields. The work of foreign scientists in this field is not sufficiently well known: several papers of a theoretical nature, and only one experimental paper [13] have been published.

High frequency fields may be used in the problem of controlled thermonuclear synthesis for several different purposes (for example, they may be used for heating the plasma). Although this line of work was started some time ago, it is not discussed in the present paper. Here, we are interested in proposals for using high frequency fields in two other ways. First, it was pointed out in some of the proposals that the method can be used to produce field configurations that are nearly the same as the field configuration in an ideal trap. In this case, we are dealing with methods of containing the plasma both by high frequency fields alone, and in combination with stationary or quasistationary fields. Second, in systems in which the plasma is contained by stationary or quasistationary fields, high frequency fields are used to stabilize the most dangerous types of instability. Here, the

Plasma Containment and Stabilization By Means of High Frequency Fields

Lumped constant systems. It is clear that when using lumped constant systems, the oscillational frequency of the field must be kept as low as possible, since increasing the frequency (for a fixed total field energy) raises the active power taken from the generator supplying the oscillations. The lower limit of the frequency will be approximately the thermal velocity of the ions divided by the characteristic dimension of the system. This is due to the fact that during one period of change in the high frequency field, the perturbation of the plasma surface must not exceed the allowable limits. In other words, as the field pressure on the plasma surface varies from zero to its maximum value, the perturbation of the surface must be small in comparison with the distance from the surface to the walls of the chamber. This condition holds both for systems in which the action on the plasma comes exclusively from the high frequency field, and for combined systems. In the latter case, the rate of perturbation of the surface may be determined by the velocity of propagation of Alfvén waves for the stationary wave $v_A = H_0 / \sqrt{4\pi\rho}$, while in the first case it is determined by the thermal velocity of the ions. For the conditions under which studies are being made or are being proposed, the appropriate frequencies lie in the 1-10 Mc range, i.e., in the 300-30 m wavelength range. These values are many times greater than the dimensions of the equipment used, and are thus simply lumped constant systems. They are characterized by the use of vacuum tube oscillation generators and ceramic circuit condensers. The inductance is the winding on the gas discharge chamber. Let us consider how these systems may be used to contain a plasma. As a typical example take the traveling wave system [1].

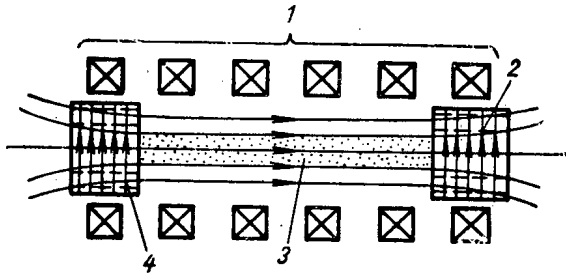


Fig. 7. Trap with high frequency mirrors: 1) magnetic winding; 2) endovibrator; 3) plasma; 4) lines of force of electric field.

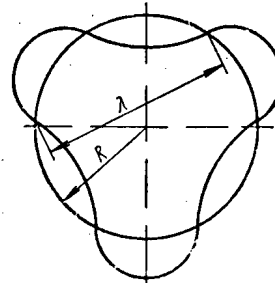


Fig. 8. Bending of a plasma spiral carrying current, for $n = 3$.

It was pointed out above that in traps with sharp point geometry in the magnetic field, the conditions are satisfied for stability to perturbations of convective type, which are one variety of magnetohydrodynamic instability. The windings producing the magnetic field are connected bucking, i.e., the currents in the windings are of opposite sign. As a result of this, the magnetic field intensity is zero at the center of the chamber, and is everywhere rising toward the periphery. However, there are gaps in these traps through which particles can escape. Assume that the magnetic field is produced by a winding in which the alternating currents in neighboring turns are displaced in phase by some angle (Fig. 4).

If the phase shift angle φ between the current in neighboring turns lies between zero and π , the amplitude value of the magnetic field intensity will change in the direction of the z axis (see Fig. 4), so that the waves seem to travel. If the system is wound into a torus, the wave will rotate in the same way as in an induction motor. In this case, the gap, i.e., the place where the magnetic field intensity is small, will move along with the wave. If the velocity of the wave is quite large, the particle is not able to get out of the effective volume. The velocity of the wave is $v = \omega/\kappa$, where κ is the wave number $2\pi/\lambda$, and λ is the wavelength in space. The condition for the smallness of the plasma surface perturbation because of the presence of the moving gap reduces to $\omega < \pi u/l$, where u is the velocity of sound in the plasma, and is equal in practice to the thermal velocity of the ions.

For a phase shift of π , i.e., in a system with sharp point geometry, the field intensity varies over the cross section of the chamber (without plasma) as shown by curve 1 of Fig. 5. If the current flows in the same direction in all the turns, the field will be practically uniform. It is clear that if the phase shift angle between neighboring windings is $0 < \varphi < \pi$, some intermediate case will occur (for example, curve 2 of Fig. 5). Here the field does not drop to zero, but it is a minimum in the center, and increases toward the periphery everywhere. Accordingly, the plasma is in a "well," the depth of which is determined by the phase shift angle φ , the values of R (the radius of the turn), and

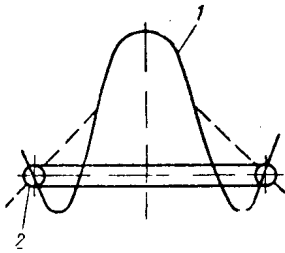


Fig. 9. Magnetic field intensity distribution in a system with dynamic stabilization of a plasma spiral. 1) Field intensity H ; 2) plasma spiral.

l (see Fig. 4). The increase in field on going away from the plasma boundary favors stability: if the plasma surface is deformed, the resulting additional field pressure tries to bring the plasma boundary back to its previous state [2]. If the cylinder is wound into a torus (see Fig. 4), the toroidal effect causes the magnetic field distribution to become asymmetric over the cross section: the field intensity about the inner surface of the chamber will be greater than about the outer surface, but the "well" is still there, and the equilibrium conditions are maintained (Fig. 6). Other modifications of the traveling wave system are possible; for example, the field may rotate along the small radius of the torus. Other types of discharge using rotating fields are not impossible [3, 4].

The system just described has been realized in experimental setups on which a series of studies have been made. Some of the results of these studies are given below. It is important to note that using high frequency fields opens up new possibilities in the direction of changing the field configuration with time so as to get rid of the defects inherent in stationary fields. If the changes in field configuration are rapid enough, a state of affairs may be reached where, on the average, conditions are satisfied which approximate the conditions for an ideal trap, at the same time satisfying the requirements needed to maintain stability. It is not impossible however that these requirements are insufficient.

Using rotating magnetic fields does not of course exhaust all the possibilities for containing a hot plasma with high frequency fields in lumped constant systems. An attempt may be made to combine rotating fields with stationary or quasistationary fields. However, this case does not show any essential advantages, since having stationary fields present, together with the associated spatial irregularities and the possibilities for particle drift, can reduce to nothing the positive features inherent in high frequency fields. In any case, we do not at the present time know of any well-founded proposals that are substantially different from those described above.

Distributed constant systems. In plasma containment in distributed constant systems, we have $E_{\sim} = H_{\sim}$, and the effect on the plasma is caused by the pressure of both the magnetic and the electric field. Accordingly, there is no instant of time at which the field pressure on the plasma is near zero. It has been shown in [5] that a plasma may be contained by means of a standing wave. An attempt may be made to compensate for the toroidal effect by using the pressure of a wave of this type.

The following possibility is discussed in [6]. Along the outside of the periphery of the torus (see Fig. 1) is located a system of endovibrators, the fields from which produce electromagnetic wave pressure in a direction opposite to the difference in magnetic pressures arising from the toroidal effect. In this case it is possible to get a resultant field configuration which satisfies the conditions for equilibrium of the plasma. The same paper gives a method for containing the plasma by means of endovibrators located at the ends of a trap with a constant main field (Fig. 7). It would seem possible in this system to make a considerable increase in the length of time the particles exist in the trap. This proposal has been realized in an experimental setup on which studies are being made [7, 8]. The question is left unresolved of particle drift at the points where the lines in the constant magnetic field intersect with the lines in the wave field.

In addition to these proposals, the paper [4] was given at the Second International Conference on the Peaceful Uses of Atomic Energy. This paper describes a system consisting of a spherical endovibrator, which produces electromagnetic fields rotating about all three axes. The extent to which this proposal has been realized is not known.

This essentially exhausts the basic proposals made up to the present time on plasma containment by high frequency fields.

Dynamic plasma stabilization methods. At the present time, proposals have been made for using dynamic stabilizing methods: first, for stabilizing the magnetohydrodynamic current instabilities in a quasistationary plasma spiral, and, second, to stabilize the instabilities of convective type in adiabatic traps.

The system for dynamic stabilization of a plasma spiral carrying a current [9, 10] may be represented in the following way. It is well known that a plasma spiral with a current induced in it from an external magnetic field can be in equilibrium with the field producing it if certain definite conditions are satisfied which are superimposed on the form of the field, thus:

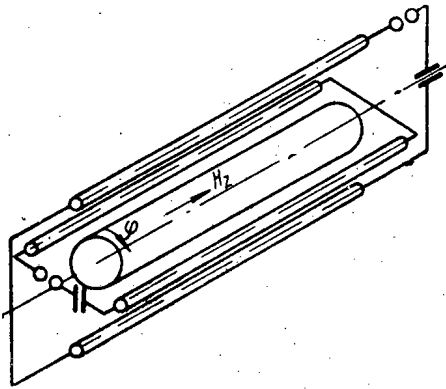


Fig. 10. Schematic diagram of the Blevin and Thoneman system [13].

$$H_{\text{orb}} = \frac{\bar{H}}{4} \left(1 + \frac{2}{l} \right),$$

where H_{orb} is the magnetic field intensity at the place where the spiral is located on the equilibrium orbit, \bar{H} is the mean field intensity inside the spiral, and $l = 2 \left(\ln \frac{8R}{r} - 2 \right)$ is the inductance per centimeter length of the spiral.

If the derivative of the field along the radius in the region of the equilibrium orbit has a quite small negative derivative, the spiral will be stable in both the vertical and the horizontal plane for the condition that circular form is maintained. But it is also known that a spiral of this sort carrying current is unstable to deformations tending to distort the circular form. The most dangerous deformation in this case is bending. Figure 8 shows the typical picture of deformation of a current spiral.

Deformations of this type may be compensated for by a magnetic field in a direction perpendicular to the plane of the spiral.

The degree of compensation is determined by the magnitude of the derivative of the field intensity along the radius $\partial H / \partial R$ in the vicinity of the equilibrium orbit. We shall call the quantity $\partial H / \partial R$ the steepness of change of the field. It has been shown that the smaller the wavelength of the bending, the greater will be the steepness of the field required to compensate for the deformation. Compensating for deformations in the plane of the spiral requires the field intensity to increase with radius, i.e., $\partial H / \partial R$ must be positive (Fig. 9, solid line). However, in this case the spiral becomes unstable to bending in the direction perpendicular to the plane of the spiral. To compensate for this deformation, the field intensity must drop off with radius, i.e., $\partial H / \partial R$ (see Fig. 9, dotted line) must be less than zero. Obviously, these conditions are mutually contradictory. They may be satisfied if the form of the field varies with time in such a way as to compensate for the instability in the plane of the spiral in one half-period, and for the instability in the plane perpendicular to it in the next half-period. The equation describing the behavior of such a system is similar to the equation for the oscillations of an overturned pendulum on a vibrating suspension, the equations for the stability of which are well known (see for example [11]). These conditions, as applied to the problem under discussion, reduce to the inequality

$$\frac{\partial H}{\partial R} \sim > \frac{2I}{cR^2} n^2 \ln \frac{\lambda}{\pi r_0} = H_{\phi} \frac{r_0}{R^2} n^2 \ln \frac{\lambda}{\pi r_0}$$

or, if we assume that the maximum value of the variable component of the field in the region of instability of the orbit varies linearly with the radius, the inequality is of the form

$$\frac{H_{\sim}}{H_{\phi}} > a r_0 \left(\frac{n}{R} \right)^2 \ln \frac{\lambda}{\pi r_0}.$$

For the frequency of the alternating field it is necessary to have

$$\omega > \frac{4\pi u}{\lambda} \sqrt{\ln \frac{\lambda}{\pi r_0}}.$$

Here H_{\sim} is the maximum intensity of the high frequency component of the magnetic field, I is the current in the plasma spiral, R is the large radius of the torus, a is the small radius of the torus, λ is the wavelength of the perturbation, n is the number of lengths of the perturbation that fit on the perimeter of the spiral (for example, for the deformation in Fig. 8, $n=3$), r_0 is the radius of the cross section of the plasma spiral, and ω is the angular frequency of the high frequency component of the field.

It may be seen from the last inequality that this frequency is, in order of magnitude, equal to the thermal velocity of the ions divided by the characteristic dimension of the system. Thus, we get the same range of frequencies as that required to contain the plasma with a traveling wave field.

At the present time, experimental studies are being made on this method, the results of which for the most part support the initial assumptions. Details of these experiments will be published later on.

We shall now give a short discussion of the proposals relating to compensating for convective instability in adiabatic traps in toroidal systems. These proposals have been formulated in [7]. In essence, they reduce to compensating for the convective instability which leads to the formation of plasma "tongues" by electron drift currents in the plasma. These currents are produced on the plasma surface by the action of high frequency fields. It has been shown that the pressure of the high frequency electromagnetic fields on the plasma surface leads to drift of the electrons in the surface layer of the plasma in a direction opposite to the direction of the drift resulting from irregularity in the stationary magnetic field. The drift currents from the high frequency field have a component constant in time, since they occur as a result of quadratic effects. These currents are proportional to vector products of the type $[\vec{H} \sim \text{rot } \vec{H} \sim]$ and $[\vec{E} \sim \text{rot } \vec{E} \sim]$, as well as to the product $\vec{E} \text{ div } \vec{E}$. If the high frequency fields are of sufficiently large amplitude, they can compensate for the deformation of the surface occurring as a result of instabilities of convective type. The compensation conditions reduce to the inequality

$$\frac{H^2}{8\pi p_l} > \frac{A}{4} \left(\frac{\pi R}{L} \right)^2 \left(\frac{H_{\max}}{H_{\min}} - 1 \right),$$

where A is a coefficient of the order of unity, R is the radius of the plasma, L is the distance between the mirrors, p_l is the plasma pressure, and H_{\max}/H_{\min} is the mirror ratio.

A proposal for compensating for instabilities of the plasma surface in adiabatic traps has also been described in [12], in which the suggestion is made of using comparatively low frequency fields with a frequency of the order of several megacycles. In this case, the only thing that is important is the effect of the magnetic field, in comparison with which the electric field intensity is small. The paper only gives theoretical studies made on quite reasonable assumptions. It is assumed that both high frequency and stationary fields are absent inside the plasma. Apparently, these assumptions were made for convenience of theoretical treatment, but there is some doubt as to whether or not they hold.

Definite interest attaches to the proposal made in [13], on the basis of which experiments are being made at the present time. This proposal may be realized both in adiabatic traps and in toroidal systems. The content of the proposal is as follows. A plasma in a longitudinal stationary magnetic field is acted upon by an additional high frequency rotating magnetic field, which is produced by currents from the attenuating discharge of a condenser battery, flowing in a system of rods running in the direction of the main field (Fig. 10). The high frequency rotating field produces drift currents in the plasma in the direction of rotation of the field, i.e., in the φ direction. These currents have a component constant in time, since they arise as a result of a quadratic effect, and are proportional to $[\vec{H} \sim \text{rot } \vec{H} \sim]$. An additional stationary field H_z is produced by the drift currents flowing inside the plasma. If the direction of rotation of the high frequency field is taken such that the field from the drift current combines with the main field inside the plasma, the plasma becomes paramagnetic. Paramagnetism of the plasma is known to exert a beneficial effect on the stability. Actually, in the experiments that have been made a stable plasma formation has been observed, separated from the walls of the vessel, as ascertained by superhigh-speed photography, as well as by means of probes and microwave measurements. However, the experiments have so far been made on a straight tube with a uniform field, so that there was nothing to prevent free outflow of particles along the field lines to the ends of the tube. The question of whether or not stability is maintained in adiabatic traps and toroidal systems is still open.

Discussion of Experimental Results and Conclusions

A short presentation has been given above of the basic proposals made up to the present time on the use of high frequency electromagnetic fields to contain and stabilize a plasma. Experimental studies have been started on the basis of some of these proposals. The results of the studies made were reported at the International Conference on Plasma Physics and Controlled Thermonuclear Synthesis held in Salzburg in September 1961, and were published in part in [14-16].

The experimental results obtained still do not give any basis for drawing definite conclusions as to the underlying possibilities of using the methods given above. Only the first steps have been taken along these lines. Nevertheless, the results are of great interest since new physical phenomena have been discovered which form no part of our original ideas.

Mention was made above of the drift currents occurring as a result of quadratic effects. It has been discovered in experimental studies on the traveling wave system that the presence of such currents has a substantial effect on the characteristics of the system. The drift current, to a considerable degree, determines such parameters as the effective conductivity of the plasma, and the way in which the high frequency field penetrates the plasma.

For the simplest case, where the high frequency fields are relatively small while the gas densities are large, the constant component of the drift current is given by the equation

$$I_{dr} = \frac{e\delta r_0 \kappa \hat{H}^2}{8mv},$$

where r_0 is the plasma radius, κ is the wave number for the wavelength in space, δ is the thickness of the skin layer assuming normal skin effect, i.e., for the case where the thickness of the skin layer is greater than the electron mean free path, ν is the effective frequency of collisions between an electron and the neutral and charged particles, and \hat{H} is the maximum value of the magnetic field component in the direction of motion of the wave. The value of the field is taken at the plasma boundary. The measured values of the drift current for small fields and large initial pressures are quite close to the calculated values. The measurements made on the thickness of the skin layer with magnetic probes are also in good agreement with the calculated values. However, the state of affairs changes radically as the magnetic field intensity is increased and the initial gas pressure is lowered. It turns out that having a drift current present leads to a condition where the conductivity ceases to increase with increase in the degree of ionization of the plasma and in the electron temperature. The expression for this anomalous effective conductivity σ_{eff} may be written in the form

$$\sigma_{eff} = \frac{\sigma_n}{1 + \left(\frac{e\delta\kappa\hat{H}^2}{\sqrt{2}mc\nu} \right)},$$

where σ_n is the normal conductivity.

Hence it follows that for $\frac{e\delta\kappa\hat{H}^2}{\sqrt{2}mc\nu} > 1$, the conductivity lowering effect becomes substantial. Physically, this means that when the radial component of the magnetic field $\hat{H}_r = \kappa\delta\hat{H}_z$ becomes such that the Larmor frequency in the field exceeds the collision frequency, "magnetization" of the electrons occurs. The expression for \hat{H}_r is obtained from the equation $\text{div } \vec{H} = 0$, for the condition that the z dependence is of the form $\cos(\omega t + \kappa z)$, while the r dependence is of the form $e^{-r/\delta}$.

Actually, the reduction in conductivity as a result of magnetization of the electrons decreases the Q of the circuit, and leads to excessive consumption of plasma energy. The magnetization also affects the magnitude of the drift current, the expression for which takes the form

$$I_{dr} = \frac{\pi r_0 \delta e n_e \nu_f}{1 + \left(\frac{e\delta\kappa\hat{H}^2}{\sqrt{2}mc\nu} \right)^2} \left(\frac{e\delta\kappa\hat{H}^2}{\sqrt{2}mc\nu} \right)^2,$$

where n is the electron density, and ν_f is the phase velocity of the wave in the direction of the rotation of the field, $\nu_f = \omega/\kappa$. It may be seen from the above equation that the directed velocity of the electrons in the drift current cannot exceed the phase velocity of the wave, which, in the system studied, was about $5 \cdot 10^7$ cm/sec. Accordingly, having a drift current flowing can scarcely start up electron oscillations in the plasma, since the above velocity is much less than the thermal velocity of the electrons.

However, as far as the electrodynamic current instability is concerned, it may be shown that the magnetic field of the drift current is always considerably less than the intensity of the main high frequency field, so that it is again in this case scarcely possible for instability to occur. Nevertheless, the presence of the drift current has such a large effect on all the processes that it is difficult to say what effect it will have if the high frequency magnetic field intensities are subsequently increased to any considerable extent. The example given provides a clear illustration of the importance of nonlinear effects in systems using high frequency magnetic fields. As was shown above, such nonlinear effects occur, and are used in other systems: in compensating for the instabilities in adiabatic traps, in systems using a rotating magnetic field with a stationary longitudinal field present, etc. Thus, new theoretical problems arise, along with the need to look for new theoretical methods of investigating nonlinear effects.

However, as far as experimental methods for the subsequent development of high frequency systems are concerned, difficulties arise having both engineering and fundamental aspects. The existing engineering methods make it possible to carry out physical investigations that clear up a number of fundamental questions in the process of looking for the most promising lines of work. This of course requires complex engineering developments, which, however,

are completely attainable with the present day level of development of engineering. What are needed are more highly developed and more powerful generators (approximately up to 1000 MW for a pulse length of ~ 1 msec), circuit condensers with an energy capacity per unit volume a factor of 50-100 greater than those in existence, development of methods for increasing the dielectric strength of circuits, development of ceramic chambers meeting the operating requirements in high vacuum, etc. All these problems have to do with engineering. However, the choice of suitable materials, and the development of the technology of preparing samples requires serious physics studies.

The fundamental side is more important. Even in case the physics studies show that the action of high frequency fields on a plasma lead to the desired results in containment and thermalization of a hot plasma, it turns out that satisfying the energy balance conditions in a future thermonuclear reactor is considerably more difficult than is the case with stationary or quasistationary fields.

It was shown in [1] that for the existing conducting materials at normal temperature, the ohmic losses from a greatly enhanced skin effect are such that the losses themselves will be mainly what determines the energy balance. The Q values obtainable at the present time in radio systems using either lumped or distributed constants are fundamentally not good enough to make an energetically favorable nuclear synthesis reaction possible. Accordingly, the lines of work involving high frequency methods of containing and stabilizing the plasma can only be said to be promising if it is possible to make a marked reduction in the losses in the circuits and endovibrators. Fundamental possibilities are opened up by the use of superconductors in which a superconducting state is maintained at high magnetic field intensities. Such superconductors have been obtained quite recently, and success in their further development may exert a decisive influence in the problem under discussion.

Of course, at the present time, the greatest amount of attention must be concentrated principally on making physics studies and looking for physical ways of making a fundamental solution of the problem. As for the engineering development possibilities, it would be premature at present to set up any projects in this direction based on existing engineering facilities. There is every reason to assume that by the time physical means have been found of solving the problem, new engineering methods will have appeared, since the rapid development of engineering in general, and of radio-engineering in particular, is such that it is at present difficult to imagine what the possibilities will be in the comparatively near future.

It should be noted in conclusion that the lines of work involving the use of high frequency electromagnetic fields in the problem of controlled thermonuclear synthesis have only begun to develop. Further studies are needed at higher field intensities. More powerful generating equipment must be built, along with circuits with higher breakdown strength, more heat resistance discharge chambers, etc. It may be assumed that even in the next few years our knowledge in the field of study of the interaction between a plasma and high frequency electromagnetic fields will become substantially more complete, and that this very interesting line of investigation will occupy a permanent place among the other lines in which a search is being made for means of controlling thermonuclear synthesis.

LITERATURE CITED

1. S. M. Osovets, In Collection: Plasma Physics and the Problem of Controlled Thermonuclear Reactions, Vol. 4 [in Russian], Moscow, Academy of Sciences Press, USSR, p. 3 (1958).
2. T. F. Volkov, *ibid.*, p. 109.
3. B. A. Trubnikov, *ibid.*, p. 309.
4. J. Butler, A. Hatch, and A. Ulbrich, Paper No. 350, presented by the USA at the Second International Conference on the Peaceful Uses of Atomic Energy, Geneva (1958).
5. R. Z. Sagdeev, In Collection: Plasma Physics and the Problem of Controlled Thermonuclear Reactions, Vol. 3 [in Russian], Moscow, Academy of Sciences Press, USSR, p. 346 (1958).
6. A. A. Vedenov, et al., In the book: Transactions of the Second International Conference on the Peaceful Uses of Atomic Energy. Papers by Soviet scientists, Vol. 1 [in Russian], Moscow, Atomizdat, p. 143 (1958).
7. T. F. Volkov, V. M. Glagolev, and B. B. Kadomtsev, Paper No. 228 at the International Conference on Plasma Physics and Controlled Thermonuclear Synthesis [in Russian], Salzburg, MAGATÉ (1961).
8. Yu. I. Arsen'ev, et al., *ibid.*, paper No. 218.
9. S. M. Osovets, *Zh. éksp. i teor. fiz.*, 39, 311 (1960).
10. M. L. Levin and M. S. Rabinovich, See [7], paper No. 251.
11. L. D. Landau and E. M. Lifshits, *Theoretical Physics, Mechanics*, Vol. 1 [in Russian], Moscow, Fizmatgiz, p. 121 (1958).

12. E. Weibel, *The Physics of Fluids*, 3, 945 (1960).
13. H. Blevin and P. Thoneman, See [7], paper No. 65.
14. V. G. Andreev, *ibid.* paper No. 250.
15. R. A. Demirkhanov, *Zh. éksperim. i teor. fiz.*, 42, 338 (1962).
16. R. A. Demirkhanov, et al., *Zh. tekhn. fiz.*, 32, 180 (1962).

All abbreviations of periodicals in the above bibliography are letter-by-letter transliterations of the abbreviations as given in the original Russian journal. *Some or all of this periodical literature may well be available in English translation.* A complete list of the cover-to-cover English translations appears at the back of this issue.

CALCULATION OF THE THERMODYNAMIC PROPERTIES
OF CESIUM VAPOR UP TO 1500°K AND A PRESSURE OF 22 BARS

N. I. Agapova, B. L. Paskar', and L. R. Fokin

Translated from Atomnaya Énergiya, Vol. 15, No. 4,

pp. 292-302, October, 1963

Original article submitted December 27, 1962

This paper gives an analysis of the original data, together with tables of the thermodynamic properties of cesium on the saturation curve and in the superheated and wet vapor region, and an estimate is made of the accuracy of the results. An attempt is made to calculate the thermodynamic properties of cesium vapor up to 1500°K and 22 bars.

The method of calculation is the same as that used previously in determining the thermodynamic properties of potassium [1]. Here, the cesium vapor is regarded as an equilibrium dissociating mixture of mon- and diatomic ideal gases ($Cs_2 \rightleftharpoons 2Cs_1$),* while the wet vapor (in calculating the velocity of sound) is regarded as a medium that is uniform from the gas dynamic point of view. In calculating the properties of the saturated vapor, the specific volume and the compressibility of the liquid have been neglected.

Initial Data

The caloric functions of the condensed phase needed for the calculations—the heat capacity, the entropy, and the enthalpy—were taken from [2, 3], in which the melting point is taken to be 301.8°K [4], while the heat of fusion is taken as $\Delta I_{301.8}^0 = 2137.2$ J/g-atom (here, and in the rest of the paper, the condensed phase is assumed to be mon-atomic, while the molecular mass is $\mu_c = \mu_1 = 132.91$).

The heat capacity C_{pc}^0 has been studied experimentally at temperatures from 20 to 310°K in [5], where the characteristic temperature was found to be $\theta_D(Cs) = 44^\circ K$. These data have been used in [2, 3] to calculate the enthalpy $|I_{298.15}^0 - I_0^0|_c = 7778.2$ J/g-atom, and the entropy $S_{c,298.15}^0 = 84.35 \pm 1.7$ J/g-atom · °K.

In addition to this, the heat capacity of liquid cesium had been measured in 1913 [6] at temperatures from 28 to 100°C, and the equation found was

$$C_{pc}^0 = 33.47 - 0.0188 \text{ J/g-atom} \cdot \text{deg}.$$

It is known that beyond the melting point, C_{pc}^0 of the liquid first decreases (as a result of destruction of the quasicrystalline structure), and then increases, and in the critical range $C_{pc}^0 \rightarrow \infty$. There is very little experimental data on the heat capacity in the liquid state for cesium and other alkali metals, which makes it difficult to sample and extrapolate the values by similitude methods.

We consider that the calculation of the caloric functions of liquid cesium made in [2], assuming that the heat capacity is constant ($C_{pc}^0 = 31.80$ J/g-atom · deg) from the melting point to 1500°K, represents the present day level of knowledge since any other extrapolation can be just as inaccurate. The method that we have used for calculating the saturation pressure [1] is based on determining the partial pressures of mon- and diatomic ideal vapor over liquid cesium from a consideration of the appropriate phase equilibrium conditions. The original data used in this case were those on the heats of sublimation of the components, and the heat capacity C_{pc}^0 . Brute force extrapolation of the latter to the high temperature range is, in our opinion, more justifiable than straight extrapolation of the different pieces of experimental data on the saturation pressure since it is clear in the first method what liquid and vapor model is being used to obtain the results.

The heat of sublimation ΔI_{01}^0 of Cs_1 vapor from the condensed phase at 0°K is given in a number of papers and varies from 79699 J/g-atom [2, 3] to 78619 J/g-atom [7]. The value of ΔI_{01}^0 is found from an analysis of the experimental data on the saturation pressure, which, for cesium, were taken in the temperature range 307.5-943°K [7].

* The subscripts 1, 2 and "c" refer to atoms, molecules, and the condensed phase respectively. The index 0 (at the top) designates the standard state.

TABLE 1. Saturated State of Cesium Vapor (Temperature Table)

T, °K	p_g , bar	α''	μ''	$v'' \cdot 10^3$ m ³ /kg	v'' , m ³ /kg	$\sigma \cdot 10^3$ N/m	i'' , kJ/kg	s'' , kJ/kg·°K	r'' , kJ/kg	i'' , kJ/kg	s'' , kJ/kg·°K
500	2.489·10 ⁻⁴	0.9930	133.38	0.586	1252	45	122.878	0.81153	553.77	676.65	1.9191
550	1.246·10 ⁻³	0.9872	133.77	0.596	274.5	41	134.841	0.83433	548.63	683.47	1.8318
600	4.723·10 ⁻³	0.9792	134.31	0.607	78.65	39	146.803	0.85515	543.09	689.90	1.7603
650	1.450·10 ⁻²	0.9689	135.01	0.617	27.61	36	158.766	0.87430	537.16	695.93	1.7007
700	3.771·10 ⁻²	0.9567	135.85	0.628	11.36	34	170.729	0.89203	530.90	701.63	1.6505
750	8.602·10 ⁻²	0.9430	136.81	0.639	5.299	31	182.692	0.90854	524.37	707.06	1.6077
800	1.761·10 ⁻¹	0.9283	137.85	0.649	2.740	29	194.654	0.92398	517.63	712.29	1.5710
850	3.304·10 ⁻¹	0.9128	138.97	0.660	1.539	28	206.617	0.93848	510.74	717.36	1.5394
900	5.767·10 ⁻¹	0.8963	140.13	0.670	0.9260	26	218.579	0.95216	503.82	722.40	1.5119
950	9.464·10 ⁻¹	0.8814	141.29	0.681	0.5907	24	230.542	0.96509	496.93	727.47	1.4882
1000	1.474	0.8662	142.44	—	0.3961	—	242.505	0.97737	490.08	732.59	1.4675
1050	2.195	0.8513	143.58	—	0.2770	—	254.467	0.98904	483.29	737.76	1.4493
1100	3.147	0.8370	144.70	—	0.2008	—	266.430	1.00017	476.60	743.02	1.4334
1150	4.363	0.8236	145.77	—	0.1504	—	278.393	1.01081	470.05	748.44	1.4195
1200	5.878	0.8110	146.78	—	0.1156	—	290.355	1.02099	463.66	754.01	1.4074
1250	7.712	0.7993	147.73	—	0.09122	—	302.318	1.03075	457.41	759.73	1.3967
1300	9.897	0.7883	148.65	—	0.07347	—	314.280	1.04014	451.29	765.57	1.3873
1350	12.45	0.7780	149.51	—	0.06032	—	326.243	1.04917	445.29	771.56	1.3790
1400	15.36	0.7685	150.31	—	0.05041	—	338.206	1.05787	439.43	777.64	1.3717
1450	18.66	0.7598	151.05	—	0.04277	—	350.169	1.06627	433.73	783.90	1.3654
1500	22.35	0.7519	151.73	—	0.03677	—	362.131	1.07438	428.18	790.33	1.3598

T, °K	c_p^* , kJ/kg·deg	c_p^{*sp} , kJ/kg·deg	c_p^{*sp} , kJ/kg·deg	c_p^{*sp} , kJ/kg·deg	α^{*sp} , deg/bar	$\alpha^{*sp} = \frac{dT}{dp}$, deg/bar	α^{*sp} , m/sec	α^{*tp} , m/sec	k^{*sp}	k^{*tp}	
500	0.23925	-0.9674	0.1821	0.1152	17.628	2604.10	1130.10 ²	221.6	186.6	1.575	1.116
550	0.23925	-0.8652	0.1952	0.1254	14.183	8856	2752.10	229.9	196.5	1.546	1.129
600	0.23925	-0.7806	0.2092	0.1359	11.598	3512	8689	237.9	205.9	1.524	1.141
650	0.23925	-0.7092	0.2229	0.1457	9.616	1584	3341	245.6	214.9	1.507	1.153
700	0.23925	-0.6474	0.2352	0.1540	8.067	791.0	1498	253.2	223.5	1.496	1.166
750	0.23925	-0.5929	0.2452	0.1602	6.828	429.4	757.9	260.7	231.8	1.491	1.178
800	0.23925	-0.5439	0.2528	0.1643	5.832	250.7	423.4	268.1	239.7	1.489	1.190
850	0.23925	-0.4996	0.2581	0.1666	5.018	155.6	256.1	275.3	247.4	1.490	1.203
900	0.23925	-0.4591	0.2612	0.1673	4.346	101.7	165.4	282.3	254.8	1.492	1.215
950	0.23925	-0.4218	0.2622	0.1666	3.787	69.32	112.9	289.2	262.1	1.496	1.228
1000	0.23925	-0.3874	0.2618	0.1649	3.316	49.13	80.83	295.9	269.2	1.500	1.241
1050	0.23925	-0.3557	0.2602	0.1627	2.918	36.00	60.18	302.4	276.2	1.504	1.254
1100	0.23925	-0.3264	0.2578	0.1600	2.579	27.14	46.35	308.8	283.1	1.508	1.267
1150	0.23925	-0.2993	0.2548	0.1571	2.288	20.97	36.78	315.0	289.9	1.512	1.280
1200	0.23925	-0.2741	0.2513	0.1540	2.038	16.56	29.93	321.0	296.6	1.516	1.293
1250	0.23925	-0.2508	0.2476	0.1509	1.821	13.33	24.93	326.8	303.3	1.519	1.307
1300	0.23925	-0.2292	0.2438	0.1480	1.632	10.92	21.16	332.5	309.9	1.521	1.320
1350	0.23925	-0.2091	0.2401	0.1451	1.467	9.086	18.29	338.1	316.5	1.522	1.334
1400	0.23925	-0.1904	0.2364	0.1425	1.323	7.669	16.06	343.5	323.1	1.523	1.347
1450	0.23925	-0.1730	0.2327	0.1400	1.120	6.550	14.30	348.8	326.6	1.524	1.360
1500	0.23925	-0.1567	0.2293	0.1376	1.083	5.652	12.88	353.9	336.1	1.524	1.373

TABLE 2. Thermodynamic Properties of Cesium (Superheated Vapor)

T, °K	α	v, m ³ /kg	i, kJ/kg	s, kJ/kg · °K	c _p ^o , kJ/kg · deg	c _p ^o , kJ/kg · deg	h, m/sec	α	v, m ³ /kg	i, kJ/kg	s, kJ/kg · °K	c _p ^o , kJ/kg · deg	c _p ^o , kJ/kg · deg	h, m/sec		
															p = 0.01 bars	p = 0.015 bars
650	0.97832	40.221	697.56	1.7262	0.20345	0.13070	1.5402	248.9								
700	0.98801	43.527	707.94	1.7402	0.17930	0.11156	1.5977	263.7	0.98217	28.933	796.03	1.7136	0.19014	0.11958	1.5723	261.2
750	0.99287	46.750	715.70	1.7522	0.16840	0.10299	1.6293	276.9	0.98936	31.112	715.09	1.7261	0.17421	0.10740	1.6136	274.4
800	0.99548	49.932	723.98	1.7628	0.16312	0.09889	1.6459	286.7	0.99326	33.251	723.59	1.7371	0.16642	0.10436	1.6384	285.7
850	0.99700	53.093	732.06	1.7727	0.16040	0.09579	1.6546	296.4	0.99591	35.398	731.89	1.7470	0.16236	0.09824	1.6489	296.8
900	0.99791	56.242	740.04	1.7818	0.15882	0.09365	1.6594	305.5	0.99687	37.475	739.83	1.7562	0.16012	0.09655	1.6559	305.1
950	0.99849	59.384	747.96	1.7903	0.15802	0.09200	1.6621	314.2	0.99774	39.574	747.82	1.7649	0.15882	0.09557	1.6599	313.9
1000	0.99887	62.521	755.84	1.7984	0.15749	0.09061	1.6637	322.5	0.99832	41.669	755.74	1.7730	0.15804	0.09500	1.6622	322.3
1050	0.99914	65.656	763.70	1.8061	0.15719	0.08937	1.6646	330.6	0.99871	43.761	763.63	1.7807	0.15754	0.09464	1.6636	330.5
1100	0.99933	68.789	771.56	1.8134	0.15695	0.08822	1.6652	338.4	0.99899	45.851	771.50	1.7880	0.15723	0.09441	1.6645	338.4
1150	0.99946	71.929	779.49	1.8204	0.15682	0.08813	1.6655	346.1	0.99919	47.940	779.36	1.7950	0.15702	0.09427	1.6650	346.0
1200	0.99956	75.051	787.24	1.8271	0.15674	0.08808	1.6657	353.6	0.99934	50.028	787.29	1.8017	0.15689	0.09418	1.6653	353.5
1250	0.99963	78.181	795.08	1.8335	0.15665	0.08800	1.6659	360.9	0.99945	52.116	795.05	1.8081	0.15680	0.09413	1.6654	360.8
1300	0.99969	81.311	802.98	1.8396	0.15667	0.08805	1.6656	368.0	0.99954	54.203	802.89	1.8142	0.15676	0.09411	1.6654	368.0
1350	0.99974	84.440	810.74	1.8455	0.15669	0.08808	1.6653	375.0	0.99961	56.290	810.72	1.8201	0.15676	0.09412	1.6654	375.0
1400	0.99977	87.569	818.58	1.8512	0.15672	0.08812	1.6649	381.8	0.99966	58.375	818.56	1.8258	0.15678	0.09416	1.6648	381.8
1450	0.99980	90.698	826.42	1.8567	0.15674	0.08820	1.6643	388.5	0.99971	60.462	826.40	1.8313	0.15684	0.09423	1.6642	388.5
1500	0.99983	93.827	834.26	1.8620	0.15680	0.08830	1.6635	395.1	0.99974	62.548	834.25	1.8367	0.15693	0.09433	1.6634	395.1
p = 0.02 bars																
700	0.97643	21.637	705.05	1.6944	0.20061	0.12787	1.5510	250.1	0.97080	17.260	704.07	1.6792	0.21071	0.13554	1.5328	257.2
750	0.98589	23.293	714.49	1.7074	0.17989	0.11170	1.5994	273.0	0.98246	18.602	713.90	1.6928	0.18546	0.11590	1.5865	271.6
800	0.99105	24.911	723.20	1.7187	0.16967	0.10379	1.6276	284.8	0.98884	19.906	722.82	1.7043	0.17288	0.10618	1.6193	283.9
850	0.99493	26.507	731.54	1.7288	0.16431	0.09969	1.6435	295.2	0.99255	21.190	731.28	1.7146	0.16624	0.10110	1.6382	294.6
900	0.99884	28.092	739.67	1.7381	0.16135	0.09744	1.6525	304.7	0.99481	22.462	739.49	1.7239	0.16256	0.09832	1.6492	304.3
950	0.99939	29.669	747.69	1.7467	0.15992	0.09615	1.6577	313.6	0.99623	23.727	747.56	1.7327	0.16042	0.09672	1.6556	313.4
1000	0.99976	31.243	755.65	1.7549	0.15898	0.09538	1.6608	322.1	0.99720	24.988	755.55	1.7409	0.15912	0.09576	1.6594	322.0
1050	0.99982	32.814	763.55	1.7626	0.15792	0.09490	1.6627	330.3	0.99785	26.246	763.48	1.7486	0.15830	0.09516	1.6617	330.2
1100	0.99985	34.383	771.54	1.7700	0.15700	0.09460	1.6638	338.2	0.99832	27.502	771.38	1.7560	0.15777	0.09478	1.6632	338.2
1150	0.99982	35.951	779.31	1.7770	0.15722	0.09440	1.6646	345.9	0.99865	28.757	779.26	1.7630	0.15742	0.09433	1.6641	345.9
1200	0.99982	37.517	787.16	1.7836	0.15704	0.09428	1.6650	353.4	0.99890	30.011	787.13	1.7697	0.15719	0.09438	1.6646	353.4
1250	0.99927	39.083	795.01	1.7900	0.15692	0.09429	1.6652	360.8	0.99909	31.264	794.98	1.7761	0.15703	0.09428	1.6643	360.7
1300	0.99936	40.649	802.85	1.7962	0.15683	0.09417	1.6652	367.9	0.99923	32.517	802.83	1.7823	0.15694	0.09423	1.6650	367.9
1350	0.99948	42.215	810.70	1.8021	0.15683	0.09417	1.6650	374.9	0.99935	33.770	810.68	1.7881	0.15690	0.09421	1.6648	374.9
1400	0.99955	43.780	818.54	1.8078	0.15684	0.09419	1.6647	381.8	0.99944	35.022	818.52	1.7939	0.15689	0.09423	1.6645	381.8
1450	0.99961	45.345	826.39	1.8133	0.15688	0.09426	1.6641	388.5	0.99951	36.274	826.37	1.7994	0.15693	0.09428	1.6641	388.5
1500	0.99966	46.909	834.23	1.8186	0.15697	0.09435	1.6634	395.0	0.99957	37.526	834.22	1.8047	0.15701	0.09437	1.6633	395.0
p = 0.03 bars																
700	0.96526	14.343	703.11	1.6666	0.22046	0.14292	1.5171	255.5								
750	0.97996	15.475	713.31	1.6807	0.19992	0.12090	1.5748	270.4	0.97237	11.567	712.15	1.6614	0.20148	0.12791	1.5543	268.2
800	0.98666	16.371	722.44	1.6925	0.17604	0.10853	1.61143	283.0	0.98233	12.491	721.69	1.6737	0.18225	0.11344	1.5970	281.5
850	0.99168	17.045	731.62	1.7029	0.16816	0.10251	1.6332	294.9	0.98816	13.214	730.52	1.6844	0.17194	0.10828	1.6236	293.0
900	0.99378	18.799	739.31	1.7124	0.16377	0.09919	1.6459	303.9	0.99173	14.017	738.95	1.6940	0.16617	0.10093	1.6397	303.2
950	0.99550	19.765	747.43	1.7212	0.16121	0.09728	1.6535	313.1	0.99491	14.813	747.17	1.7029	0.16279	0.09841	1.6493	312.6
1000	0.99664	20.817	755.45	1.7291	0.15966	0.09614	1.6580	321.8	0.99653	15.604	755.26	1.7112	0.16073	0.09689	1.6552	321.4
1050	0.99742	21.867	763.40	1.7372	0.15868	0.09542	1.6608	330.1	0.99667	16.393	763.25	1.7190	0.15943	0.09594	1.6589	329.8
1100	0.99798	22.914	771.33	1.7445	0.15804	0.09497	1.6625	338.1	0.99731	17.180	771.21	1.7264	0.15888	0.09533	1.6612	337.9
1150	0.99838	23.961	779.21	1.7515	0.15762	0.09467	1.6636	345.8	0.99784	17.965	779.12	1.7335	0.15802	0.09494	1.6626	345.7
1200	0.99868	25.006	787.09	1.7582	0.15734	0.09447	1.6643	353.3	0.99824	18.750	787.01	1.7402	0.15764	0.09467	1.6636	353.2
1250	0.99891	26.051	794.95	1.7646	0.15715	0.09435	1.6646	360.7	0.99854	19.535	794.88	1.7466	0.15738	0.09450	1.6641	360.5
1300	0.99908	27.095	802.81	1.7708	0.15703	0.09428	1.6648	367.9	0.99877	20.318	802.75	1.7528	0.15721	0.09440	1.6644	367.8
1350	0.99922	28.139	810.65	1.7767	0.15697	0.09426	1.6647	374.9	0.99895	21.102	810.61	1.7587	0.15711	0.09435	1.6644	374.8
1400	0.99933	29.183	818.50	1.7824	0.15695	0.09427	1.6644	381.7	0.99910	21.885	818.46	1.7644	0.15707	0.09434	1.6642	381.7
1450	0.99941	30.227	826.35	1.7880	0.15688	0.09431	1.6649	388.4	0.99922	22.668	826.32	1.7699	0.15707	0.09437	1.6637	388.4
1500	0.99948	31.270	834.20	1.7933	0.15701	0.09440	1.6632	395.0	0.99931	23.450	834.17	1.7753	0.15712	0.09444	1.6631	395.0
p = 0.04 bars																

1010

Table 2. (Continued)

T, °K	α	v , m ³ /kg	i , kJ/kg	s , kJ/kg·°K	c_p , kJ/kg·deg	c_v , kJ/kg·deg	k	a , m/sec	α	v , m ³ /kg	i , kJ/kg	s , kJ/kg·°K	c_p , kJ/kg·deg	c_v , kJ/kg·deg	k	a , m/sec
p=0.05 bars																
750	0.96581	9.2231	711.01	1.6461	0.21162	0.13546	1.5369	266.2	0.95939	7.6608	709.89	1.6334	0.22135	0.14266	1.5219	264.5
800	0.97805	9.8992	720.94	1.6589	0.18829	0.11766	1.5841	280.0	0.97383	8.2317	720.21	1.6484	0.19418	0.12194	1.5723	278.7
850	0.98526	10.556	730.01	1.6699	0.17666	0.10800	1.6147	291.9	0.98239	8.7841	729.52	1.6579	0.17931	0.11067	1.6064	291.0
900	0.98969	11.202	738.60	1.6798	0.16854	0.10264	1.6337	302.5	0.98767	9.3256	738.25	1.6680	0.17088	0.10433	1.6280	301.8
950	0.99253	11.841	746.51	1.6888	0.16435	0.09952	1.6453	312.1	0.99106	9.8605	746.66	1.6771	0.16590	0.10062	1.6415	311.6
1000	0.99442	12.476	755.06	1.6971	0.16180	0.09764	1.6525	321.1	0.99332	10.391	754.86	1.6856	0.16285	0.09838	1.6499	320.7
1050	0.99572	13.109	763.11	1.7050	0.16018	0.09646	1.6570	329.6	0.99487	10.919	762.96	1.6934	0.16082	0.09697	1.6532	329.3
1100	0.99664	13.738	771.09	1.7124	0.15912	0.09570	1.6595	337.7	0.99597	11.446	770.97	1.7009	0.15966	0.09607	1.6586	337.5
1150	0.99731	14.365	779.02	1.7194	0.15841	0.09520	1.6618	345.5	0.99677	11.971	778.93	1.7080	0.15881	0.09547	1.6608	345.4
1200	0.99780	14.997	786.93	1.7262	0.15794	0.09487	1.6629	353.1	0.99736	12.495	786.86	1.7147	0.15823	0.09507	1.6622	353.0
1250	0.99818	15.625	794.82	1.7326	0.15761	0.09465	1.6636	360.5	0.99781	13.018	794.76	1.7212	0.15784	0.09480	1.6631	360.4
1300	0.99847	16.252	802.69	1.7388	0.15739	0.09451	1.6640	367.7	0.99816	13.541	802.64	1.7274	0.15757	0.09463	1.6636	367.6
1350	0.99870	16.879	810.56	1.7447	0.15725	0.09444	1.6641	374.8	0.99843	14.064	810.51	1.7333	0.15739	0.09453	1.6638	374.7
1400	0.99888	17.506	818.42	1.7504	0.15718	0.09441	1.6639	381.6	0.99865	14.587	818.36	1.7390	0.15729	0.09448	1.6637	381.6
1450	0.99902	18.132	826.28	1.7560	0.15716	0.09443	1.6636	388.4	0.99883	15.109	826.24	1.7445	0.15725	0.09448	1.6634	388.3
1500	0.99914	18.759	834.14	1.7613	0.15720	0.09449	1.6629	394.9	0.99897	15.631	834.11	1.7499	0.15727	0.09454	1.6628	394.9
p=0.06 bars																
750	0.94691	5.7090	707.73	1.6130	0.23965	0.15611	1.4975	261.5	0.95749	4.8981	717.37	1.6118	0.21624	0.13805	1.5351	274.2
800	0.96556	6.1479	718.77	1.6272	0.20549	0.13023	1.5521	276.3	0.97116	5.2406	727.55	1.6241	0.19329	0.12381	1.5779	287.5
850	0.97672	6.5693	728.52	1.6391	0.18642	0.11584	1.5912	289.2	0.97970	5.5729	736.85	1.6348	0.17996	0.11084	1.6075	299.3
900	0.98366	6.9801	737.54	1.6494	0.17547	0.10763	1.6173	300.5	0.98523	5.8990	745.64	1.6443	0.17196	0.10482	1.6272	309.8
950	0.98813	7.3845	746.14	1.6587	0.16896	0.10279	1.6341	310.7	0.98894	6.2210	754.10	1.6530	0.16702	0.10129	1.6399	319.4
1000	0.99112	7.7848	754.48	1.6672	0.16495	0.09985	1.6448	320.0	0.99149	6.5405	762.37	1.6610	0.16386	0.09900	1.6482	328.3
1050	0.99318	8.1825	762.66	1.6752	0.16239	0.09799	1.6516	328.8	0.99331	6.8582	770.51	1.6686	0.16178	0.09751	1.6536	336.7
1100	0.99464	8.5785	770.74	1.6827	0.16072	0.09679	1.6561	337.1	0.99464	7.1747	778.56	1.6758	0.16038	0.09652	1.6572	344.8
1150	0.99570	8.9732	778.74	1.6898	0.15960	0.09600	1.6590	345.1	0.99562	7.4903	786.55	1.6826	0.15942	0.09585	1.6596	352.6
1200	0.99649	9.3670	786.70	1.6966	0.15883	0.09546	1.6609	352.8	0.99636	7.8054	794.50	1.6891	0.15875	0.09539	1.6611	360.1
1250	0.99709	9.7602	794.63	1.7031	0.15829	0.09510	1.6621	360.2	0.99694	8.1199	802.43	1.6953	0.15828	0.09508	1.6621	367.4
1300	0.99755	10.153	802.54	1.7093	0.15793	0.09486	1.6629	367.5	0.99739	8.4341	810.33	1.7012	0.15796	0.09488	1.6626	374.5
1350	0.99791	10.545	810.42	1.7152	0.15768	0.09470	1.6632	374.6	0.99775	8.7481	818.22	1.7070	0.15775	0.09476	1.6628	381.4
1400	0.99820	10.937	818.30	1.7210	0.15752	0.09462	1.6632	381.5	0.99805	9.0618	826.11	1.7125	0.15762	0.09471	1.6626	388.1
1450	0.99844	11.329	826.18	1.7265	0.15744	0.09460	1.6630	388.2	0.99828	9.3754	833.99	1.7178	0.15757	0.09472	1.6621	394.7
1500	0.99863	11.721	834.05	1.7318	0.15742	0.09463	1.6624	394.8								
p=0.08 bars																
750	0.94691	5.7090	707.73	1.6130	0.23965	0.15611	1.4975	261.5	0.95749	4.8981	717.37	1.6118	0.21624	0.13805	1.5351	274.2
800	0.96556	6.1479	718.77	1.6272	0.20549	0.13023	1.5521	276.3	0.97116	5.2406	727.55	1.6241	0.19329	0.12381	1.5779	287.5
850	0.97672	6.5693	728.52	1.6391	0.18642	0.11584	1.5912	289.2	0.97970	5.5729	736.85	1.6348	0.17996	0.11084	1.6075	299.3
900	0.98366	6.9801	737.54	1.6494	0.17547	0.10763	1.6173	300.5	0.98523	5.8990	745.64	1.6443	0.17196	0.10482	1.6272	309.8
950	0.98813	7.3845	746.14	1.6587	0.16896	0.10279	1.6341	310.7	0.98894	6.2210	754.10	1.6530	0.16702	0.10129	1.6399	319.4
1000	0.99112	7.7848	754.48	1.6672	0.16495	0.09985	1.6448	320.0	0.99149	6.5405	762.37	1.6610	0.16386	0.09900	1.6482	328.3
1050	0.99318	8.1825	762.66	1.6752	0.16239	0.09799	1.6516	328.8	0.99331	6.8582	770.51	1.6686	0.16178	0.09751	1.6536	336.7
1100	0.99464	8.5785	770.74	1.6827	0.16072	0.09679	1.6561	337.1	0.99464	7.1747	778.56	1.6758	0.16038	0.09652	1.6572	344.8
1150	0.99570	8.9732	778.74	1.6898	0.15960	0.09600	1.6590	345.1	0.99562	7.4903	786.55	1.6826	0.15942	0.09585	1.6596	352.6
1200	0.99649	9.3670	786.70	1.6966	0.15883	0.09546	1.6609	352.8	0.99636	7.8054	794.50	1.6891	0.15875	0.09539	1.6611	360.1
1250	0.99709	9.7602	794.63	1.7031	0.15829	0.09510	1.6621	360.2	0.99694	8.1199	802.43	1.6953	0.15828	0.09508	1.6621	367.4
1300	0.99755	10.153	802.54	1.7093	0.15793	0.09486	1.6629	367.5	0.99739	8.4341	810.33	1.7012	0.15796	0.09488	1.6626	374.5
1350	0.99791	10.545	810.42	1.7152	0.15768	0.09470	1.6632	374.6	0.99775	8.7481	818.22	1.7070	0.15775	0.09476	1.6628	381.4
1400	0.99820	10.937	818.30	1.7210	0.15752	0.09462	1.6632	381.5	0.99805	9.0618	826.11	1.7125	0.15762	0.09471	1.6626	388.1
1450	0.99844	11.329	826.18	1.7265	0.15744	0.09460	1.6630	388.2	0.99828	9.3754	833.99	1.7178	0.15757	0.09472	1.6621	394.7
1500	0.99863	11.721	834.05	1.7318	0.15742	0.09463	1.6624	394.8								
p=0.10 bars																
750	0.94691	5.7090	707.73	1.6130	0.23965	0.15611	1.4975	261.5	0.95749	4.8981	717.37	1.6118	0.21624	0.13805	1.5351	274.2
800	0.96556	6.1479	718.77	1.6272	0.20549	0.13023	1.5521	276.3	0.97116	5.2406	727.55	1.6241	0.19329	0.12381	1.5779	287.5
850	0.97672	6.5693	728.52	1.6391	0.18642	0.11584	1.5912	289.2	0.97970	5.5729	736.85	1.6348	0.17996	0.11084	1.6075	299.3
900	0.98366	6.9801	737.54	1.6494	0.17547	0.10763	1.6173	300.5	0.98523	5.8990	745.64	1.6443	0.17196	0.10482	1.6272	309.8
950	0.98813	7.3845	746.14	1.6587	0.16896	0.10279	1.6341	310.7	0.98894	6.2210	754.10	1.6530	0.16702	0.10129	1.6399	319.4
1000	0.99112	7.7848	754.48	1.6672	0.16495	0.09985	1.6448	320.0	0.99149	6.5405	762.37	1.6610	0.16386	0.09900	1.6482	328.3
1050	0.99318	8.1825	762.66	1.6752	0.16239	0.09799	1.6516	328.8	0.99331	6.8582	770.51	1.6686	0.16178	0.09751	1.6536	336.7
1100	0.99464	8.5785	770.74	1.6827	0.16072	0.09679	1.6561	337.1	0.99464	7.1747	778.56	1.6758	0.16038	0.09652	1.6572	344.8

TABLE 2. (Continued)

$T, ^\circ K$	α	$v, m^3/kg$	$i, kJ/kg$	$s, kJ/kg \cdot ^\circ K$	$c_p, kJ/kg \cdot deg$	$c_v, kJ/kg \cdot deg$	k	$a, m/sec$	α	$v, m^3/kg$	$i, kJ/kg$	$s, kJ/kg \cdot ^\circ K$	$c_p, kJ/kg \cdot deg$	$c_v, kJ/kg \cdot deg$	k	$a, m/sec$
$\rho = 0.20$ bars																
850	0.94467	2.5851	722.94	1.5762	0.22429	0.14296	1.5289	281.1	0.93222	2.0548	720.76	1.5601	0.23794	0.15257	1.5118	278.7
900	0.94058	2.7396	733.51	1.5883	0.20081	0.12565	1.5684	294.2	0.95143	2.1973	731.92	1.5729	0.21033	0.13234	1.5534	292.1
950	0.97110	2.9285	743.16	1.5988	0.18620	0.11494	1.5976	305.9	0.96426	2.2347	741.96	1.5838	0.19287	0.11959	1.5854	304.2
1000	0.97823	3.0038	752.22	1.6051	0.17695	0.10820	1.6181	316.4	0.97301	2.4685	751.31	1.5934	0.18168	0.11147	1.6087	315.1
1050	0.98320	3.2566	760.31	1.6166	0.17094	0.10386	1.6323	326.1	0.97914	2.4600	760.20	1.6020	0.17435	0.10619	1.6252	325.0
1100	0.98676	3.4178	769.35	1.6244	0.16694	0.10101	1.6420	335.0	0.98353	2.7298	768.78	1.6110	0.16944	0.10270	1.6366	334.2
1150	0.98936	3.5779	777.62	1.6318	0.16421	0.09908	1.6486	343.5	0.98675	2.8585	777.16	1.6175	0.16608	0.10033	1.6446	342.8
1200	0.99129	3.7370	785.79	1.6387	0.16232	0.09776	1.6531	351.5	0.98915	2.9864	785.41	1.6245	0.16374	0.09870	1.6501	351.0
1250	0.99277	3.8956	793.87	1.6453	0.16099	0.09685	1.6563	359.2	0.99098	3.1137	793.52	1.6311	0.16209	0.09757	1.6539	358.8
1300	0.99391	4.0538	801.89	1.6516	0.16003	0.09621	1.6584	366.7	0.99241	3.2406	801.62	1.6375	0.16090	0.09676	1.6566	366.3
1350	0.99481	4.2116	809.87	1.6576	0.15933	0.09576	1.6607	373.9	0.99352	3.3671	809.65	1.6435	0.16004	0.09629	1.6583	373.6
1400	0.99553	4.3691	817.82	1.6634	0.15887	0.09546	1.6605	380.9	0.99442	3.4934	817.63	1.6493	0.15942	0.09581	1.6593	380.7
1450	0.99610	4.5265	825.76	1.6690	0.15854	0.09527	1.6608	387.7	0.99514	3.6195	825.60	1.6549	0.15899	0.09555	1.6599	387.5
1500	0.99658	4.6837	833.68	1.6743	0.15833	0.09518	1.6606	394.4	0.99573	3.7454	833.53	1.6603	0.15870	0.09540	1.6599	394.2
$\rho = 0.30$ bars																
850	0.92024	1.7017	718.68	1.5467	0.25052	0.16135	1.4977	276.5	0.92548	1.3551	727.38	1.5394	0.23580	0.15001	1.5195	287.0
900	0.94254	1.8228	730.36	1.5691	0.21932	0.13861	1.5405	290.2	0.94457	1.4445	738.52	1.5514	0.21124	0.13228	1.5561	299.9
950	0.95736	1.9389	740.79	1.5714	0.19925	0.12402	1.5746	302.6	0.95783	1.5309	748.65	1.5618	0.19407	0.12059	1.5848	311.5
1000	0.96787	2.0517	750.41	1.5812	0.18625	0.11462	1.6001	313.8	0.96723	1.6152	758.11	1.5710	0.18407	0.11280	1.6063	322.2
1050	0.97312	2.1622	759.49	1.5901	0.17767	0.10846	1.6185	324.0	0.97403	1.6980	767.11	1.5794	0.17666	0.10755	1.6221	331.9
1100	0.98033	2.2712	768.22	1.5982	0.17189	0.10435	1.6315	333.4	0.97904	1.7797	775.81	1.5871	0.17152	0.10394	1.6334	341.0
1150	0.98416	2.3790	776.71	1.6058	0.16792	0.10156	1.6407	342.2	0.98281	1.8606	784.29	1.5944	0.16791	0.10143	1.6415	349.5
1200	0.98703	2.4860	785.04	1.6128	0.16515	0.09962	1.6472	350.5	0.98569	1.9409	792.62	1.6012	0.16532	0.09966	1.6473	357.6
1250	0.98991	2.5923	793.24	1.6196	0.16318	0.09827	1.6516	358.4	0.98793	2.0208	800.84	1.6078	0.16344	0.09839	1.6513	365.3
1300	0.99091	2.6985	801.36	1.6259	0.16175	0.09731	1.6548	366.0	0.98970	2.1004	808.97	1.6137	0.16207	0.09748	1.6541	372.8
1350	0.99224	2.8041	809.42	1.6320	0.16072	0.09663	1.6569	373.3	0.99111	2.1797	817.05	1.6196	0.16107	0.09683	1.6560	380.0
1400	0.99331	2.9095	817.43	1.6378	0.15997	0.09615	1.6582	380.4	0.99225	2.2589	825.08	1.6253	0.16033	0.09638	1.6572	387.0
1450	0.99417	3.0147	825.42	1.6434	0.15944	0.09583	1.6589	387.3	0.99319	2.3379	833.08	1.6307	0.15981	0.09608	1.6577	393.7
1500	0.99488	3.1198	833.38	1.6488	0.15907	0.09563	1.6592	394.1								
$\rho = 0.50$ bars																
800	0.96932	1.6750	724.56	1.5228	0.25053	0.16007	1.5091	284.2	0.92010	0.95001	734.24	1.5224	0.23241	0.14469	1.5282	295.3
900	0.99210	1.1482	736.34	1.5556	0.22220	0.13981	1.5409	297.4	0.93865	1.0106	745.28	1.5337	0.21684	0.13035	1.5603	307.5
1000	0.94809	1.2187	746.94	1.5445	0.20316	0.12616	1.5717	309.5	0.95201	1.0685	755.44	1.5436	0.19598	0.12081	1.5859	318.9
1050	0.95953	1.2871	756.75	1.5569	0.19017	0.11692	1.5955	320.4	0.96178	1.1250	764.96	1.5525	0.18565	0.11354	1.6055	329.2
1100	0.96785	1.3541	766.03	1.5647	0.18124	0.11061	1.6134	330.5	0.96905	1.1804	774.05	1.5606	0.17839	0.10847	1.6202	338.8
1150	0.97401	1.4201	774.92	1.5726	0.17501	0.10625	1.6266	339.8	0.97454	1.2332	782.84	1.5686	0.17321	0.10489	1.6311	347.7
1200	0.97865	1.4853	783.56	1.5799	0.17059	0.10319	1.6361	348.6	0.97876	1.2894	791.40	1.5750	0.16947	0.10234	1.6390	356.1
1250	0.98221	1.5500	792.09	1.5868	0.16742	0.10102	1.6430	356.8	0.98208	1.3432	799.80	1.5816	0.16674	0.10049	1.6448	364.1
1300	0.98498	1.6143	800.32	1.5933	0.16511	0.09945	1.6480	364.7	0.98467	1.3967	808.08	1.5870	0.16471	0.09914	1.6489	371.7
1350	0.98717	1.6782	808.52	1.5995	0.16340	0.09832	1.6515	372.3	0.98676	1.4500	816.27	1.5938	0.16321	0.09816	1.6518	379.1
1400	0.98893	1.7419	816.66	1.6055	0.16214	0.09750	1.6539	379.5	0.98845	1.5031	824.41	1.5996	0.16209	0.09746	1.6538	386.2
1450	0.98955	1.8054	824.75	1.6111	0.16122	0.09692	1.6555	386.6	0.98984	1.5560	832.49	1.6050	0.16126	0.09696	1.6549	393.1
1500	0.99151	1.8687	832.79	1.6166	0.16054	0.09652	1.6563	393.4								
$\rho = 0.60$ bars																
800	0.96932	1.6750	724.56	1.5228	0.25053	0.16007	1.5091	284.2	0.92010	0.95001	734.24	1.5224	0.23241	0.14469	1.5282	295.3
900	0.99210	1.1482	736.34	1.5556	0.22220	0.13981	1.5409	297.4	0.93865	1.0106	745.28	1.5337	0.21684	0.13035	1.5603	307.5
1000	0.94809	1.2187	746.94	1.5445	0.20316	0.12616	1.5717	309.5	0.95201	1.0685	755.44	1.5436	0.19598	0.12081	1.5859	318.9
1050	0.95953	1.2871	756.75	1.5569	0.19017	0.11692	1.5955	320.4	0.96178	1.1250	764.96	1.5525	0.18565	0.11354	1.6055	329.2
1100	0.96785	1.3541	766.03	1.5647	0.18124	0.11061	1.6134	330.5	0.96905	1.1804	774.05	1.5606	0.17839	0.10847	1.6202	338.8
1150	0.97401	1.4201	774.92	1.5726	0.17501	0.10625	1.6266	339.8	0.97454	1.2332	782.84	1.5686	0.17321	0.10489	1.6311	347.7
1200	0.97865	1.4853	783.56	1.5799	0.17059	0.10319	1.6361	348.6	0.97876	1.2894	791.40	1.5750	0.16947	0.10234	1.6390	356.1
1250	0.98221	1.5500	792.09	1.5868	0.16742	0.10102	1.6430	356.8	0.98208	1.3432	799.80	1.5816	0.16674	0.10049	1.6448	364.1
1300	0.98498	1.6143	800.32	1.5933	0.16511	0.09945	1.6480	364.7	0.98467	1.3967	808.08	1.5870	0.16471	0.09914	1.6489	371.7
1350	0.98717	1.6782	808.52	1.5995	0.16340	0.09832	1.6515	372.3	0.98676	1.4500	816.27	1.5938	0.16321	0.09816	1.6518	379.1
1400	0.98893	1.7419	816.66	1.6055	0.16214	0.09750	1.6539	379.5	0.98845	1.5031	824.41	1.5996	0.16209	0.09746	1.6538	386.2
1450	0.98955	1.8054	824.75	1.6111	0.16122	0.09692	1.6555	386.6	0.98984	1.5560	832.49	1.6050	0.16126	0.09696	1.6549	393.1
1500	0.99151	1.8687	832.79	1.6166	0.16054	0.09652	1.6563	393.4								

TABLE 2. (Continued)

T, °K	α	$v, m^3/kg$	$i, kJ/kg$	$s, kJ/kg \cdot ^\circ K$	$c_p, kJ/kg \cdot deg$	$c_{v1}, kJ/kg \cdot deg$	κ	$a_1, m/sec$	α	$v, m^3/kg$	$i, kJ/kg$	$s, kJ/kg \cdot ^\circ K$	$c_p, kJ/kg \cdot deg$	$c_{v1}, kJ/kg \cdot deg$	κ	$a_1, m/sec$
p = 4.0 bars								p = 4.5 bars								
1150	0.83547	0.16505	750.54	1.4263	0.25011	0.15418	1.5179	316.6								
1200	0.85976	0.17451	762.61	1.4366	0.23314	0.14282	1.5396	327.8	0.84608	0.15398	760.19	1.4278	0.23865	0.14622	1.5324	325.9
1250	0.87963	0.18372	773.91	1.4458	0.21938	0.13367	1.5587	338.4	0.86745	0.16225	771.76	1.4372	0.22433	0.13671	1.5517	336.6
1300	0.89594	0.19273	784.58	1.4542	0.20829	0.12636	1.5750	348.4	0.88509	0.17033	782.67	1.4458	0.21267	0.12903	1.5685	346.7
1350	0.90937	0.20156	794.76	1.4619	0.19941	0.12055	1.5887	357.9	0.89969	0.17826	793.06	1.4536	0.20324	0.12287	1.5827	356.3
1400	0.92051	0.21025	804.55	1.4690	0.19223	0.11594	0.6000	366.8	0.91185	0.18604	803.02	1.4609	0.19563	0.11794	1.5946	365.4
1450	0.92979	0.21881	814.02	1.4757	0.18659	0.11258	1.6093	375.3	0.92201	0.19371	812.64	1.4676	0.18948	0.11401	1.6043	374.0
1500	0.93758	0.22726	823.23	1.4819	0.18201	0.10939	1.6166	383.3	0.93057	0.20128	821.98	1.4740	0.18453	0.11088	1.6121	382.1
p = 5.0 bars								p = 6.0 bars								
1200	0.83303	0.13760	757.90	1.4198	0.24361	0.14928	1.5258	324.0								
1250	0.85576	0.14511	769.69	1.4294	0.22885	0.13948	1.5453	334.8	0.83373	0.11949	765.80	1.4158	0.23677	0.14432	1.5342	331.7
1300	0.87463	0.15245	780.82	1.4382	0.21672	0.13150	1.5624	345.1	0.85477	0.12570	777.32	1.4248	0.22393	0.13588	1.5517	342.1
1350	0.89032	0.15964	791.40	1.4461	0.20682	0.12504	1.5770	354.8	0.87241	0.13177	788.23	1.4331	0.21329	0.12894	1.5669	352.0
1400	0.90343	0.16670	801.53	1.4535	0.19877	0.11983	1.5894	364.0	0.88726	0.13774	798.67	1.4407	0.20453	0.12328	1.5800	361.3
1450	0.91443	0.17365	811.30	1.4604	0.19223	0.11565	1.5996	372.7	0.89981	0.14360	808.70	1.4477	0.19732	0.11868	1.5909	370.2
1500	0.92371	0.18051	820.77	1.4668	0.18693	0.11230	1.6079	381.0	0.91045	0.14939	818.42	1.4543	0.19141	0.11435	1.6000	378.7
p = 7.0 bars								p = 8.0 bars								
1250	0.81332	0.10128	762.21	1.4041	0.24341	0.14839	1.5247	328.8								
1300	0.83620	0.10666	774.04	1.4134	0.23014	0.13964	1.5424	339.4	0.81880	0.09244	770.96	1.4034	0.23549	0.14290	1.5342	336.3
1350	0.85553	0.11193	785.25	1.4219	0.21897	0.13237	1.5580	349.4	0.83962	0.09710	782.43	1.4121	0.22397	0.13538	1.5501	347.0
1400	0.87194	0.11710	795.95	1.4297	0.20966	0.12635	1.5716	358.9	0.85738	0.10167	793.38	1.4200	0.21424	0.12909	1.5640	356.7
1450	0.88587	0.12219	806.24	1.4369	0.20192	0.12141	1.5831	368.0	0.87255	0.10616	803.88	1.4274	0.20607	0.12387	1.5760	365.8
1500	0.89774	0.12719	816.17	1.4436	0.19551	0.11736	1.5927	376.6	0.88555	0.11058	814.00	1.4343	0.19926	0.11957	1.5861	374.6
p = 9.0 bars								p = 10.0 bars								
1300	0.80244	0.08143	768.07	1.3945	0.24012	0.14572	1.5268	334.5								
1350	0.82456	0.08560	779.77	1.4033	0.22837	0.13803	1.5429	344.8	0.81027	0.07644	777.24	1.3955	0.23226	0.14039	1.5364	342.7
1400	0.84353	0.08970	790.93	1.4115	0.21834	0.13155	1.5571	354.5	0.83033	0.08015	788.59	1.4037	0.22202	0.13375	1.5507	352.5
1450	0.85982	0.09372	801.62	1.4190	0.20984	0.12611	1.5694	363.8	0.84763	0.08380	799.47	1.4114	0.21327	0.12814	0.5633	361.0
1500	0.87384	0.09768	811.93	1.4260	0.20269	0.12159	1.5799	372.7	0.86259	0.08739	809.93	1.4185	0.20583	0.12344	1.5741	370.9
p = 12.0 bars								p = 14.0 bars								
1350	0.78380	0.06277	772.56	1.3818	0.23876	0.14435	1.5248	338.9								
1400	0.80563	0.06589	784.23	1.3903	0.22830	0.13753	1.5394	348.9	0.78311	0.05577	780.235	1.3787	0.23338	0.14063	1.5296	345.6
1450	0.82479	0.06897	795.41	1.3981	0.21921	0.13169	1.5524	358.4	0.80360	0.05843	791.66	1.3868	0.22414	0.13466	1.5428	355.2
1500	0.84132	0.07199	806.16	1.4054	0.21138	0.12672	1.5637	367.5	0.82156	0.06104	802.66	1.3942	0.21608	0.12952	1.5544	364.5
p = 16.0 bars								p = 18.0 bars								
1450	0.78400	0.05057	788.20	1.3769	0.22826	0.13717	1.5342	352.3	0.76578	0.04449	784.97	1.3681	0.23170	0.13929	1.5265	349.6
1500	0.80312	0.05287	799.39	1.3845	0.22008	0.13192	1.5460	361.6	0.78588	0.04655	796.34	1.3758	0.22349	0.13399	1.5384	359.0
p = 20.0 bars								p = 22.0 bars								
1500	0.76970	0.04151	793.47	1.3684	0.22640	0.13579	1.5315	356.6	0.75447	0.03742	790.77	1.3610	0.22889	0.13736	1.5251	354.3

TABLE 3. Thermodynamic Velocity of Sound and Adiabatic Exponent k for Wet Cesium Vapor

T°, K	x=0.95		x=0.90		x=0.85		x=0.80		x=0.75		x=0.7		x=0.65		x=0.6	
	a,	k	a,	k	a,	k	a,	k	a,	k	a,	k	a,	k	a,	k
	m/sec		m/sec		m/sec		m/sec		m/sec		m/sec		m/sec		m/sec	
550	191.4	1.128	186.2	1.126	180.9	1.125	175.4	1.124	169.7	1.122	163.8	1.121	157.7	1.118	151.4	1.116
600	200.6	1.140	195.2	1.138	189.5	1.137	183.7	1.135	177.7	1.133	171.5	1.131	165.1	1.128	158.4	1.126
650	209.4	1.152	203.6	1.150	197.7	1.148	191.6	1.146	185.4	1.144	178.9	1.141	172.1	1.138	165.1	1.134
700	217.7	1.164	211.7	1.162	205.6	1.160	199.2	1.157	192.6	1.154	185.8	1.151	178.8	1.147	171.5	1.143
750	225.7	1.176	219.5	1.173	213.0	1.171	206.4	1.168	199.6	1.164	192.5	1.160	185.1	1.156	177.5	1.151
800	233.4	1.188	226.9	1.185	220.2	1.182	213.3	1.178	206.2	1.174	198.8	1.170	191.2	1.165	183.2	1.159
850	240.8	1.200	234.1	1.196	227.1	1.193	220.0	1.189	212.6	1.184	204.9	1.179	196.9	1.173	188.7	1.166
900	248.0	1.212	241.0	1.208	233.8	1.204	226.4	1.200	218.7	1.193	210.7	1.187	202.5	1.180	193.9	1.172
950	255.0	1.224	247.8	1.219	240.3	1.214	232.6	1.209	224.6	1.203	216.3	1.194	207.8	1.188	198.9	1.178
1000	261.9	1.236	254.3	1.231	246.6	1.225	238.6	1.219	230.4	1.212	221.8	1.204	212.9	1.194	203.8	1.184
1050	268.6	1.248	260.8	1.242	252.8	1.236	244.5	1.229	236.0	1.220	227.1	1.211	217.9	1.201	208.3	1.189
1100	275.2	1.260	267.2	1.254	258.8	1.246	250.3	1.238	241.4	1.229	232.2	1.218	222.7	1.206	212.8	1.193
1150	281.7	1.273	273.4	1.265	264.8	1.257	255.9	1.247	246.8	1.237	237.2	1.225	227.4	1.212	217.1	1.196
1200	288.2	1.285	279.6	1.277	270.6	1.267	261.5	1.256	252.0	1.244	242.1	1.231	231.9	1.219	221.2	1.199
1250	294.3	1.295	285.6	1.287	276.4	1.277	266.9	1.265	257.1	1.252	246.9	1.237	236.4	1.220	—	—
1300	300.9	1.310	291.7	1.299	282.1	1.287	272.3	1.273	262.1	1.259	251.5	1.242	240.6	1.224	—	—
1350	307.2	1.322	297.6	1.310	287.7	1.296	277.5	1.281	266.9	1.265	256.0	1.246	244.7	1.226	—	—
1400	313.4	1.334	303.4	1.320	293.2	1.305	282.6	1.288	271.7	1.270	260.4	1.250	248.6	1.227	—	—
1450	319.6	1.346	309.2	1.330	298.6	1.314	287.2	1.295	276.4	1.275	264.6	1.253	252.5	1.228	—	—
1500	325.7	1.357	315.0	1.340	304.0	1.322	292.6	1.301	280.9	1.279	268.7	1.254	256.1	1.227	—	—

The values for the saturation pressures of cesium vapor, found from the equations of [7], are based principally on the data of [8], and lie above the values found in [9, 10].

We assume that the values for the saturation temperatures found in [8] may have been too low, and so the values of the saturation pressure are too high, in view of the fact that the authors of this paper measured the temperature of the thermostat while the cesium vapor was in a vessel along the axis of which ran a tungsten filament heated to 1500°K. The value of the heat of sublimation taken from [2, 3] is $\Delta I_{01}^0 = 79699 \pm 1255$ J/g-atom.

The heat of dissociation D_0^0 is a very important parameter, the accuracy of measurement of which to a large extent determines the accuracy when calculating the thermodynamic properties of the dissociating gas. The value of D_0^0 for Cs_2 in the normal state is found in [11] ($D_0^0 = 0.45$ eV), and [12] ($D_0^0 = 0.45 \pm 0.04$ eV) from an analysis of spectroscopic data [13, 14] by graphical extrapolation, using the Berdzh-Shponer method. The same value of D_0^0 is used in [15]. Recently, in [16], from similarity of the molecular constants, based, for the alkali metals, on the value $D_0^0(Na_2) = 0.76$ eV, a value was obtained of $D_0^0(Cs_2) = 0.453$ eV. In spite of the good agreement between the above values of $D_0^0(Cs_2)$, it should be kept in mind that the initial spectroscopic data are not good enough to make a reliable extrapolation. Noting this as well as the general nature of the accuracy of determining the heats of dissociation of alkali metals, the value used is $D_0^0(Cs_2) = 0.45 \pm 0.04$ eV = 43,431 \pm 6695 J/mole, from which it follows that $\Delta I_{02}^0 = 2\Delta I_{01}^0 - D_0^0 = 115,967 \pm 6695$ J/mole.

The thermodynamic functions of mon- and diatomic gases in the standard state needed for the calculations were taken from [15], where they were found for atoms up to 2500°K (including the contribution from electron levels), and for molecules up to 1500°K (including anharmonic vibrations, rotation-vibration interaction, etc.).

In accordance with the method used, the above initial data are satisfactory for the calculations. Further, an attempt has been made to find the values of the specific volumes v' and the surface tension σ for the liquid up to 800-900°K.

The density of liquid cesium has been studied experimentally up to 396°K [17, 18]. The extrapolation of these values to the boiling point was based on the following assumptions. It is known, first, that the densities of the liquid alkali metals sodium [19], potassium [20], and rubidium [21] are satisfactorily described by equations of the type $\rho = \rho_{mp}[1 - a(T - T_{mp})]$ up to 1100°K (ρ_{mp} is the density at the melting point T_{mp}). Second, these metals and cesium have similar structures in the crystal and liquid states. Finally, the coefficient a in the above equation obeys some sort of a law, as may be seen from the following data:

Element	Na	K	Rb	Cs	
$a \cdot 10^4, \text{ deg}^{-1}$	2.58	2.7	3.55	3.95 [17]	3.4 [16]

It has been assumed, on the basis of an analysis of the data, that up to the boiling point the density of liquid cesium (Table 1) may be calculated from the equation

$$\rho' = (1840 \pm 30) [1 - (3.9 \pm 0.6) \times 10^{-4} (T - T_{\text{mp}})] \text{ kg/m}^3.$$

The surface tension σ of cesium has only been measured in the temperature range from 335 to 550°K [22]. It was shown in [23] that the values of σ , known up to 723°K for sodium, are satisfactorily described by the Bachinskii formula (parachor equation)

$$\sigma = c(\rho' - \rho'')^4.$$

Using the theoretical value $\sigma_{\text{mp}} \approx 6 \cdot 10^{-2} \text{ J/m}^2$ [24] at the melting point, and the values of ρ' calculated above, the parachor equation has been used to find the approximate values of the surface tension of cesium up to the boiling point (see Table 1). The error in these data at 900°K is probably ~30%.

Results and Analysis of Calculations

The initial data as described above has been used to calculate the thermodynamic properties of cesium for superheated, saturated, and wet vapor at temperatures from 400 to 1500°K in steps of 50°, and for pressures from 0.01 to 22 bars in varying steps, and the data has been used to compile tables and plot the appropriate diagrams.

Table 1, for the saturated state (by temperature), contains the following data: saturation pressure p_s , degree of dissociation of the vapor α'' (ratio of the number of moles reacted Cs_2 to the initial number), molecular mass of the vapor μ'' , specific volume v' (up to 900°K), specific enthalpy and entropy i' and s' for the liquid, values of v'' , i'' , and s'' for the vapor, surface tension σ (up to 900°K), heat of evaporation \underline{r} , heat capacities along the saturation curve c_s' and c_s'' , the heat capacities $c_p''^{\text{sp}}$ and $c_v''^{\text{sp}}$, the differential adiabatic throttle effect $\alpha''_{\text{th}}^{\text{sp}}$, the velocity of sound a''^{sp} , the adiabatic exponent $k''^{\text{sp}} = -\frac{v''}{p} \left(\frac{\partial p}{\partial v} \right)_s^{\text{sp}}$ on the single phase side of the vapor region (index sp), and the values of $c_v''^{\text{tp}}$, $\alpha''_{\text{th}}^{\text{tp}}$, α''^{tp} , and k''^{tp} on the wet vapor side (index tp).

Note that for a cesium-ideal inert gas mixture, the total pressure of the system at which the cesium vapor is in the saturated state is

$$p = p_s \frac{1 + \alpha_s + \nu_n}{1 + \alpha_s},$$

where $\nu_n = \mu_2/d\mu_n$ is the number of moles of neutral gas with the molecular weight μ_n , and d is the concentration of cesium vapor per unit mass of inert gas.

The starting point for the enthalpy and entropy was taken to be the state of the condensed phase at 0°K. In the paper and in the tables the thermal unit, following All Union State Standard-8850-61, is the Joule, where 1 J is equal to 0.23884 cal. If the tables are given to four significant figures, this guarantees a smoothness of ± 1 in the last significant figure. The value of the universal gas constant used in the calculations is $R = (8.314414 \pm 0.0003) \text{ kJ/mole} \cdot \text{deg}$ (1 bar = 10^5 N/m^2).

A total of 50 isobars was calculated in the superheated vapor range for the quantities α , v , i , s , c_p , c_v , k , and a , 40 of which are given in Table 2. The values of the thermodynamic velocity of sound a and the adiabatic exponent k for wet cesium vapor at degrees of dryness $x \geq 0.60$ are given in Table 3.

The following comments are to be made on the results of the calculations:

1. The calculated saturation pressures of cesium vapor are ~30% lower at 400°K, and ~30% higher at 1500°K than the values given by the equations of An. N. Nesmeyanov [7]. This is due to the difference in the values taken for the heats of sublimation, and to the fact that the results of the fundamental work in the range 300-400°K [8] possibly give too high pressures. From 500 to 700°K our values are in better agreement with the experimental data of [9, 10] than with the data of [7].

2. As is the case with other alkali metals [1], the way in which a number of the calculated thermodynamic properties of cesium vapor change on the saturation curve shows peculiarities. These include the bend points in the curves giving the degree of dissociation and the heat of evaporation as a function of temperature, and the occurrence of a maximum in the heat capacity c_p'' . A complete analysis of these phenomena can only be made on the basis of experimental work.

3. The isobars of the heat capacity c_p of dissociating gases are known to have maxima, which, for cesium in the range of parameters studied, are cut off by the saturation curve. It is also obvious that beyond the maximum, as the temperature increases, the heat capacity c_p on the isobar will first decrease (as a result of reducing the fraction of dissociating molecules), and then increase (as a result of the increase in the heat capacity C_{pi}^0 for atoms). The corresponding minima for cesium vapor on the isobars 0.01 and 0.02 bar occur about 1300°K.

4. It has already been emphasized in [1] that the values of the so-called adiabatic sound exponent

$$k = -\frac{v}{p} \left(\frac{\partial p}{\partial v} \right)_s$$

are not the same as the thermal adiabatic exponent, given by the equation $pv^k = \text{const}$. The differences may reach 20-30% for cesium vapor in the range of parameters studied. However, the functions of k are nevertheless nearly the same, and the values of k^{sp} and k^{tp} are given in Table 1 as an illustration of the way in which they change, and of the jump on the saturation curve.

5. In the method of calculation used, a "model" of matter is employed which makes it possible to evaluate the error in the results. The errors in calculating the properties of superheated vapor resulting from the inaccuracy mentioned above in determining the heat of dissociation at 1500°K and 22 bars are $\delta\alpha \approx 7.5\%$, $\delta v \approx 2.5\%$, and $\delta c_p \approx 10\%$.

The error in calculating the saturation pressure for a dissociating mixture of ideal gases at 1500°K is hard to reduce to less than 20-25%, as a result of errors in determining the heat of sublimation in the heat capacity C_{pc}^0 . In this case the error in determining the heat of evaporation may reach 10-15%.

The difference between the properties of the components of cesium vapor and those of an ideal gas are difficult to evaluate, since at the present time not enough is known about the parameters of the interaction potentials, for example, of cesium atoms in the triplet state. It is nevertheless probable that the depth of the well in this potential curve is $\epsilon/k < 1200^\circ\text{K}$, while the equilibrium interatomic distance is $r_e < 6.5 \text{ \AA}$. Even this rough estimate enables us to assume that as a result of the vapor departing from an ideal gas, the saturation pressure of cesium at 1500°K may exceed the calculated value by $\sim 20\%$.

6. In analyzing the errors, it is interesting to find the possible effect of thermal ionization of Cs_1 atoms on the heat capacity of the vapor at the maximum temperature of 1500°K used in the calculations and the minimum pressure of 0.01 bar. The formulation of the problem is obvious: for cesium, the ionization potential $u_{11} = 3.78 \text{ eV}$ is not large, while the heat capacity is a quantity that is very sensitive to such effects.

It is easily found from Saha's equation that the degree of ionization is $\alpha_{11} \approx 2 \cdot 10^{-5}$ for the reaction $\text{Cs}_1 = \text{Cs}^+ + e^-$ with the parameters under discussion. The increase in heat capacity from thermal ionization is found in the same way as for dissociation. In our case, $\Delta c_{p11} \approx 6.3 \cdot 10^{-4} \text{ kJ/kg} \cdot \text{deg}$, which amounts to $\sim 4\%$ of the calculated value of the heat capacity of a dissociating mixture of ideal gases.

On the whole, calculating the error shows that the insufficiencies and inaccuracies in the initial data leave something to be desired in the accuracy of the results obtained, and improving this requires extensive experimental work.

LITERATURE CITED

1. M. P. Vukalovich, V. N. Zubarev, and L. R. Fokin, *Teploenergetika*, No. 8, 10 (1962).
2. L. V. Gurvich, et al., *Thermodynamic Properties of Individual Materials* [in Russian], Moscow, Academy of Sciences Press, USSR (1962).
3. *Thermodynamic Properties of the Elements*. D. Stull and G. Sinke, ACS, Washington (1956).
4. K. Clusius and H. Stern, *Z. angew. Phys.*, 6, 194 (1954).
5. T. Dauphinee, D. Martin, and H. Preston-Thomas, *Proc. Roy. Soc.*, A233, 214 (1955).
6. M. Rengade, *Compt. rend.*, 156, 1897 (1913).
7. An. N. Nesmeyanov, *Vapor Pressure of the Chemical Elements* [in Russian], Moscow, Academy of Sciences Press, USSR (1961).
8. J. Taylor and I. Langmuir, *Phys. Rev.*, 51, 753 (1937).
9. A. Kröner, *Ann. Physik. ser.*, 4, 40, 438 (1913).
10. M. Hackspill, *Ann. Chim. Phys.*, ser., 8, 28, 613 (1913).

11. G. Herzberg, Molecular spectra and molecular structure. I. Spectra of diatomic molecules, 2nd ed. Toronto-N.Y.-London (1950).
12. A. Gaydon, Dissociation energies and spectra of diatomic molecules, 2nd ed., London (1953).
13. F. Loomis and P. Kusch, Phys. Rev., 46, 286 (1934).
14. W. Finkelburg, Phys. Zs., 39, 98 (1938).
15. W. Evans, et al., J. Res. Nat. Bur. Standards, 55, 83 (1955).
16. G. Somayajulu, J. Chem. Phys., 33, 1541 (1960).
17. M. Hackspill, Compt. rend., 152, 259 (1911).
18. Eckhardt and Graefe, Z. anorgan. und allgem. Chem., 23, 378 (1900).
19. P. A. Andreev, et al., Liquid Metal Coolants for Nuclear Reactors [in Russian], Leningrad, Sudpromgiz (1959).
20. E. Rink, Compt. rend., 189, 40 (1929); Ann. chim., 18, 435 (1932).
21. S. Cohen, Nucl. Sci. and Engng., 2, 530 (1957).
22. O. A. Timofeecheva, et al., Dokl. AN SSSR, 143, 618 (1962).
23. M. Sittig, Sodium (Production, Properties, and Use) [in Russian], Moscow, Gosatomizdat (1961).
24. S. I. Zadumkin, Izv. AN SSSR, Division of Engineering Sciences, Metallurgy Fuel Series, No. 6, 119 (1960).

All abbreviations of periodicals in the above bibliography are letter-by-letter transliterations of the abbreviations as given in the original Russian journal. Some or all of this periodical literature may well be available in English translation. A complete list of the cover-to-cover English translations appears at the back of this issue.

ENLARGED RADIOCHEMICAL EQUIPMENT USING THE RADIATION
FROM SPENT NUCLEAR REACTOR FUEL ELEMENTS

V. L. Karpov, A. Kh. Breger, M. E. Eroshov, V. E. Drozdov,
G. N. Lisov, S. G. Stoenko, D. M. Torgovitskii, V. I. Vainshtein,
and N. P. Syrkus

Translated from Atomnaya Energiya, Vol. 15, No. 4,
pp. 302-308, October, 1963

Original article submitted January 11, 1963

Graphs are given for determining the instantaneous and mean γ power from the fission fragments in fuel elements as a function of operating schedule in the nuclear reactor and in the radiochemical equipment, as well as graphs for finding the variation with the same parameters of the energy of the γ radiation produced in the radiochemical equipment.

A description is given of the construction of an enlarged installation for carrying out radiochemical reactions using radiators made of (up to 100) nuclear reactor fuel elements. The maximum activity of the fuel elements in the equipment may reach $\sim 10^6$ g-equiv Ra in the initial period of operation.

One of the most promising sources of γ radiation for carrying out radiochemical reactions on a large scale is that provided by nuclear reactor fuel elements [1].

In recent years, a number of installations have been made, and projects have been developed in which use is made of the γ radiation from the fuel elements of various nuclear reactors (for example, MTR (USA), DIDO (England), HIFAR (Australia), EL-3 (France), and VVR-Ts (USSR) [2-9]). A large part of the equipment when using fuel elements consists of all-purpose devices intended for irradiating different objects.

The data in the literature show that so far, in working with fuel elements, the way these sources of γ radiation were used was to a considerable extent haphazard, and was determined by the nature of the operation (program) of the nuclear reactor, and the usual conditions under which the spent fuel elements were stored. What were used were mainly old fuel elements, i.e., that had been stored up to six months after discharge from the reactor. The question of laying out the most rational program for using the fuel elements from the point of view of utilizing the γ power has been posed and discussed in [10-12]. However, use of the results obtained in these papers is limited to fuel elements that have operated in the reactor for a time t_r equal to 40 days. For practical purposes, in a number of cases, particularly where it is desired to calculate the γ power of fuel elements from power reactors (which usually operate for a long period), data are required for considerably larger values of t_r . Accordingly, using the results of [13], we have calculated the mean γ power of the spent fuel elements during the time t_e that they are operating in the radiochemical equipment, as well as the total γ energy developed in the apparatus during this time for values of $0 \leq t_e \leq 400$ days and $10 \text{ days} \leq t_r \leq 500$ days, with the time required to transport the fuel elements from the reactor to the equipment being $t_{re} = 1$ day.

The calculation is made in the following way. Graphs were constructed giving the instantaneous γ power from the U^{235} fission products, expressed as a fraction of the thermal power ϵ of the reactor, as a function of the time t_r and of $t_t = t_e + t_{re}$ (days) (Fig. 1). Then, by making a graphical integration of the curves of Fig. 1 between the limits of the time t_{re} equal to 1 day and t_t , the values were obtained for the γ energy developed by the fission fragments in the time t_e , i.e.,

$$\epsilon^{(t_{re}=1)} = k \int_1^{t_t} \epsilon(t) dt, \quad (1)$$

where k is a dimensional factor.

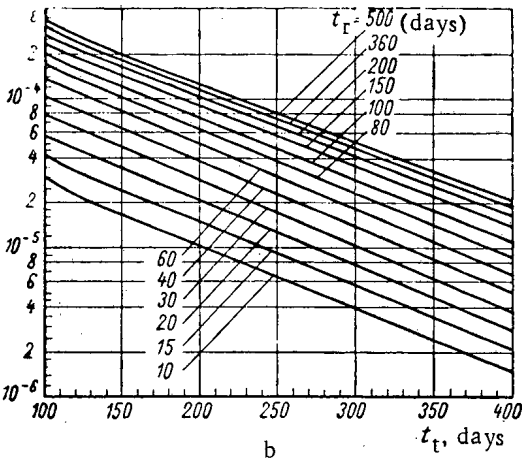
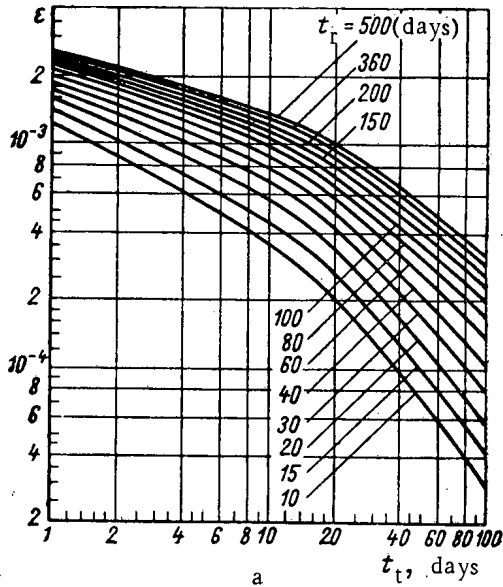


Fig. 1. Instantaneous γ power ϵ of spent fuel elements, expressed as fractions of the thermal power of the reactor, as a function of t_t for different values of t_r : a) for $1 \text{ day} \leq t_t \leq 100 \text{ days}$; b) for $100 \text{ days} \leq t_t \leq 400 \text{ days}$.

accumulated in working with these radiation sources which will obviously be needed for a large scale operation in the future.

The apparatus provides for a large variety of fuel element assemblies to be used as radiators of different shapes and sizes, as well as containing different numbers of fuel elements (1-100).

Depending on the radiochemical reaction to be carried out, the radiator may consist either of a single fuel element or of a set of fuel elements forming a hollow cylinder or coaxial cylinders, parallel planes, etc. The number of fuel elements required to assemble a desired radiator is determined by the activity, and the particular radiochemical process.

To get large dose power in the radiator for a given number of fuel elements of a given activity the holder is made in such a way that the fuel elements can be arranged in several rows.

An important fact which must be kept in mind in using fuel elements is the relatively rapid decay in the γ activity of the fuel elements with time (see Fig. 1). Depending on the drop-off in activity, the fuel elements are replaced approximately every 100-200 days of operation in the equipment.

The results of the integration are given in Fig. 2. Here, the ordinates are fractions of the thermal power of the reactor, multiplied by the time in hours. To obtain ϵ_Σ for any value of $t_{re} = n$ days, it is necessary on the graph (see Fig. 2) to find the difference between the numerical values of the integrals:

$$\epsilon_\Sigma^{(t_{re} = n)} = k \int_1^{t_t} \epsilon(t) dt - k \int_1^n \epsilon(t) dt. \quad (2)$$

Then the mean γ power $\bar{\epsilon}$ was found for the time they were operating in the radiochemical apparatus in fractions of the thermal power of the reactor:

$$\bar{\epsilon} = \frac{1}{t_e} \int_{t_r}^{t_t} \epsilon(t) dt. \quad (3)$$

Figure 3 gives curves of $\bar{\epsilon}$ as a function of t_e and t_r for $t_{re} = 1$ day. The value of $\bar{\epsilon}$ may be found for any $t_{re} = n$ days by means of the formula

$$\bar{\epsilon}^{(t_{re} = n)} = \frac{\epsilon_\Sigma^{(t_{re} = n)}}{24 \cdot t_e}, \quad (4)$$

where t_e is expressed in days.

Figure 4 shows curves of ϵ_Σ and $\bar{\epsilon}$ as a function of t_e and t_r for $t_e = t_r$ and $t_{re} = 1$ day, i.e., when the radiochemical equipment gets the fuel elements as soon as the reactor is shut down, and they are used in the apparatus until the next shutdown.

Use and Physical Parameters of the Equipment

Realizing the need to go from laboratory radiochemical studies to large scale experiments and then to industrial radiochemical processes, an enlarged installation has been developed and built, intended for carrying out various radiochemical reactions using fuel elements as the γ sources. This installation is in operation at the present time. During operation the experience will be

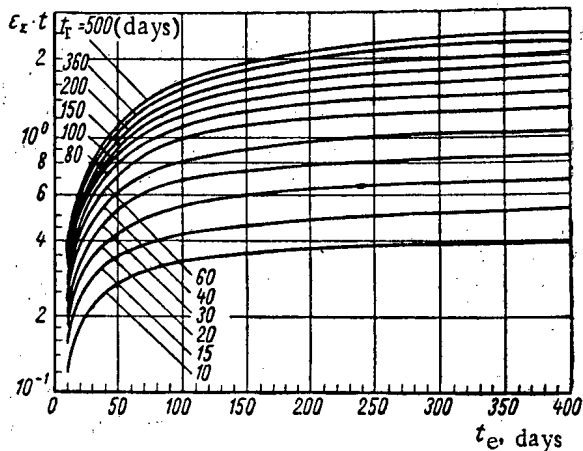


Fig. 2. γ energy ϵ_{Σ} of spent fuel elements developed in the time t_e days as a function of t_e for different values of t_r .

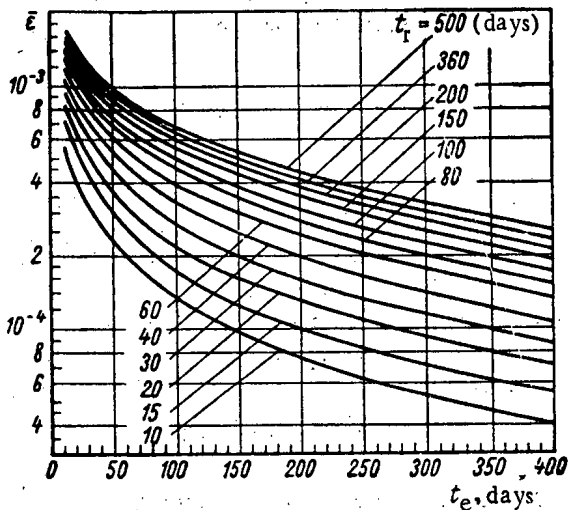


Fig. 3. Mean γ power $\bar{\epsilon}$ of spent fuel elements, expressed in fractions of the thermal power of the reactor, during the time t_e days, as a function of t_e for different values of t_r .

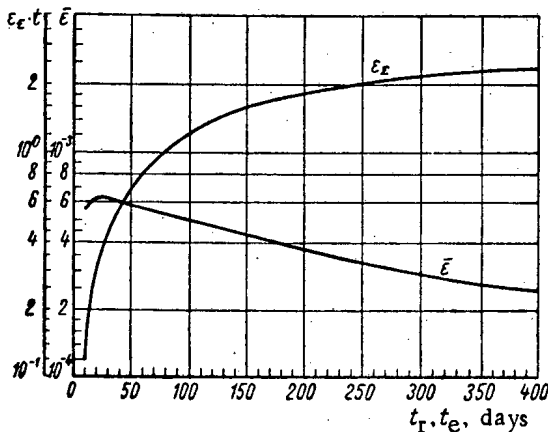


Fig. 4. Energy and mean γ power of spent fuel elements as a function of t_r and t_e (for $t_r = t_e$).

The results of calculating the dose power at the center of a hollow cylindrical radiator for $t_r = 60$ days and $t_e = 5-200$ days at a thermal power of $w = 300$ kW for a fuel element are given in Fig. 5. It follows from the graphs that the dose power when t_e varies from 5 to 200 days decreases for an inside radiator diameter of $D_i = 12$ cm from 2000 to 65 r/sec, while for $D_i = 70$ cm, it drops from 1500 to 50 r/sec.

In the first stage, the equipment uses fuel elements that have been stored for 60 days and have a total activity of 270,000 g-equiv Ra. This makes it possible to realize dose powers up to 200 r/sec in the center of a cylindrical radiator for a diameter of 70 cm and up to 800 r/sec for a diameter of 12 cm.

At the same time it is also possible to carry out certain radiochemical reactions on the outside of the radiator. The dimensions of the chamber make it possible to set various objects as far as 3 m from the center of the radiator. The equipment is designed for using spent fuel elements from different reactors.

Building Housing the Equipment (Fig. 6)

The main parts of the equipment are shown in Fig. 7. The equipment is designed in such a way that irradiation may be done in three ways:

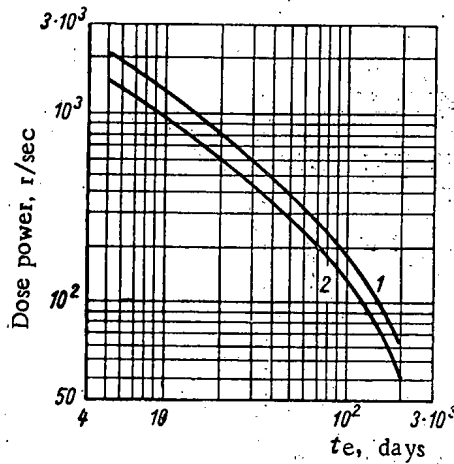


Fig. 5. Dose power in the center of a cylindrical radiator made up of n fuel elements, as a function of t_e : 1) $D_1 = 12$ cm, $n = 40$; 2) $D_1 = 70$ cm, $n = 100$.

to it rails for a movable carriage used to take the radiator containing the fuel elements into the operating chamber and out again. The mechanism used to move the carriage is able both to take the radiator (fastened to the floor of the carriage) out of storage and into the radiation chamber and back again, and at the same time take the object to be tested to the radiation tank when using underwater irradiation. The carriage is remotely controlled and has a capacity of 1.5 tons.

- 1) in a radiator (inside and outside) drawn up into a radiation chamber above the storage tank;
- 2) inside a radiator kept in a holder under a layer of water;
- 3) inside a radiator kept in a holder from which the water has been removed.

The $5 \times 6 \times 5.2$ m working chamber is provided with a three-ton traveling crane, a manipulator, a viewing window, and a television setup. The entrance to the chamber is a labyrinth with a door fitted with a protective interlock. The operating chamber is connected by communication and experimental channels with both the control desk and the laboratory parts of the building.

The water storage is in a $1.5 \times 1.5 \times 6.75$ m 1Kh18N9T steel tank holding the radiator tank containing tubular sockets for the fuel elements. The storage tank has a capacity of 15 m^3 . The radiator tank can hold up to 100 fuel elements with a total activity reaching $\sim 10^6$ g-equiv Ra. The spacing of the tubular cells is such as to ensure subcriticality, thus eliminating the possibility of a chain reaction. One of the walls of the storage tank has fastened

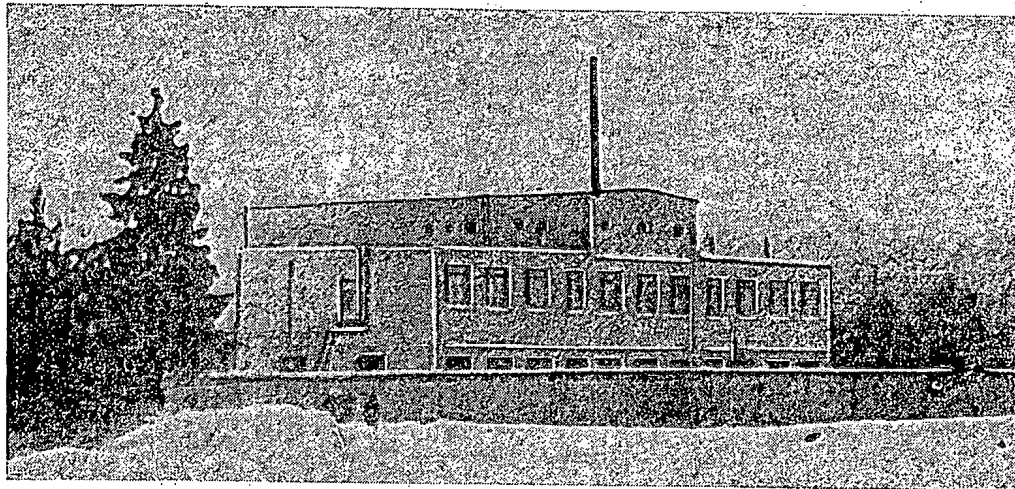


Fig. 6. General view of building housing the equipment.

The rotating loading device is intended to bring the channel in the fuel element container into coincidence with the inclined loading chute of the storage tank. The fuel elements in special containers are brought to the equipment in a truck, and by means of a 10-ton crane dolly, the fuel elements are lifted to the rotating loading mechanism. Before the fuel elements are let down into the loading chute of the storage tank a check is made on the air tightness and surface contamination of the fuel elements by analyzing a sample of water taken from the container. The good fuel elements are dropped through the neck of the container into the storage tank under a protective layer of water. A rod operated by hand is used both for underwater loading of the tubular cells in the radiator tank and for underwater loading with fuel elements of the radiator assembled on the cart.

Provisions are made for rapid replacement of the water in the holder as well as for pumping it in the following ways: 1) tank-filter-tank; 2) tank-filter-waste; 3) tank-filter-storage container.

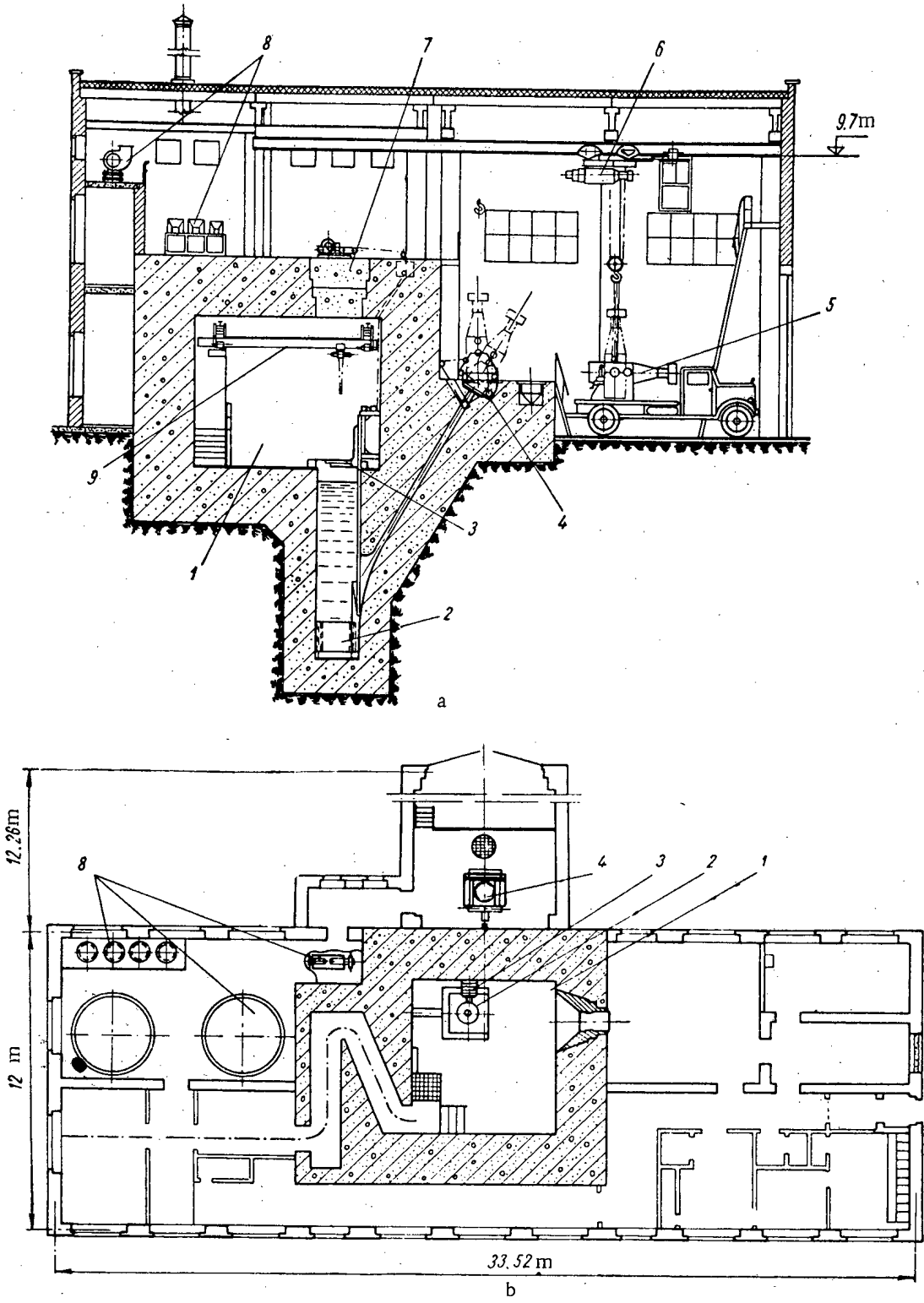


Fig. 7. Vertical (a) and horizontal (b) sections of the equipment: a) working chamber with walls of ordinary concrete 200 cm thick; 2) water storage holder with sockets for holding the fuel elements; 3) mechanism for moving the carriage to which the assembled radiator is fastened; 4) rotating loading device; 5) fuel element container; 6) crane dolly; 7) removable shield plug; 8) ventilation equipment; 9) traveling crane.

The following precautions have been taken to ensure safe working conditions around the equipment:

1) placing monitor and signal apparatus in all the rooms which is connected to the interlocks so that it is impossible to open the door to the labyrinth and to the operating chamber if the dose there is more than the allowable value, or when the ventilator is not working;

2) dividing the rooms into clean and presumably clean zones; the personnel passes from one zone to another through an air lock and a check point;

3) two input and two exhaust ventilating systems where the air supplied and exhausted is purified by filters;

4) the air is pumped out from above the water level and the storage tank, which prevents contamination of the air in the chamber by active aerosols;

5) remote control of the mechanisms for raising the radiators and the traveling cranes in the radiation chamber;

6) using fuel elements placed in ampules, and checking the air tightness and surface cleanness of the ampules;

7) collecting all the special waste and dead storage in one place.

The auxiliary rooms in the installation satisfy all technical health requirements and provide extensive facilities for experimentation.

The building housing the equipment is T-shaped in plan (see Fig. 7b). The building has brick walls self-supporting on flat concrete foundations. The ceilings are made of insulating sheets. The depth of the storage well, which is dictated by personnel safety considerations, is 7.7 m from the floor of the operating chamber. The walls of the chamber are made of monolithic reinforced concrete ($\gamma = 2.2 \text{ ton/m}^3$). The walls are 2 m thick. Using heavy concrete in this case turned out to be a good idea since it did not reduce the volume of the chamber to any great extent and the cost of the work is not proportionately greater.

The ceiling of the chamber has an opening for making repairs that is closed with a fabricated plug having a total weight of 9 tons. The construction of the building, in view of the need to have a deep storage well, required special organization of the work. The storage well was constructed by excavation. Special requirements were placed on the hydraulic insulation of the subterranean part of the equipment.

The equipment in the installation includes a settling tank (150 m^3) with a special unit for switching around piping, placed in a nearby tower sunk into the ground to the level of the floor of the settling tank. The building housing the equipment is surrounded by a radiation danger zone.

The over-all data on the building are:

Total volume	4450 m^3
Built-up area	360 m^2
Volume of earth works	5700 m^3
Volume of concrete and reinforced concrete work	1200 m^3
Amount of air removed	8900 m^3/h
Surface of heating equipment	240 m^2
Electric power required	Up to 200 kW

A motor road leads to the building, designed to carry loads up to twenty tons.

Transportation of Fuel Elements

Before the fuel elements are transported, they are put into special cladding ampules. This greatly reduces the contamination of the water storage basin. The fuel elements are put into the ampules by remote control, behind a shield, and may be either "dry" or "wet," depending on whether the operation is carried out in a "hot" chamber or in a water basin.

The ampule is a cylindrical vessel with a screw-on cover using special metal and plastic packing.

The ampules containing the fuel elements are mounted in the container in a protective socket above the water basin or in a "hot" chamber. A lifter mounted on the container lets the fuel element down into the container. The

construction of the container is such that it is air tight and the inside may be filled with water. The container is transported on a specially designed truck. While the fuel elements are being transported the heat is conducted away through the layer of water between the ampule and the inner wall of the container.

Inside the building, the container is taken off the truck by a traveling crane and put on a device which aligns the axis of the container with the axis of the inclined loading chute of the storage well. After washing with a circulating loop containing a pump mounted on the container, and when the surface of the ampule is as clean as possible, it is let down through the channel into the storage well. Then, under a protective layer of water, the ampule is removed from the holder on the lowering cable and taken from the loading hatch to the socket in the storage holder.

The experience from the design, building, and operation of the enlarged installation may be of use in designing and constructing similar equipment.

The authors recognize their duty of noting the participation in the development of the installation by P. P. Moiseenko, L. M. Dunaev, L. M. Suroegin, Yu. G. Savin, and I. G. Abramov.

LITERATURE CITED

1. A. Kh. Breger, *Khim. prom-st'*, No. 6, 12 (1959).
2. *Nucleonics*, 15, No. 7, 108; No. 8, 102; No. 11, 170 (1957).
3. J. Martens and F. Minuth, Selected list of neutron and γ -irradiation facilities in operation, being built or planned. Washington, Govt. Print. Office (1957).
4. H. Stockman, et al., *Nucleonics*, 15, 94 (1957).
5. S. Jefferson, G. Murray, and F. Rogers, Large Radiation Sources in Industry, Vol. 1, Conference Proceedings, Warsaw (September 8-12, 1959). International Atomic Energy Agency, Vienna (1960).
6. P. Leveque, *ibid.*, p. 95.
7. D. George and J. Gregory, *ibid.*, p. 141.
8. B. I. Vainshtein, A. Kh. Breger, and N. P. Syrkus, *Khim. prom-st'*, No. 7, 6 (1959).
9. A. Kh. Breger, et al., *Kauchuk i rezina*, No. 4, 17 (1960).
10. A. Kh. Breger, Radioactive Isotopes and Nuclear Radiation in the National Economy of the USSR, Vol. 1 [in Russian], Moscow, Gostoptekhizdat, p. 169 (1961).
11. Yu. S. Ryabukhin and A. Kh. Breger, *Atomnaya énergiya*, 5, 533 (1958).
12. A. Kh. Breger, Yu. S. Ryabukhin, and F. A. Makhlis, *Dokl. AN SSSR*, 136, 671 (1961).
13. E. Crauch, AERA C/M 324, Harwell (July, 1957).

All abbreviations of periodicals in the above bibliography are letter-by-letter transliterations of the abbreviations as given in the original Russian journal. Some or all of this periodical literature may well be available in English translation. A complete list of the cover-to-cover English translations appears at the back of this issue.

A RADIOCHEMICAL INVESTIGATION OF THE YIELDS OF RARE-EARTH ELEMENTS FROM U^{238} PHOTOFISSION

K. A. Petrzhak and R. V. Sedletskii

Translated from Atomnaya Énergiya, Vol. 15, No. 4,
pp. 308-313, October, 1963
Original article submitted December 27, 1962

Employing radiochemical methods of isolating fragments without a carrier, and the isotope dilution method ("active by active" variant), the authors investigated rare-earth elements and other U^{238} photofission fragments at maximum bremsstrahlung energy 14 MeV. The relation between the fission product yield and the mass number was determined.

Introduction

An investigation of the mass distribution of fragments during heavy nuclear fission gives valuable information on the properties of fission itself and on the effect of the mass and charge of the nucleus and its excitation energy on this process. The advantage of photofission at low excitation energies in comparison with other types of fission is that absorption of a γ -quantum does not lead to a change in the charge and mass of the nucleus. It has been shown that two groups of fragments, a light and a heavy one [1], are formed during photofission of elements heavier than thorium at low excitation energies. In the case of symmetric fission, isotopes of rare-earth elements form part of the heavy group.

There have been comparatively few investigations into the yields of rare-earth elements during all types of fission. There is only one paper on the photofission of heavy nuclei [2] and this deals with the yields of rare-earth elements during U^{238} fission by γ -quanta with a maximum energy of 100 and 250 MeV. It was of interest to investigate the yields of these fragments by the example of U^{238} photofission at low excitation energies because this eliminates indeterminacy of the mass and charge of the nucleus undergoing fission.

EXPERIMENTAL

The lack of information on yields of the rare-earth element fraction is not accidental, and is due mainly to difficulties of separation.

The "conventional" radiochemical method is little suited for an investigation of this group of fragments, particularly those with a short half-life, or radioactive isotopes of an element like promethium, which has no known stable isotopes. The essential point here is that gravimetric amounts of rare-earth elements cannot be separated rapidly and reliably by ion-exchange chromatography or continuous electrophoresis [3], which can only be employed for microamounts of these elements. The method employed in [4] for determining the yields of rare-earth elements is one of the possible compromise solutions.

Another essential point should be noted. When the yield curve of the fission fragment masses is investigated by the radiochemical method, the absolute β -activity of the preparations is measured. These measurements are usually carried out in an end-window counter, the measured samples having a high surface density. The shortcomings of such a method are well known, whereas there are obvious advantages in measuring the absolute activity of fission fragments in a 4π -counter when the investigated material does not contain weighed gravimetric amounts of a stable carrier. The recording efficiency in this case is nearly 100%.

These were the factors determining the problem of separating rare-earth elements from irradiated material without a stable isotopic carrier. In [3, 5] it was shown that this fragment group can be separated from uranium and thorium without a carrier, followed by separation of the group elements by continuous electrophoresis. For investigating the yields of these elements we used the method in [5].

TABLE 1. Yields of U^{238} Photofission Fragments at a Maximum Bremsstrahlung Energy of 14 MeV

Fragment	Half-life	Ratio of fragment yield to Ce^{143} yield	Only one experiment
Y^{93}	11 h	0.996 ± 0.096	4.3 ± 0.4
Ru^{103}	39.8 days	0.955 ± 0.028	4.11 ± 0.12
Ru^{105}	4.4 h	0.832 ± 0.020	3.59 ± 0.09
$Ag^{111} *$	7.6 days	0.064 ± 0.025	0.27 ± 0.11
$Ag^{113} *$	5.3 h	0.066 ± 0.025	0.28 ± 0.11
La^{141}	3.7 h	1.45 ± 0.21	6.2 ± 0.9
Ce^{143}	33.4 h	1.0	4.3
Pr^{145}	6.0 h	0.989 ± 0.167	4.2 ± 0.7
Nd^{147}	11.3 days	1.03 ± 0.28	4.4 ± 1.2
Nd^{149}	1.8 h	0.52 ± 0.12	2.2 ± 0.5
Pm^{151}	27.5 h	0.25 ± 0.05	1.1 ± 0.2

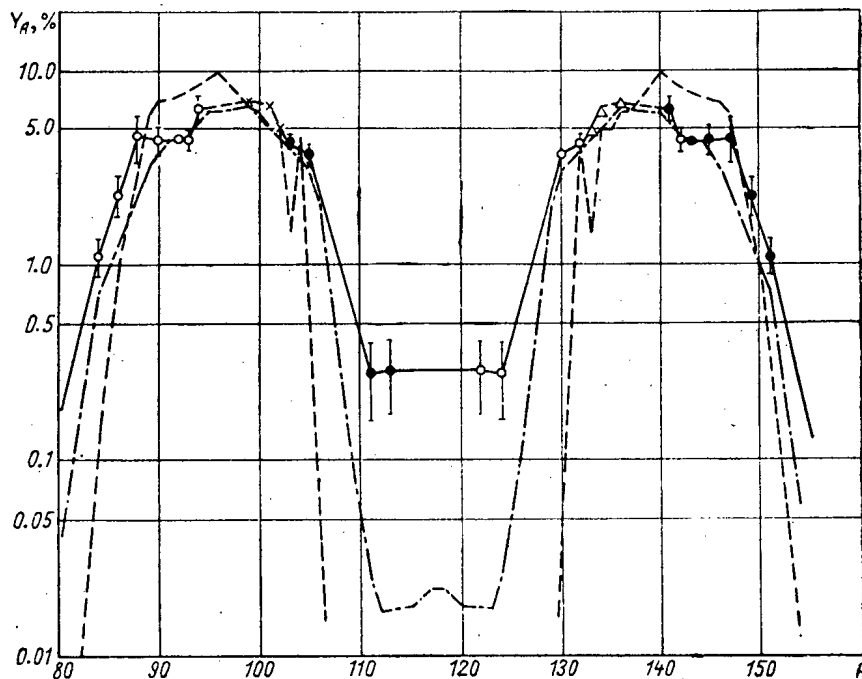
* Only one experiment.

The yields of ruthenium and silver isotopes from U^{238} fission were investigated simultaneously by the method of separating without a carrier. Hume's method [6], somewhat modified in view of the necessity of separating isotopes of silver and the rare-earth group, was used for separating ruthenium isotopes. During the investigation of silver isotope yields, we used thallium as the nonisotopic carrier to solve this problem, thallium being separated from silver in the final stages of radiochemical analysis.

The maximum bremsstrahlung energy of 14 MeV was used for investigating the mass distribution of U^{238} fission fragments. 0.7-1.0 g samples of pressed and calcined uranous-uranic oxide were irradiated in the betatron accelerator chamber of the Lensovet Leningrad Technological Institute. The maximum electron energy was 15 MeV. The bremsstrahlung intensity was 5-8 r/min at 1 meter from the target. The electrons were decelerated in the substance of the irradiated material. The

electron-induced, neutron-induced and photoneutron-induced fission fractions were determined theoretically and experimentally in [7-9] and found to be negligible.

The known values of the photonuclear reaction thresholds for a number of elements (In^{115} , Sb^{121} , Ag^{109} , Br^{81} , Br^{79} , Cu^{63} , N^{14} , Zn^{64} , P^{31} , Zr^{90} , Mo^{92} , Fe^{54}) were used for calibrating the maximum bremsstrahlung energy of the betatron.



Relation between fission fragment yields and mass number: ●) main points; ○) mirror points (our results for U^{238} photofission at 14 MeV); ×) main points; △) mirror points (results in [22] for U^{238} photofission at 13 MeV); - · - · -) U^{238} photofission at 8 MeV [1]; - - - -) spontaneous fission of U^{238} [19-21].

During irradiation, the energy stability was monitored by observing the voltage from a coil in the magnetic field of the betatron. The constancy of radiation intensity was assessed from ionization chamber readings. The irradiation time was generally 10-12 h.

We investigated the relative yields of the following U^{238} photofission fragments: La^{141} , Ce^{143} , Pr^{145} , Nd^{147} , Nd^{149} , Pm^{151} , Y^{93} , Ru^{103} , Ru^{105} , Ag^{111} , Ag^{113} . Ce^{143} served as the standard fragment.

The chemical yield in each experiment was monitored directly by adding in the first stage of analysis a known activity of the corresponding long-life "label" isotopes (La^{140} , Ce^{144} , Pr^{143} , Pm^{147} , Y^{90} , Ru^{106} , Ag^{100}), followed by analysis of the activity decay curve of the separated material. This method of determining the chemical yield is based on Hahn's isotope dilution method [10, 11].

TABLE 2. Principal Characteristics of the Yield Curves for U^{238} Photofission and Spontaneous Fission

Yield curve parameters	U^{238} spon- taneous fission [19-21]	U^{238} (γ_8 MeV, f) [1]	U^{238} (γ_{14} MeV, f) (our results)
Position of the heavy peak	140	138	141
Position of the light peak	96	98	94
Maximum yield	9.6	6.4	6.2
Peak halfwidth	13	15	17
Peak/valley ratio	> 190	310	23
d log Y/dA at A > 151	- 0.50*	- 0.35*	- 0.20

*From the mirror points.

Where an appreciable amount of the radioactive isotope used for monitoring the chemical yield accumulated during irradiation (e.g., Pr^{143}), blank experiments were carried out under the same irradiation conditions. The daughter decay products were separated from the parent ones in the same period of time after the betatron had been switched on as that in the "working" experiments. The relative activities of short-life and long-life isotopes, e.g., Pr^{145} and Pr^{143} , were determined in the blank experiments. Further, the activity added was such that the activity of the long-life isotope accumulated during irradiation was only a very small fraction of the former.

This method of determining the chemical yield may also be used for investigating long-life isotopes formed during fission. In this case the irradiated material is cooled in a period of time adequate for virtually complete decay of the short-life isotopes. Any short-life isotope of the investigated element is then used as the label.

The radioactive label isotopes were first purified to remove possible radioactive impurities. A solution was prepared and this was used for the chemical yield labels. The specific activity of the radioactive label-isotope solution was monitored in each experiment by simultaneous sampling of this solution (a weighed drop applied to thin copper foil) and a "standard" solution (a weighed drop applied to a collodion film across a ring). The activity of the standard, and therefore the specific activity of the solution was then determined.

The material used for measuring the β -activity of the separated fragments was measured as follows. The exact location of the peaks of the rare-earth element fractions in the continuous electrophoresis cell was determined by measuring the activity of identical amounts of the solution in an end-window counter. After separation, the fractions of the solution were evaporated to dryness in quartz dishes. The latter were roasted to decompose the ammonium salts of ethylenediaminetetracetic acid and treated with concentrated hydrochloric acid. The hydrochloric acid solutions of fractions containing radioactive isotopes of rare-earth elements without a carrier were added dropwise to organic films "mounted" on rings. The samples were dried carefully under an infrared lamp and placed in a 4π -counter. The material used for measuring the activity of the separated ruthenium and silver isotopes was prepared in the same way. The activity of the fission fragments without a carrier was measured in a 4π -counter operating under proportional conditions. The counter background was 2-3 counts/min [12, 13]. The operation of the counter was monitored before each series of experiments against a standard Tl^{204} source whose exact activity was known.

The decay curves of the radioactive isotopes of the separated element were analyzed to determine: (1) the amount of the activity in the investigated isotope, by means of the half-life; (2) the chemical yield, from the con-

tent of the long-life label isotope. The relative activities of the separated fragments were determined. The activity of Ce^{143} serving as the standard. The relative activities of the investigated photofission fragments were determined as the mean of results of three to seven irradiations.

To determine the mass of the additional fragment, or the "mirror" point on the mass yield curve, the average number of prompt neutrons emitted per fission event must be known. According to [14] and [15], the number of prompt neutrons emitted during spontaneous fission of U^{238} is 2.1 ± 0.1 and 2.1 ± 0.08 respectively. If it is assumed that the relation between $\bar{\nu}$ and the excitation energy of the split nucleus has the same character for photofission as for neutron-induced nuclear fission, i.e., increases by one unit with an increase in excitation energy by 7-9 MeV [16], then we may assume that $\bar{\nu} = 3$ for U^{238} photofission by γ -quanta with a maximum energy of 14 MeV.

Having plotted the relative mass yield curve for $\bar{\nu} = 3$, and standardized the area enveloped by the curve to 200%, we obtained the absolute yields of the fragments.

The cumulative fragment yields found were considered as equal to the total yields of chains with corresponding mass numbers because the independent yields of the final terms calculated in accordance with the hypothesis of equal charge displacement [17, 18] are small and outside the limits of accuracy of our results. The data obtained are given in Table 1.

The Pm^{149}/Pm^{151} and Nd^{147}/Nd^{149} yield ratios were determined; they were 2.07 ± 0.08 and 1.99 ± 0.06 respectively. For the investigation of the mass yield ratios 149 and 151, the residence time of the irradiated sample was 12-13 h so as to ensure virtually complete decay of Nd^{149} . Further, it was assumed that the independent yield of Pm^{149} was small, i.e., the Nd^{147}/Nd^{149} yield ratio is thereby the ratio of the total yields of chains with mass numbers 147 and 149. Knowing these ratios, one may calculate the chain yields for these mass numbers.

From the results obtained we plotted the curve of the relation between the fission product yields and mass number (see the figure). The latter also gives the fragment yield distribution for spontaneous fission of U^{238} [19-21] and photofission by γ -quanta with maximum energy 8 MeV [1].

We did not obtain data on fragment yields in the mass range 94-103 and 132-141. Therefore, in these ranges the curve of the fragment mass distribution was drawn as a dotted line through the fragment yields for U^{238} photofission by γ -quanta with maximum energy 13 MeV, given in [22]. Since the difference in the excitation energies is small, it may be assumed that the fragment mass distribution curve in these ranges is similar to that obtained with maximum γ -quanta energy 14 MeV. It is interesting to note that in these ranges the yield curve obtained with γ -quanta energy 8 MeV [1] is almost the same.

When the curves (see the figure) for spontaneous fission were plotted, it was assumed that $\bar{\nu} = 2$, and that for photofission at 8 and 13 MeV $\bar{\nu} = 3$. Smooth mass yield curves were not constructed, assuming that local deviations from the above nature of these relations are the rule rather an exception.

The principal characteristics of the mass distribution curves shown in the figure are given in Table 2.

We also investigated the relation between the change in the 151/143 mass yield ratio and maximum bremsstrahlung energy in the range 8-14 MeV:

Maximum bremsstrahlung energy, MeV	Pm^{151}/Ce^{143} yield ratio
8.0	0.30 ± 0.01
10.0	0.27 ± 0.03
12.0	0.31 ± 0.01
14.0	0.25 ± 0.05

The error in the determination of the maximum bremsstrahlung energy was estimated as ± 0.3 MeV.

DISCUSSION OF THE RESULTS

A comparison of the mass yield curves in the figure and an examination of Table 2 reveal the regular nature of the excitation energy increase of the nucleus undergoing fission. A reduction of the mass yields in the peaks of light and heavy fragment groups and an increase in the symmetrical fission yields are observed. With increasing excitation energy the width of the main mass distribution peaks increases. We may evidently also assume that the

yields of markedly asymmetric masses increase with increasing excitation energy. Extrapolation at masses > 151 for U^{238} photofission at 14 MeV gives a $d \log Y/dA$ value which is less (in absolute value) than for spontaneous fission and fission by quanta with maximum energy 8 MeV.

It is difficult to compare our data for yields of 145-151 asymmetric masses with those of other investigators because we do not know of any directly measured yields in this mass range for U^{238} photofission at low or medium excitation energies. We can only compare the yields of the mirror-image masses. However, it should be mentioned that recent data on the relation between the number of prompt neutrons and the fragment mass [23-26] render such a comparison qualitative rather than quantitative.

It may be seen from our data that we did not find a change in the 151/143 asymmetric mass yield ratio with a change in maximum bremsstrahlung energy from 8 to 14 MeV. This justifies the conclusion that there is no change in fragment yields in the 143-151 mass range, or that the change in yields in the excitation energy range 6.8-11.5 MeV is very small. This probably agrees with arguments that only the yields of markedly asymmetric masses at $A > 153$ and $A < 83$ depend greatly on the excitation energy [27]. However, a comparison of mass distribution for U^{238} spontaneous fission and photofission at 8 and 14 MeV with data in [1] on photofission at 5.5-8 MeV shows a marked change in yields for the mass range 140-147 as one passes from spontaneous to induced fission.

In [22] the yields for U^{238} photofission by γ -quanta with maximum energy MeV in the mass range 99-105 were investigated in detail; it was found that at a mass number 105 there is a deviation in the smooth course of the curve. This was interpreted as a "fine structure," additional to the heavy peak and due to the high probability of formation of fission fragments with complete shells of 50 protons (Sn_{50}^{130}). Our data for this mass region appear to corroborate this deviation at a mass of 105.

It should be mentioned that there is another viewpoint as regards the nature of local deviations from the smooth mass yield distribution curve. The authors of [26], who investigated hot neutron-induced U^{238} fission, relate such deviations to simple variation of the probability of emission from prompt fission fragments in relation to the mass, and they consider that the hypothesis of greater probability of magic nuclei in a fission event does not correspond with the facts.

We are very grateful to V. P. Shvedov and A. V. Stepanov for permission to use the continuous electrophoresis apparatus and for their help in this work.

LITERATURE CITED

1. R. Duffield, R. Schmitt, and R. Sharp, Report No. 678, Presented by the American Delegation to the Second International Conference on the Peaceful Uses of Atomic Energy, Geneva (1958).
2. A. K. Lavrukina, et al., In the symp.: Physics of the Fission of Atomic Nuclei [in Russian], Moscow, Gosatomizdat, p. 210 (1962).
3. V. P. Shvedov, et al., Radiokhimiya, 6, 711 (1960).
4. A. Pappas and S. Alstad, J. Inorg. Nucl. Chem., 17, 195 (1960); 15, 222 (1960).
5. R. V. Sedletskii and K. A. Petrzhak, Radiokhimiya, 4, 99 (1962).
6. D. Hume, National Nuclear Energy Series. Plutonium Project Record, Vol. 9, book 3. Radiochemical Studies of the Fission Products, p. 261 (1951).
7. R. Schmitt and R. Duffield, Phys. Rev., 105, 1277 (1957).
8. I. A. Vasil'ev and K. A. Petrzhak, Z. éksperim. i teor. fiz., 35, 1135 (1958).
9. H. Richter and C. Coryell, Phys. Rev., 95, 1550 (1954).
10. O. Hahn, Applied Radiochemistry, Ithaca, N.Y., Cornell University Press (1936).
11. O. Hahn, Z. Phys. Chem., 103, 461 (1923).
12. K. A. Petrzhak and R. V. Sedletskii, Pribery i tekhnika éksperimenta, 2, 32 (1960).
13. K. A. Petrzhak and R. V. Sedletskii, Pribery i tekhnika éksperimenta, 5, 177 (1961).
14. B. D. Kuz'minov, et al., Zh. éksperim. i teor. fiz., 37, 406 (1959).
15. R. Sher and I. Leroy, Nucl. Energy. A., 12, 101 (1960).
16. Yu. S. Zamyatnin, In the symp.: Physics of the Fission of Atomic Nuclei [in Russian], Moscow, Gosatomizdat, p. 103 (1962).
17. L. Glendenin, C. Coryell, and R. Edwards, National Nuclear Energy Series. Plutonium Project Record, Vol. 9, book 3. Radiochemical Studies of the Fission products, p. 489 (1951).
18. A. Pannas, Proceedings of the First International Conference on the Peaceful Uses of Atomic Energy, Geneva (1958).

19. P. Kuroda and M. Menon, Nucl. Sci. Engng., 10, 70 (1961).
20. B. Young and H. Thode, Canad. J. Phys., 38, 1 (1960).
21. G. Wetherill, Phys. Rev., 92, 907 (1953).
22. D. Wiles and C. Coryell, Phys. Rev., 96, 696 (1954).
23. V. F. Apalin, et al., Atomnaya énergiya, 8, 15 (1960).
24. J. Freser and I. Milton, Phys. Rev., 93, 818 (1954).
25. S. Whetstone, Phys. Rev., 114, 581 (1959).
26. H. Farrar and R. Tomlinson, Canad. J. Phys., 40, 943 (1962).
27. T. Sugihara, et al., Phys. Rev., 108, 1264 (1957).

All abbreviations of periodicals in the above bibliography are letter-by-letter transliterations of the abbreviations as given in the original Russian journal. *Some or all of this periodical literature may well be available in English translation.* A complete list of the cover-to-cover English translations appears at the back of this issue.

THE EFFECT OF THE IRON MINERALS IN ORES ON OXIDATION
OF URANIUM IN ACID

G. M. Alkhazashvili, G. M. Nesmeyanova, and L. N. Kuz'mina

Translated from *Atomnaya Énergiya*, Vol. 15, No. 4,
pp. 313-317, October, 1963
Original article submitted December 17, 1962

This paper gives the results of an investigation into the effect of iron minerals on extraction of uranium from pitchblende in dilute sulfuric acid containing oxidizing agents. From these results a more efficient method may be selected for extraction of uranium according to the composition of the ore material.

This work confirms the opinion that Fe(II) ions have an unfavorable effect on oxidation of uranium by a mixture of nitric and sulfuric acids; this shows that relatively dilute solutions of mixed acids (<100 g/liter) cannot be used for extracting uranium from ores with high pyrite contents. It is also shown that the presence of limonite, magnetite, pyrite and siderite makes it possible to extract uranium by dilute sulfuric acid containing MnO_2 .

The method selected for bringing uranium into solution depends largely on the ore composition [5, 8]. As the various components contained in non-uranium minerals pass into solution they exert a marked effect on leaching-out of uranium from the ores. To characterize the process taking place during uranium leaching, it is therefore necessary to have data on the behavior of the individual minerals and the nature of the effect of admixtures on leaching.

In [1] it was shown by way of example of uranium oxides that the presence of elements of variable valence (Fe, Mn, Cu, Ni, Co, V) in the solution not only increases the degree of uranium extraction, but also makes it possible to dissolve uranium at relatively low sulfuric acid concentrations. Confirmation was provided by an investigation of dissolution of uranium from pitchblende in [2, 3], where it was shown that the iron in pitchblende greatly accelerates oxidation of uranium in acid. The process may be speeded up and the degree of uranium dissolution increased by adding Fe(III) ions to the reaction mixture [1, 2].

The extent to which the iron minerals in uranium ores affect the oxidation of uranium depends on their solubility. Leaching of uranium from ores containing readily soluble iron minerals may therefore be carried out under milder conditions than from ores with minerals soluble in acids only with difficulty [4, 5].

Data in [2, 4] gave the results of dissolution of various minerals in acid: pitchblende, hematite, siderite, magnetite, limonite, pyrite and covellite. Later, experiments were carried out on mixtures of pitchblende with each of these minerals and then with a mixture of all of them. H_2SO_4 (concentration 5-100 g/liter) served as solvent, and MnO_2 and HNO_3 were used as oxidizing agents. The duration of the experiments was 3 h at 20°C and 1 h at 90°C, the reason for selecting these times being the relatively high extraction of uranium from pitchblende in the absence of mineral additions.

The consumption of sulfuric acid and oxidizing agent was calculated with respect to principal admixtures in pitchblende and for each mineral separately; the ratio of pitchblende to an iron mineral was 1:2.

A comparison of the results of mineral dissolution in sulfuric acid showed that uranium is extracted from pitchblende far more readily than iron from limonite, hematite and pyrite. For example, at the above sulfuric acid concentration, 18-48% uranium is extracted from pitchblende in 30 min at 90°C. Under these conditions only 0.7% iron is extracted from hematite, even when the H_2SO_4 concentration is 100 g/liter. At concentrations of 5-400 g/liter, 2-4% iron is extracted from pyrite, irrespective of the duration of the experiment (15-300 min). When magnetite is treated with H_2SO_4 , Fe(II) passes into solution more readily than Fe(III). If the H_2SO_4 concentration < 50 g/liter, very little iron is extracted from magnetite; with an increase to 100-400 g/liter, extraction of Fe(II) and Fe(III) increases to 33-78% and 24-63% respectively in 3 h.

TABLE 1. Extraction of Iron from Minerals at 90°C in 3 h in Relation to the H₂SO₄ Concentration, %

Mineral	H ₂ SO ₄ concentration, g/liter						
	1.0	5.0	50	100	150	250	400
Limonite	8.3	2.4	36.2	49.2	65.2	44.3	77.1
Hematite	—	—	—	14.1	19.5	36.0	46.0
Magnetite	—	—	—	26.8*	34.7	49.4	67.2
				12.4	16.1	23.4	30.9
Pyrite	12.3	4.0	3.0	3.0	3.0	3.0	2.6
	14.0	8.8	—	24.1	29.1	36.3	39.0
Siderite	44.1	64.0	99.1	100	—	—	—
	29.0	33.0	46.4	72.2	74.6	76.6	77.8

*The figures below the lines give extraction of iron in presence of MnO₂.

TABLE 2. Extraction of Uranium from Pitchblende to an H₂SO₄ Solution + MnO₂ In the Presence of Various Minerals, %

Expt. No.	Mineral	H ₂ SO ₄ concentration, g/liter		
		5	25	100
1	—	47.2	55.4	65.0
2	Hematite	56.4	56.1	62.8
3	Limonite	56.8	63.8	64.4
4	Magnetite	66.5	—	85.3
5	Pyrite	85.4	85.6	88.6
6	Siderite	68.1	93.6	100.0
7	Covellite	71.4	82.0	96.6
8	Covellite + siderite	83.5	97.3	99.8
9	—	65.1	71.5	91.0
10	Hematite	74.2	81.1	95.3
11	Limonite	80.0	98.3	100.0
12	Magnetite	92.2	94.6	100.0
13	Pyrite	95.6	96.3	100.0
14	Siderite	85.2	96.8	100.0
15	Covellite	91.2	94.8	99.8
16	Covellite + siderite	85.1	88.3	99.8

Remark. Experiments 1-8 carried out at 20°C, experiments 9-16 at 90°C. Analyses of these minerals were given in [2, 4].

At an H₂SO₄ concentration of 1 g/liter, 75.8% iron is extracted from siderite in 5 h. At 100-400 g/liter H₂SO₄, siderite dissolves completely in 2 h.

Addition of an oxidizing agent (e.g., MnO₂) to the solution increases extraction of uranium from pitchblende: to 46-65% at 20°C (30 min), and to 65-91% at 90°C, depending on the sulfuric acid concentration. Extraction of iron from siderite is also greatly increased by addition of MnO₂, but extraction of iron from magnetite and siderite is reduced (Table 1).

The results of the experiments on dissolution of iron minerals show that the iron concentration in the solution varies in relation to the mineralogical composition of the ore. Therefore, the degree of uranium extraction or the duration of leaching depend on the type of iron minerals in the ore.

TABLE 3. Transfer of Uranium from Pitchblende to an $H_2SO_4 + HNO_3$ Solution in the Presence of Various Minerals, %

Expt. No.	Mineral	Concentration of the acid mixture, g/liter		
		10	50	100
1	—	15.0	17.8	27.5
2	Hematite	21.4	30.0	32.4
3	Limonite	17.1	27.8	75.0
4	Magnetite	19.6	28.9	83.6
5	Pyrite	42.0	42.1	55.0
6	Siderite	22.0	29.0	88.6
7	Covellite	22.5	38.6	48.9
8	Covellite and siderite	31.5	46.2	48.4
9	—	23.2	91.0	91.4
10	Hematite	97.4	98.6	99.0
11	Limonite	88.0	92.6	100.0
12	Magnetite	58.6	95.2	96.0
13	Pyrite	25.2	71.7	83.4
14	Siderite	24.4	78.6	86.0
15	Covellite	63.4	68.8	86.0
16	Covellite and siderite	78.0	90.0	98.6

Remark. Experiments 1-8 were carried out at 20°C; experiments 9-16 at 90°C.

When pitchblende is treated with an H_2SO_4 solution containing MnO_2 , additions of iron minerals to the reaction mixture greatly accelerate the process and increase extraction of uranium into the solution. Iron minerals show decreasing effect on uranium in the following order: siderite, pyrite, magnetite, limonite and hematite (Table 2). This sequence is particularly distinct if the process takes place at 20°C. Irrespective of the type of iron mineral added to the reaction mixture (with the exception of hematite), extraction of uranium to the solution is 100% at 90°C and an H_2SO_4 concentration of 100 g/liter. The similarity in the behavior of iron minerals at 90°C is due to the fact that at elevated temperatures the total amount of iron passing into the solution, even from relatively difficultly soluble minerals, is perfectly adequate to accelerate oxidation and dissolve uranium from pitchblende.

As regards the effect of iron minerals on dissolution of pitchblende in a nitric-sulfuric mixture (15% HNO_3 and 85% H_2SO_4), at 20°C and acid concentration 5-50 g/liter, that of siderite, magnetite, limonite and hematite is very slight (Table 3). With an increase in acid concentration to 100 g/liter, extraction of uranium is greatly increased. At 90°C the effect of ferric oxide minerals is greater than those containing Fe(II). This effect is particularly marked at low acid mixture concentrations.

Pyrite has a rather unusual effect: extraction of uranium into the solution decreases at 90°C and mixture concentration 50-100 g/liter (see Table 3, expts. 1 and 13). This may be due to the following: iron is virtually unextracted from pyrite at an acid mixture concentration of 10-50 g/liter. An increase to 100 g/liter or more increases the degree of dissolution of iron (Fig. 1), but the mixed acid only oxidized Fe(II) fairly rapidly at high concentrations (Table 4), whereas it is oxidized readily by MnO_2 in dilute sulfuric acid and even a neutral solution of an iron salt [6, 7].

As a result of the slow oxidation of Fe(II) at concentrations 100 g/liter or less, the solution contains a considerable number of Fe(II) ions; this retards oxidation of U(IV) by nitric acid [9, 10]. It should be mentioned that siderite, containing virtually no Fe(III), has the same effect on oxidation of uranium by nitric acid as pyrite.

When pitchblende mixed with the above-mentioned iron minerals is dissolved (Fig. 2), the amount of uranium transferred to the solution tends to increase, irrespective of the type of oxidizing agent used. It is characteristic that at 90°C the solvent concentration has little effect on extraction of uranium from a mixture of pitchblende and iron minerals. At 20°C, extraction of uranium by a nitric-sulfuric mixture of concentration 5 g/liter increases [due to oxidation by Fe(III) ions] from 15.2 to 42.1% and reaches 65% at a mixture concentration of 100 g/liter.

TABLE 4. Fe(II) Content of the Solution (% of Initial Content) in Relation to the $H_2SO_4 + HNO_3$ Concentration, Temperature and Time

Acid concentration, g/liter	Time, min									
	0	5	15	30	60	120	180	240	300	360
Temperature 70°C										
100	100.0	100.0	99.6	99.5	99.2	97.4	96.6	94.0	91.6	—
200	100.0	100.0	100.0	100.0	100.0	94.0	86.5	78.8	78.5	—
300	100.0	96.6	90.5	79.6	62.6	35.5	0.0	—	—	—
Temperature 90°C										
100	100.0	96.0	96.0	95.0	92.5	85.5	82.0	78.6	69.5	68.4
200	100.0	94.5	91.5	80.0	51.0	0.0	—	—	—	—

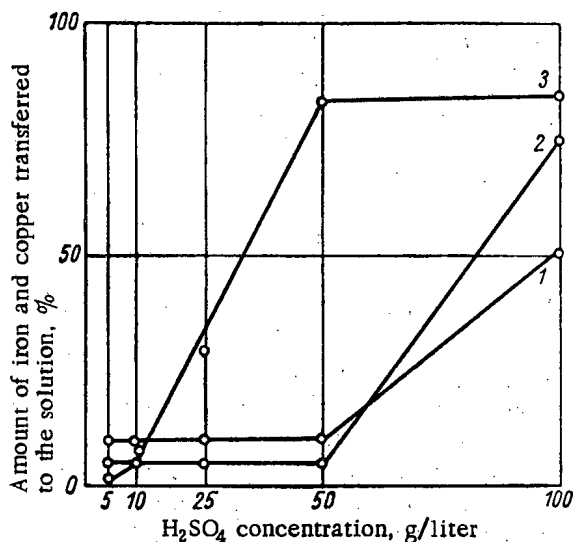


Fig. 1. Effect of the concentration of the nitric-sulfuric acid mixture on transfer of iron and copper to the solution from pyrite (1), covellite (2) and siderite (3) at 90°C in 1 h.

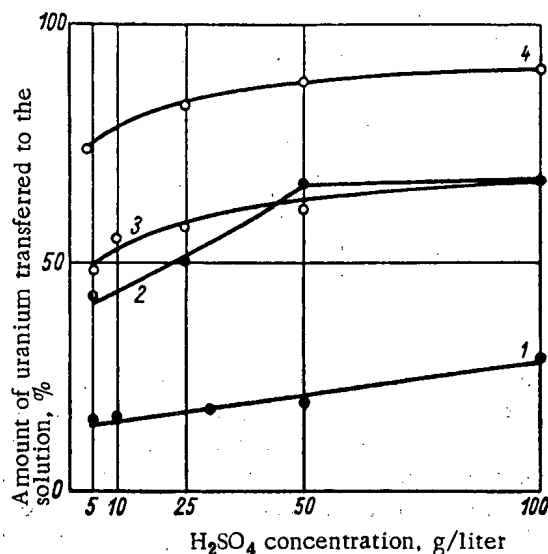


Fig. 2. Relation between extraction of uranium from pitchblende (1, 3) and a mixture of iron minerals and pitchblende (2, 4), and the concentration of sulfuric acid containing MnO_2 (O) or HNO_3 (●) as oxidizing agent at 20°C in 3 h.

We also investigated the effect of copper sulfide-covellite on extraction of uranium into the solution. By way of admixture, the mineral sample contained 20.3% iron, the copper and sulfide sulfur contents being 38.77% and 37.25% respectively. We used a 1:1 pitchblende/covellite ratio, corresponding to a 1:0.55 U/Cu ratio.

The results of the experiments (see Table 2) show that in the presence of covellite and MnO_2 , extraction of uranium increases over the whole range of H_2SO_4 concentrations. In the case of oxidation of uranium by nitric acid (see Table 3) in sulfuric acid at 20°C the degree of dissolution of uranium increases, but decreases at 90°C and an acid mixture concentration of 50-100 g/liter. A comparison of these results with data characterizing the effect of pyrite on extraction of uranium by a mixture of nitric and sulfuric acids shows that their character is identical.

However, it should be mentioned that siderite, pyrite and covellite always contain an admixture (fairly considerable in some cases) of Fe(III). When these minerals are added to the reaction mixture, Fe(III) passes into solution and reacts with uranium, acting as an additional oxidizing agent. In such cases the unfavorable effect of Fe(II) on uranium oxidation by an acid mixture is compensated by the favorable effect of the Fe(III) ions.

A comparison of the dissolution curves of pitchblende in sulfuric acid containing Fe(III) as oxidizing agent, and in a nitric-sulfuric acid mixture in the presence of covellite or pyrite shows that the relationship is almost identical (Fig. 3). In the latter case, uranium is oxidized in the same way as in the absence of nitric acid. These results confirm the conclusion drawn in [9] from an investigation of the oxidation of pure oxides.

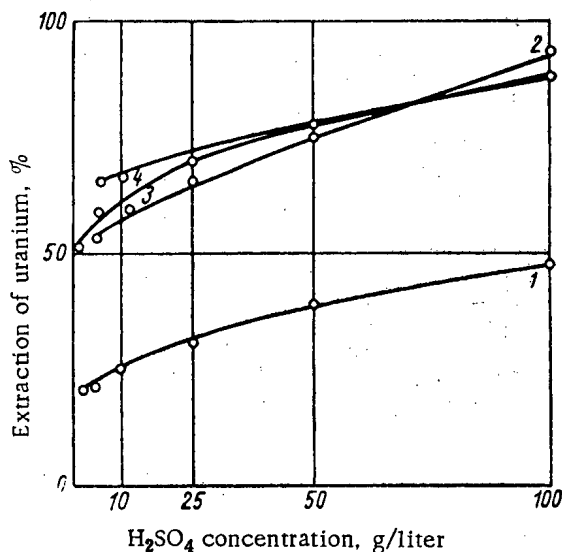


Fig. 3. The effect of the concentration of sulfuric acid (1), a nitric-sulfuric acid mixture (2), an acid mixture in the presence of pyrite and covellite (3) and sulfuric acid (4) + $\text{Fe}_2(\text{SO}_4)_3$ on the dissolution of pitchblende in 1 h.

The reduction in uranium extraction in an acid mixture when covellite is present in the reaction mixture may be compensated by adding siderite (see Table 3). In these experiments the pitchblende/siderite/covellite ratio was 1:3:1, corresponding to a U:Fe:Cu ratio of 1.0:1.5:0.55, and the Fe(III) content of siderite was 15.4%.

SUMMARY

1. When pitchblende is dissolved in H_2SO_4 containing MnO_2 or HNO_3 as oxidizing agent, the presence of iron and copper minerals greatly accelerates the process and increases the extraction of uranium into the solution.

2. Of the ferric oxide minerals, limonite has the greatest effect on extraction of uranium by sulfuric acid with MnO_2 ; of the ferrous oxide minerals, siderite, which is the most readily soluble in sulfuric acid, has the most marked effect.

3. When pitchblende is dissolved in a mixture of nitric and sulfuric acid, ferric oxide passes from the minerals into solution, thereby increasing the extraction of uranium. At acid mixture concentrations less than 100 g/liter, ferrous iron has an unfavorable effect on the process.

LITERATURE CITED

1. G. M. Nesmeyanova and G. M. Alkhazashvili, *Atomnaya énergiya*, 10, 587 (1961).
2. G. M. Alkhazashvili and G. M. Nesmeyanova, *Atomnaya énergiya*, 13, 170 (1962).
3. G. M. Nesmeyanova, *Atomnaya énergiya*, 11, 456 (1961).
4. G. M. Nesmeyanova and N. K. Chernushevich, *Atomnaya énergiya*, 9, 137 (1960).
5. A. P. Zefirov, B. V. Nevskii, and G. F. Ivanov, *Uranium Ore Processing Plants in Capitalist Countries* [in Russian], Moscow, Gosatomizdat (1962).
6. G. M. Nesmeyanova and A. I. Vikulov, *Zh. prikl. khim.*, 35, 989 (1962).
7. D. H. A. Koch, *Austral. J. Ch.*, 10, 150 (1957).
8. B. V. Nevskii, *Atomnaya énergiya*, 6, 5 (1959).
9. G. M. Nesmeyanova and G. M. Alkhazashvili, *Atomnaya énergiya*, 8, 330 (1960).
10. C. Addison and J. Lewis, *Uspekhi khimii*, 25, 1121 (1955).

All abbreviations of periodicals in the above bibliography are letter-by-letter transliterations of the abbreviations as given in the original Russian journal. Some or all of this periodical literature may well be available in English translation. A complete list of the cover-to-cover English translations appears at the back of this issue.

LETTERS TO THE EDITOR

STUDY OF THE MOTION OF INDIVIDUAL CHARGED PARTICLES
IN CORRUGATED MAGNETIC FIELDS

V. M. Balebanov, V. B. Glasko, A. L. Groshev, V. V. Kuznetsov,
A. G. Sveshnikov, and N. N. Semashko

Translated from *Atomnaya Énergiya*, Vol. 15, No. 4,
pp. 318-319, October, 1963

Original article submitted March 13, 1963

Theoretical [1, 2] and experimental [3, 4] papers have shown that flute instability of the plasma arises in traps with magnetic mirrors. This instability should not occur if the particles undergo azimuthal drift ("effective drift") in a direction opposite to the Larmor rotation, and if the drift velocity is sufficient to compensate the effect of electric fields excited in the plasma. Effective drift of charged particles may be obtained by means of space modulation of the axially symmetric magnetic field along the trap axis.

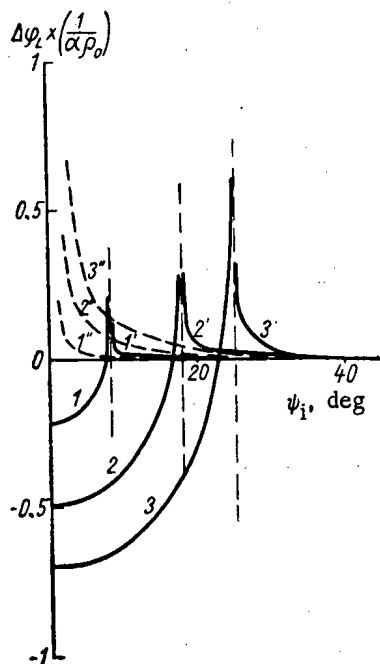


Fig. 1. Drift angle per period of the field $\Delta\varphi_L$ as a function of the injection angle ψ_i . The solid line denotes $\Delta\varphi_L$ for blocked (curves 1, 2, 3) and passed (curves 1', 2', 3') particles injected at the field minimum; the dashed line denotes $\Delta\varphi_L$ (curves 1'', 2'', 3'') for passed particles injected at the field maximum: (1) $\beta = 0.01$; 2)

$\beta = 0.05$; 3) $\beta = 0.1$; ρ_0) Larmor radius $\alpha = \frac{2\pi}{L}$.

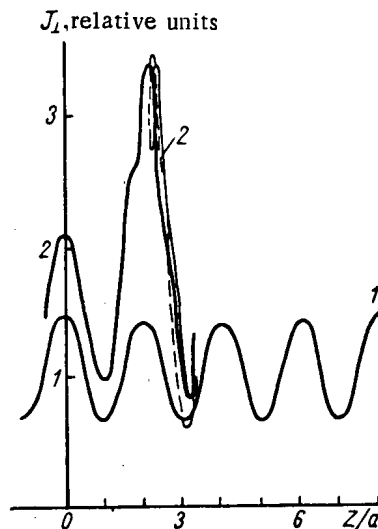


Fig. 2. Variation of J_{\perp} for particle motion in a periodic field (resonance case): 1) injection at the field minimum; 2) injection at the inflection of the lines of force of the increasing field; the solid line denotes forward motion in the direction $z > 0$; the dashed line denotes reverse motion; z/a denotes distance along the axis, in relative units.

Solution of the equations of motion of a charged particle in a linear corrugated magnetic field [5] (drift approximation) indicates the existence of a range of injection angles ψ_i (Fig. 1) in which the effective drift $\Delta\varphi$ becomes greater than zero, and also the presence of a resonance for a value of ψ_i corresponding to the boundary be-

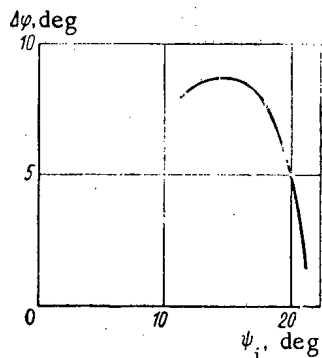


Fig. 3. Drift angle $\Delta\varphi$ as a function of injection angle ψ_i in the periodic field of ÉMO-2.

tween the passed particles and those blocked in a period of the field. Raising the depth of modulation β of the field causes an increase in the azimuthal drift velocity. Changing the injection point from the minimum of the field to its maximum widens the range of ψ_i corresponding to effective drift. The curves of Fig. 1 clearly show that the achievement of effective drift in a trap with several periods of corrugated field and with mirrors at the ends is a complex problem, since in the neighborhood of the mirrors there may be some compensation of the effective drift obtained while the particles are passing through the periodic region. This is confirmed experimentally.

By carrying out a first integration of the exact equations of motion (allowing for the axial symmetry of the magnetic field), we determined the regions for which the particles [6] are absolutely retained within the trap, corresponding to a definite group of particles with certain values of total velocity and injection angle ψ_i . The size of the region and the way in which it is filled with particle trajectories (partial or equilibrium) depends on the injection parameters. We also found sub-regions corresponding to the absolute retention of atomic ions arising from the dissociation of molecular ions in "Ogra."

Numerical integration of the exact equations of motion of particles in a periodic magnetic field gave good agreement with the analytical solution of the equations (linear approximation). Motion in the resonance case [7], where the pitch of the helical trajectory of the particle coincides with the field period L , was studied in detail. It was shown that the character of the change in the magnetic moment of the particle J_{\perp} essentially depends on the position of the injection point with respect to the field minimum (Fig. 2).

The motion of individual charged particles in a periodic magnetic field with mirrors was experimentally studied in the ÉMO-1 and ÉMO-2 installations, electron models of "Ogra," approximately 1/8 of its normal size. A narrow beam of 5 keV electrons (current up to 100 μ A) was injected into the vacuum chamber (pressure $\sim 10^{-6}$ mm Hg) in the angular range $\psi_i = 0$ to $\pm 23^\circ$. The magnetic field of the trap (~ 100 G) was produced by a stepped cylindrical coil. The value of β varied from 0 to 20%, the number of field periods between the mirrors varied from two to ten, and the reflecting ratio was 1.2.

The investigations with ÉMO-1 showed that the character of the change in drift velocity essentially depended on the positions of the injection points of the particles and their points of reflection from the mirrors with respect to the field minimum, and that in some cases, after a few reflections from the mirrors, the particles acquired effective drift.

In ÉMO-2 the drift velocity, averaged for a large number of reflections (up to several hundred), was determined by measuring the lifetime of particles after the injection of the beam had ceased [8]. The error in determining the drift velocity was no more than 10%. Significant values of drift velocity $\Delta\varphi$ (up to 10° for one reflection from the mirrors) were observed when the period of the corrugated field was large and the depth of modulation β greater than 8%. In the majority of cases the effective drift velocity increased with increasing β . The increase in β was however limited by the collision of particles with the chamber walls in regions of minimal field. In cases with large drift velocities $\Delta\varphi$ is proportional to β^2/L , in agreement with the conclusions of the drift approximation [5]. As the reflecting ratio rose, the effective drift velocity fell. For an unmodulated field with mirrors "destructive" drift was observed. The dependence of $\Delta\varphi$ on ψ_i has a maximum (Fig. 3), corresponding to transition of particles from the passed to the blocked state. It is of course not possible to observe a sharply defined resonance on account of the beam spread (angular divergence $\pm 20^\circ$) and the presence of the mirrors.

Thus by means of space modulation of the magnetic field of a trap with mirrors, it is possible to obtain a marked degree of drift velocity, but this largely depends on the reflecting ratio and the injection angle of the particles.

The authors express deep gratitude to I. N. Golovin and A. N. Tikhonov for constant interest in the work and valuable comment during discussion of the results, and also P. S. Strelkov and A. A. Roslov for help in carrying out the experiments.

LITERATURE CITED

1. M. Rosenbluth and C. Longmair, *Ann. Phys.*, **1**, 120 (1957).
2. B. Kadomtsev, *Physics of Plasma and Problems of Controlled Thermonuclear Reactions*, Vol. 4, Moscow [in Russian], Izd. AN SSSR, p. 16 (1958); *Zh. éksperim. i teor. fiz.*, **40**, 328 (1960).

3. M. S. Ioffe, R. Sobolev, and E. Yushmanov, *Zh. éksperim. i teor. fiz.*, 39, 1602 (1960); 40, 40 (1961).
4. G. F. Bogdanov, et al., Doklad. CN 10/210, presented to the International Conference on Plasma Physics and Controlled Thermonuclear Synthesis. Salzburg, MAGATÉ (1961).
5. A. Morozov and L. Solov'ev, *Zh. tekhn. fiz.*, 30, 261 (1960).
6. V. M. Balebanov, et al., see [4], Report CN 10/211.
7. V. Fedorchenko, B. Rutkevich, and B. Chernyi, *Zh. tekhn. fiz.*, 29, 1212 (1959).
8. G. Bogdanov, D. Panov, and N. Semashko, *J. Nucl. Energy, Part C*, 3, 106 (1961).

All abbreviations of periodicals in the above bibliography are letter-by-letter transliterations of the abbreviations as given in the original Russian journal. *Some or all of this periodical literature may well be available in English translation.* A complete list of the cover-to-cover English translations appears at the back of this issue.

THE OVER-ALL KINETIC ENERGY OF U^{233} AND Th^{232} FRAGMENTS

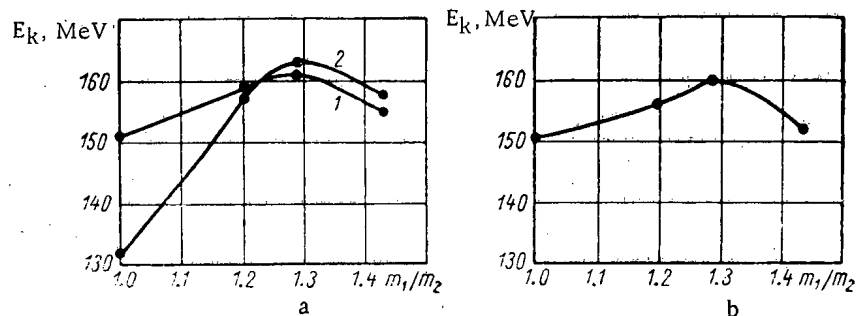
S. S. Kovalenko, K. A. Petrzhak, and V. M. Adamov

Translated from Atomnaya Énergiya, Vol. 15, No. 4,

pp. 320-321, October, 1963

Original article submitted September 14, 1962

We have measured the over-all kinetic energy of fragments for various types of fission: U^{233} and Th^{232} by 14.5-MeV neutrons and U^{233} by hot neutrons. The procedure and apparatus used were described in [1]. The U^{233} target thickness was 10 mg/cm^2 ; for Th^{232} the thickness was 50 mg/cm^2 . The over-all kinetic energy was measured for the following mass ratios of the fragments: 1, 1.2, 1.3 and 1.43. At least 10^3 fission events were recorded for each point. Further experiments were carried out to determine the effect of certain factors on the accuracy of the results. Particular attention was paid to the recording accuracy of the type of fission determined.



Relation between the over-all kinetic energy and mass ratio of fragments during fission of U^{233} (a, curve 1) and Th^{232} (b) by 14.5-MeV neutrons, and U^{233} (a, curve 2) by hot neutrons.

In [1] a single-humped curve was obtained from measurements of the unilateral spectra of the kinetic energy of symmetrical fission fragments (with resolution in an analyzer). This indicates recording of symmetrical fission, but the data were obtained only during fission by 14.5-MeV neutrons when the symmetrical fission intensity was high. The maximum error occurs during the investigation of hot neutron-induced symmetrical fission, because in this case there may be a considerable contribution from more intense (asymmetric) fission due to boundary effects in the target. It has been shown experimentally that for U^{233} fission the ratio of asymmetric fission intensity to symmetrical fission intensity, i.e., the ratio of the peak to the valley, is 180. Single-humped curves were also obtained for the unilateral spectra of symmetrical fragments. With fission by 14.5-MeV neutrons the ratio of the peak to the valley is 5, which agrees with radiochemical data. In the case of recording of unilateral spectra for mass ratios slightly different from symmetrical fission, the curves are double-humped, with a peak ratio corresponding to the selected mass ratio.

With use of 14.5-MeV neutrons a large number of α -particles is formed in the chamber as a result of an (n, α) reaction in the gas. The α -particle energy > 15 MeV because the reaction threshold is close to zero. It was therefore necessary to determine the effect of random coincidences of α -particle pulses and those of the fragments on the measured over-all kinetic energy spectra. The over-all kinetic energy of the fragments was measured during a tenfold variation in the bombarding neutron flux. The variation in the over-all value was not more than 1.5 MeV; therefore the effect of random coincidences is within the limits of experimental error.

The results of measurements of the over-all kinetic energy are given in the figure. The kinetic energy of symmetrical fragments was measured to an accuracy of ± 5 MeV; the error for the other types of fission was ± 2 MeV. Like the case of U^{235} [2], the kinetic energy of symmetrical U^{233} fission fragments with fission by 14.5 MeV neutrons

is 20 ± 5 MeV higher than for hot-neutron fission. A characteristic feature is that the dip in kinetic energy in the case of symmetrical fission of U^{233} and Th^{232} by 14.5-MeV neutrons is far smaller than that in [1, 2] for U^{235} and U^{238} by such neutrons. This may be due to the appearance of a third symmetrical peak on the mass distribution curve for U^{233} and Th^{232} . The data show that there is a similarity in the behavior of the symmetrical fragment yields and their kinetic energy during a change in the bombarding particle energy. The table gives data on the symmetrical fragment yields, measured to an accuracy of 10% [3, 4] and the kinetic energies for several nuclei. The symmetrical fragment kinetic energy for U^{233} and U^{235} is taken from our data and [1, 2], and for Pu^{239} , from [5]. The error in the kinetic energy determination for our investigations and [1, 2] is ± 5 MeV; [5] does not give the error. The difference in the symmetrical fragment yields cannot be due to the difference in the excitation energies because the bond energies of the youngest neutron for these nuclei are very similar (see the table). Although the observed effect is practically within the limits of experimental error, an examination of the data together with those for different excitation energies of the nucleus undergoing fission shows that there is some correlation between the symmetrical fragment yield and their kinetic energy. It is worth noting that the behavior of the maximum kinetic energy differs from that of the kinetic energy of symmetrical fragments and (see the table) its value increases steadily with increasing atomic weight.

Yields and Kinetic Energies of Symmetrical Fission Fragments

Indices	Nucleus		
	U^{233}	U^{235}	Pu^{239}
Kinetic energy of symmetrical fragments, MeV	140	135	147
Yield of symmetrical fragments, %	0.018	0.01	0.04
Maximum kinetic energy of the fragments $\left(\frac{m_1}{m_2} = 1.25\right)$, MeV	175	177	182
Bond energy of the youngest neutron, MeV	6.74	6.39	6.38

The results of a radiochemical investigation of the products of Ra^{226} fission by particles of different energy show that there is a slight change in the symmetrical fragment yield and a considerable change in the yields of fragments corresponding to asymmetric peaks and valleys [6]. The authors of [7] investigated the behavior of the over-all kinetic energy in relation to the mass ratio of the fragments during splitting of Ra^{226} by deuterons of different energy. A comparison of the results with those of radiochemical investigations shows that the kinetic energy changes most markedly in the mass ratio region in which the change in fragment yield is greatest. The results in [6, 7] are insufficiently accurate for any quantitative assessment. The most interesting fact in the case of Ra^{226} is that the kinetic energy of the fragments increases with increasing yield and decreases when the latter decreases. This is further evidence that a very general correlation exists between the fragment yields and their kinetic energy.

It may now be assumed that the kinetic energy of the fragments is determined by Coulomb repulsion during fission, and its value depends on the effective distance between the centers of the fragment charges. As regards the numbers of protons, symmetrical fragments from fission of nuclei heavier than thorium, and fragments corresponding to the "heavy" valley in Ra^{226} fission are included in the region of markedly deformed nuclei. Asymmetric fragments belong to the region of slightly deformed nuclei. Maximum kinetic energy corresponds to fragments with a complex neutron shell of 82 neutrons. To know the behavior characteristics of the kinetic energy of fragments, it is evidently necessary to take into account the different deformabilities of the nuclear material during fission. In [8] it was shown that with increasing nuclear deformation the shell effects disappear at a deformation parameter $\alpha_2 = 0.05$, but reappear at $\alpha_2 = 0.2-0.3$. At low excitation energies fission is adiabatic; therefore it may be assumed that in the presence of a degree of nuclear deformation at which shell effects occur in the fragments a system which is favorable from the energy viewpoint is produced. Fragments corresponding to spherical or slightly deformed nuclei may be formed at lower deformations of the nucleus undergoing fission. The probability of symmetrical fission in such a case will be defined by the ratio of the number of nuclei reaching the required deformation to the number of nuclei split in the earlier deformation stages.

Therefore, the extent to which symmetrical fission takes place adiabatically is greater, and shell effects play a more important role in the former than in asymmetric fission. With increasing excitation the degree of adiabaticity decreases and likewise the role of the shell effects. In this case symmetrical fission may occur at lower deformations of the nucleus, which leads to an increase in its probability and an increase in the kinetic energy of the fragments.

LITERATURE CITED

1. V. M. Adamov, S. S. Kovalenko, and K. A. Petrzhak, *Zh. éksperim. i teor. fiz.*, 42, 1475 (1962).
2. S. S. Kovalenko, K. A. Petrzhak, and V. M. Adamov, *Atomnaya énergiya*, 13, 474 (1962).
3. S. Katcoff, *Nucleonics*, 16, 78 (1958).
4. G. I. Marchuk and V. V. Smelov, *Neutron Physics* [in Russian], Moscow, Gosatomizdat, p. 157 (1961).
5. I. Milton and K. Frasser, *Phys. Rev. Letters*, 7, 67 (1961).
6. A. Fairhall, K. Zensen, and E. Neuzil, *Proceedings of the Second United Nations International Conference on the Peaceful Uses of Atomic Energy*, Vol. 15, Geneva, UNO, p. 452 (1958).
7. H. Britt, H. Wegner, and S. Gursky, *Phys. Rev. Letters*, 8, 98 (1962).
8. B. T. Geilikman, *Physics of the Fission of Atomic Nuclei* [in Russian], Moscow, Gosatomizdat, p. 5 (1962).

All abbreviations of periodicals in the above bibliography are letter-by-letter transliterations of the abbreviations as given in the original Russian journal. *Some or all of this periodical literature may well be available in English translation.* A complete list of the cover-to-cover English translations appears at the back of this issue.

DELAYED NEUTRONS FROM FISSION OF U^{233} BY 15-MeV NEUTRONS

B. P. Maksyutenko

Translated from Atomnaya Energiya, Vol. 15, No. 4,

pp. 321-322, October, 1963

Original article submitted April 18, 1963

A U^{233} sample of weight 3.63 g and diameter 30 mm was bombarded by a 15-MeV neutron flux and then enclosed in a polyethylene block containing 10 BF_3 -filled counters connected in parallel. A high voltage was switched into the system simultaneously in the cascade generator and the neutron flux fell to zero for a fraction of a second. Two series of bombardments were carried out (300 and 30 sec). The neutron counting efficiency was 10%.

Relative Yield of Delayed Neutrons

Group No.	Half-life, sec	Relative units
1	55	1.00 ± 0.01
2	24	0.78 ± 0.04
3	15.5	1.89 ± 0.30
4	5.2	1.20 ± 0.37
5	2.2	8.04 ± 1.04

The relative yields of all groups at preset half-lives (see the table) were determined from the over-all decay curve corresponding to bombardment for 300 sec. The value of the yield ratio of the first two groups was introduced into a system of equations describing the decay curve corresponding to 30-sec bombardment, and the relative yields of all groups except the second one were found. The error of the result for the 3-5 groups was determined from the scatter of the results of these two series of measurements, using Student's criterion. The relative yield error of the first two groups was determined from the integral count and the duration of the measurement interval. The system of equations was solved by electronic computer. The results of the calculations are given in the table.

The total yield of delayed neutrons accompanying fission of U^{233} by 15-MeV neutrons is 1.6 times greater than for fission by hot neutrons and 3.8-MeV neutrons, and is 0.780 ± 0.066 of the total yield of delayed neutrons accompanying hot-neutron fission of U^{235} .

I would like to thank N. V. Golodova for programming the calculations.

DETERMINATION OF THE PARTIAL ALPHA-DECAY PERIOD OF Pu²⁴¹

R. B. Ivanov, A. S. Krivokhatskii, L. M. Krizhanskii,
V. G. Nedovesov, and M. I. Yakunin

Translated from Atomnaya Énergiya, Vol. 15, No. 4,
pp. 322-323, October, 1963

Original article submitted January 23, 1963

The isotope Pu²⁴¹ undergoes β - and α -decay. The partial α -decay period T_α of this isotope has been frequently determined, but the results have a wide scatter. According to recent data, the partial α -decay period of Pu²⁴¹ has the following values: $T_\alpha = (5.62 \pm 0.2) \cdot 10^5$ years [1] and $(5.72 \pm 0.1) \cdot 10^5$ years [2], as against $1 \cdot 10^6 - 2.5 \cdot 10^5$ in [3-5]. The results in [1, 2] were obtained by the same method and agree closely, but differ considerably from the values in [4, 5].

Values Used in Calculating T_α For Pu²⁴¹

Mass No. of the isotope	N_i	S_i	T_i , years	T_α for Pu ²⁴¹ , years (calculated)
238	9.556	$2.078 \cdot 10^{-3}$	86.4 [7]	$3.97 \cdot 10^5$
240	0.441	$6.712 \cdot 10^{-2}$	6600 [8]	$4.34 \cdot 10^5$
242	0.423	0.473	$3.88 \cdot 10^5$ [9]	$3.47 \cdot 10^5$

We determined T_α by a different method than that in [1, 2]. The relative Pu²⁴¹ content of the mixture of plutonium isotopes was determined by mass-spectrometric analysis, together with use of ionization α -spectroscopy. By using a magnetic α -spectrometer [6] one may determine the intensity of α -transitions for each isotope and thereby find the relative number of Pu²⁴¹ α -decays. From the data obtained the partial period of Pu²⁴¹ α -decay may be calculated by means of the equation

$$T_\alpha = T_i \frac{N_i}{S_i},$$

where T_i is the half-life of the isotope; N_i is the ratio of the number of Pu²⁴¹ atoms to the number of atoms of the isotope; S_i is the ratio of the number of Pu²⁴¹ α -decays to the number of α -decays of the given isotope.

The table gives the values of N_i , S_i and T_i , and the T_α values found from these. The mean value of T_α is $(3.9 \pm 0.4) \cdot 10^5$ years, which is nearly one-and-a-half times less than in [1, 2], but agrees with [3, 4]. The authors of [2] state that the reason for the discrepancy between their results and [3] is that the number of Pu²⁴¹ α -decays in [3] is too high due to Pu²⁴². In our work this error $< 10\%$ because the measurements were carried out in a magnetic α -spectrometer. Errors occur as a result of the error in determining N_i , and statistical errors in determining S_i . The maximum value of all errors should not exceed 25%. Therefore the discrepancy between our results and [1, 2] is outside the limits of errors indicated by these authors. An explanation cannot be provided at this time.

We would like to thank N. E. Titov and A. N. Dobronravov for helping with the measurements.

LITERATURE CITED

1. H. Smith, J. Inorg. and Nucl. Chem., 17, 178 (1961).
2. F. Brown, et al., J. Inorg. and Nucl. Chem., 13, 192 (1960).
3. M. Jones, et al., Nucl. Sci. Abstrs., 10, 248 (1956).
4. S. Thompson, et al., Phys. Rev., 80, 1108 (1950).

5. D. Strominger, J. Hollander, and G. Seoborg, *Tables of Isotopes*, UCRL-1928 (1958).
6. B. S. Dzhelepov, et al., *Izv. AN SSSR, Ser. fiz.*, 23, 782 (1959).
7. D. Hoffman, G. Ford, and F. Lowrence, *J. Inorg. and Nucl. Chem.*, 5, 6 (1957).
8. J. Butler, et al., *Phys. Rev.*, 103, 634 (1956).
9. J. Mech, et al., *Phys. Rev.*, 103, 340 (1956).

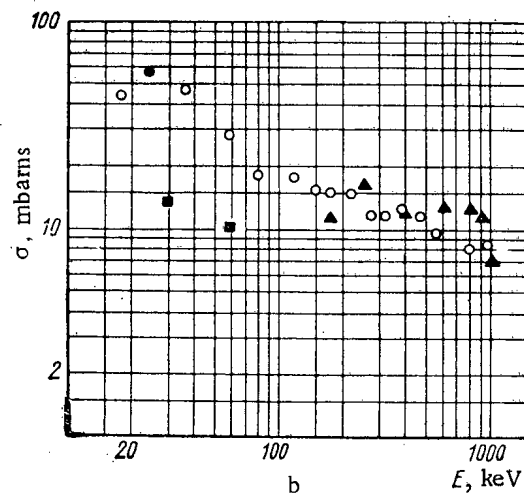
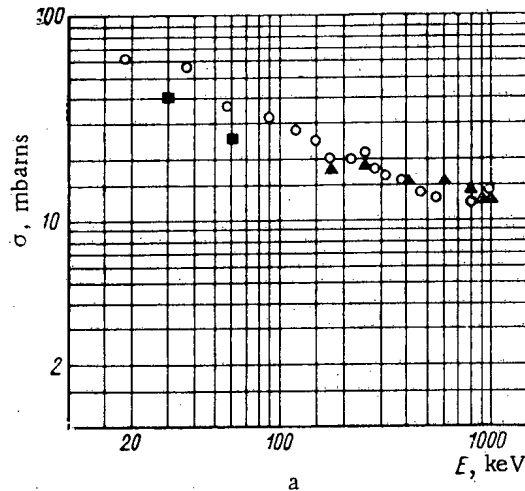
THE FAST-NEUTRON CAPTURE CROSS SECTIONS OF COPPER AND ZIRCONIUM

Yu. Ya. Stavisskii and A. V. Shapar'

Translated from *Atomnaya Énergiya*, Vol. 15, No. 4,
p. 323, October, 1963

Original article submitted January 8, 1963

The method of recording prompt gamma rays was used to measure the radiative capture cross section as a function of fast-neutron energy for natural mixtures of isotopes of copper and zirconium.



Variation of the radiative capture cross section of copper (a) and zirconium (b) as a function of neutron energy. Data of: ○) present study; ▲) [2]; ■) [3]; ●) [4].

As the neutron source we used the $T(p, n)He^3$ reaction produced in the target of a Van de Graaf accelerator. The average dispersion of the neutron energy was ± 16 keV. The gamma-ray detector used was a scintillation counter with a CaF_2 crystal. The measurements were made in ring geometry, that is, the CaF_2 crystal, shielded from the direct beam by a lead cone, was placed inside a ring of the substance being investigated. Metal specimens of copper and zirconium 2 cm thick were used.

The variation of the radiative capture cross section of neutrons as a function of energy was found by a comparison with the variation given in [1] for the fission cross section of U^{235} .

The error of each point for copper was not more than 10%. In the case of zirconium the error was considerably larger (an average of about 30%). The large error for zirconium is due to the value of the effect from the specimen by comparison with the background, which results from the smallness of the capture cross section, the relatively soft capture gamma-ray spectrum, and the low density of metallic zirconium.

To determine the absolute values of the cross section we used the radiative capture cross section for 400 keV neutrons obtained in [2], equal to 15.4 and 12.4 mbarns for copper and zirconium respectively. The results of the measurements of the present study and the data of other authors [2-4] are shown in the figure. The results of the measurements for copper are in good agreement with the data of [3], and with those of activation measurements not shown in the figure. The results for zirconium exhibit a deviation from the data of [3]. The reason for this deviation has not been determined. At a neutron energy of less than 200 keV for copper and zirconium the average distance between the levels is comparable with the energy resolution of the method. Moreover, the experiment used fairly thick specimens (2 cm). This led to a reduction in the capture cross section because of resonance blocking through scattering.

In conclusion, the authors thank A. I. Leipunskii and O. D. Kazachkovskii for their attention to the present study, as well as A. S. Kulakov for his help in making the measurements.

LITERATURE CITED

1. G. Hughes and R. Schwartz, Atlas of Neutron Cross Sections [Russian translation], Moscow, Atomizdat (1959).
2. B. Diven et al., Phys. Rev., 120, 556 (1960).
3. J. Gibbons et al., Phys. Rev., 122, 182 (1961).
4. T. S. Belanova, Atomnaya Énergiya, 14, 185 (1963).

USE OF LARGE AREA SEMICONDUCTING DETECTORS IN α -SPECTROMETRY

V. F. Kushniruk, É. Z. Ryndina, S. M. Solov'ev,
and I. I. Chuburkova

Translated from *Atomnaya Énergiya*, Vol. 15, No. 4,
p. 324, October, 1963

Original article submitted January 24, 1963

Preparing small area surface barrier detectors from n-type silicon with a specific resistance of $150 \Omega \cdot \text{cm}$ and good spectrometric properties presents no particular difficulty. On the better samples, with an area up to 0.5 cm^2 , the energy resolution was 30 keV, with a sensitive layer depth up to 100μ .

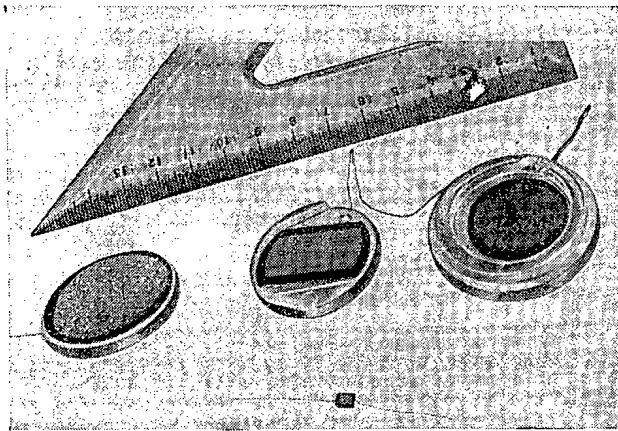


Fig. 1. General view of detectors.

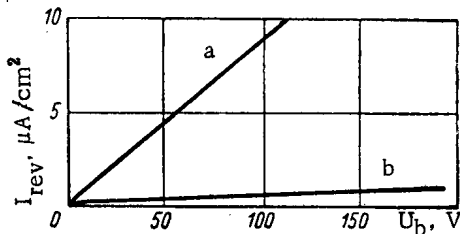


Fig. 2. Reverse current I_{rev} as a function of bias voltage U_b on the detector, taken 1 (a) and 6 (b) months after preparation.

Figure 2 gives the $I_{rev} = f(U_b)$ curves for one of the detectors, taken one and six months after preparation. For the same bias voltages, the reverse current in the detector decreased by an order of magnitude, and the operating bias increased to 150 V. This raised the signal-to-noise ratio to approximately 50, and the resolving power was improved accordingly. Thus, the detectors became suitable both for detecting α -particles and for spectrometry. The best resolution for the α -particles of the isotope mixture ThC and ThC' reaches 2% at a voltage of 60 V. It may be found from the amplitude ratio of the pulses from 6.05 and 8.78 MeV α -particles (path length in silicon about 50μ) are completely stopped in the sensitive layer of the detector for $U_b = 60 \text{ V}$. Such detectors, made of silicon with a specific resistance of $150 \Omega \cdot \text{cm}$, may be used to detect α -particles up to 12 MeV, and protons up to 2.5 MeV. Since the working area of the detectors is quite large, they may be used for spectrometry of weak α -sources.

A number of difficulties are entailed in trying to prepare larger detectors. Because of the large reverse currents, and the inhomogeneity of the silicon plates, it has so far been impossible to prepare detectors with good resolution. However, there was a considerable improvement in the characteristics of detectors that had been stored for a long period of time. This is possibly due to the fact that the formation of the inversion layer on the detector surface is not completely finished during the etching, but continues for a considerable length of time, particularly if the oxidation takes place through a film of gold. It is pointed out in [1-3] that a change in the basic characteristics of detectors keeps occurring for several days, and in [4], the time is several weeks or months.

Studies were made on detectors with an area of about 5 cm^2 , in February, 1962. The general view of the detectors is shown in Fig. 1.

The basic characteristics and the technique of preparing these detectors was presented at the conference on semiconductor detectors for use in nuclear measurements, held in 1962 in Dubna [5]. These detectors can only be used for detecting α -particles and measuring the energy of fission fragments. Because of the small working voltage (10-15 V) and the large amount of noise in the detectors (signal-to-noise ratio ~ 10), the resolution for α -particles was 8-14%.

Using silicon with a specific resistance of 900-1000 $\Omega \cdot \text{cm}$ has made it possible to get a sensitive layer depth of 110 μ on an area of 3 cm^2 , with a resolution of 100 keV.

LITERATURE CITED

1. R. Archer, J. Electrochem. Soc., 104, 619 (1957).
2. J. Blankenship, Semiconductor Nuclear Particle Detectors, Publication No. 871, Nat. Acad. of Sci., Nat. Res. Council, Washington, p. 43 (1961).
3. G. Dearnaly, *ibid.*, p. 49.
4. A. Ghiorso, *ibid.*, p. 47.
5. É. Z. Gershtein, S. M. Solov'ev, and I. I. Chuburkova, Proceedings of the Conference on Semiconductor Detectors for Nuclear Radiation [in Russian], Dubna, p. 26 (April, 1962).

THE ATTENUATION OF A HIGH-ENERGY NEUTRON FLUX IN SHIELDING

M. M. Komochkov and B. S. Sychev

Translated from Atomnaya Énergiya, Vol. 15, No. 4,

pp. 325-327, October, 1963

Original article submitted January 24, 1963

In [1] we reported experimental data on the attenuation of a neutron flux in types of concrete with different specific weights. The present study contains additional information on the attenuation of a neutron flux in iron and also offers an approximate theory which describes the experimental data fairly well.

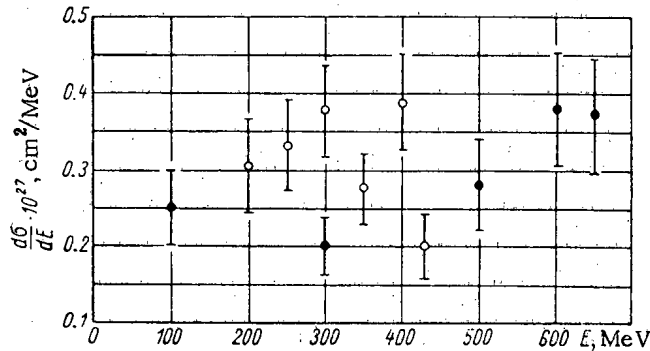


Fig. 1. Differential cross section for emission of secondary protons when protons of two different energies interact with carbon nuclei: ● $E_p = 600 \text{ MeV}$ [12]; ○ $E_p = 460 \text{ MeV}$ [13].

Values of $\Delta_{\frac{1}{2}}$ for Different Neutron Spectra

Energy of proton hitting beryllium target, MeV	Exptl. [1]	Calc.
470	29 ± 2	33 ± 2.6
250	34.5 ± 2	36 ± 2.9
350	38 ± 2	38.5 ± 3.1
480	43 ± 3	41 ± 3.3
660	42 ± 1	42.3 ± 3.3

The flux density and the energy spectrum of the neutrons were determined by solving the kinetic equation [2] for a unidirectional neutron flux hitting a semiinfinite absorber perpendicular to its surface. The angular deviations of the neutrons in the process of interaction with nuclei were ignored. This was due to the inadequacy of the data on the space-energy distribution of secondary particles when high-energy nucleons interact with nuclei. In addition, the penetration of the neutrons through the shielding must be determined essentially by the highest-energy component of the spectrum, which is deflected only through small angles.

In this approximation the kinetic equation for the distribution function of the neutron flux $N(E, x)$ is written in the form

$$\frac{\partial N(E, x)}{\partial x} = -\mu(E) N(E, x) + \int_E^{E_0} n_0 \frac{d\sigma}{dE}(E', E) N(E', x) dE', \quad (1)$$

where $\mu(E)$ is the linear coefficient of attenuation of the neutron flux; E_0 is the maximum neutron energy; n_0 is the number of nuclei per cm^3 ; $(d\sigma/dE)(E', E)$ is the differential cross section for the emission of neutrons with energy

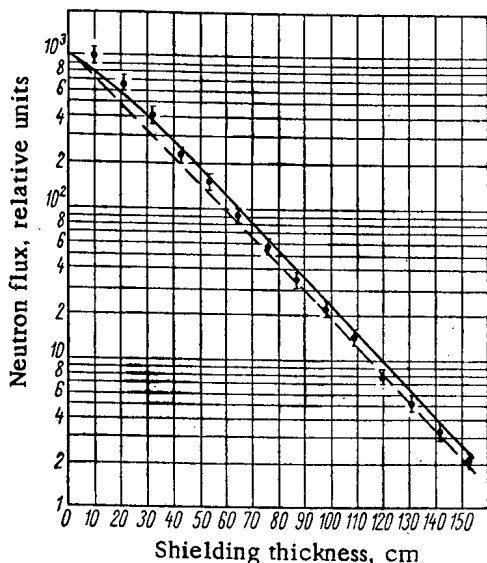


Fig. 2. Attenuation of neutron flux in steel and cast-iron shielding: ● experimental values; — calculation ($E_n > 20$ MeV); - - - calculation ($E_n > 80$ MeV).

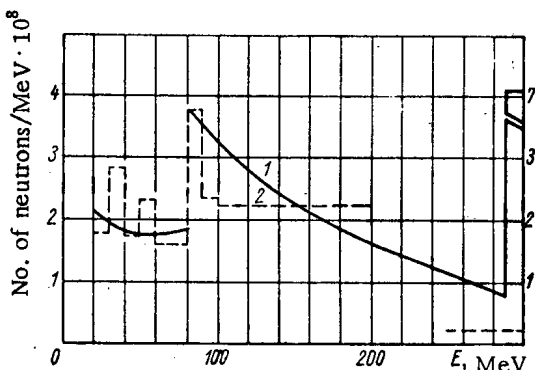


Fig. 3. Energy spectrum of neutrons beyond a heavy-concrete shield ($\rho = 3.85$ g/cm³) 460 cm thick: 1) data of the present study; 2) data of [11].

where $\eta\mu = n_0 \frac{d\sigma}{dE}$, and I_1 is the Bessel function of first order for an imaginary argument. The flux of neutrons with an energy greater than E_1 at a depth x may be written as

$$\varphi(x) = \int_{E_1}^{E_0} N(E, x) dE = e^{-\mu x} I_0(2\sqrt{\eta\mu x(E_0 - E)}), \tag{3}$$

where I_0 is the Bessel function of zero order for an imaginary argument. The value of η was found from the condition of optimum agreement between the experimental data [1] and the data calculated by formula (3) for the neutron flux at various depths; the neutron spectra in the experiments [1] were replaced by a set of monochromatic lines with the corresponding fluxes [14-16]. When (3) was compared with the experimental data, the second part of the neutron flux (energies of 20-80 MeV) was ignored, since as was seen above (Fig. 2), the rate of attenuation of this part

* The lower limit, 20 MeV, for the energy range considered is found from the threshold energy of the $C^{12}(n, 2n)C^{11}$ reaction, which was used in the experiments to determine the attenuation of a neutron flux in concrete [1].

E when a neutron with an energy E' interacts with a nucleus. We shall assume that $\mu(E) = \sigma_a(E)n_0$. The quantity $\sigma_a(E)$ —the cross section for inelastic interaction—depends to a considerable extent on the neutron energy when $E < 80$ MeV and is constant in the range from 80 MeV to several BeV [3-11]. This fact makes it possible to subdivide the integral under consideration, from $E_{\min} = 20$ MeV* to 700 MeV, into two sections. We first consider neutrons with energies greater than $E_1 = 80$ MeV, for which μ , the linear coefficient of attenuation is independent of energy. Figure 1 shows (black circles) the values of $\frac{d\rho}{dE}(E)$ obtained on the basis of [12] for the secondary charged particles (mainly protons) produced by (p, C), collisions for an initial energy of $E_p = 660$ MeV, emitted at angles $\theta < 30^\circ$ from the direction of the primary proton. If we consider the contribution made by the protons emitted at angles $\theta > 30^\circ$, the values of $d\sigma/dE$ increase somewhat in the 100-400 MeV energy range. Figure 1 also shows the values of the differential cross section for the emission of cascade protons at an energy of $E_p = 460$ MeV, obtained by means of the formula

$$\left(\frac{d\sigma}{dE}\right)_C = \left(\frac{d\sigma}{dE}\right)_{Al} \frac{\sigma_a^C}{\sigma_a^{Al}}.$$

The values of the differential cross section of the emission of cascade protons from (p, Al) collisions are taken from [13]. The data given in Fig. 1 permit us to assume that the differential cross section of neutron emission $\frac{d\sigma}{dE}(E', E)$ is independent of both E' and E , the energies of the primary and secondary neutrons. In this case we obtain a simple solution of Eq. (1) for a monochromatic neutron flux $\delta(E_0 - E)$ hitting the shielding:

$$N(E, x) = e^{-\mu x} \left[\delta(E_0 - E) + \sqrt{\frac{\eta\mu x}{E_0 - E}} I_1\left(2\sqrt{\eta\mu x(E_0 - E)}\right) \right], \tag{2}$$

of the flux at considerable depths is completely determined by the rate of attenuation of the flux of neutrons with energies of more than 80 MeV.

Let us determine the distribution function for the second part of the neutron flux $\psi(E, x)$. We shall assume that $\psi(E, x)$ satisfies the following equation:

$$\frac{d\psi}{dx} = -\mu_p(E) \psi(E, x) + \int_{E_1}^{E_0} n_0 \frac{d\sigma(E')}{dE'} N(E', x) dE'. \quad (4)$$

Here μ_p is the linear coefficient of attenuation of the neutron flux $\psi(E, x)dE$ under conditions of poor geometry. In other words, in accordance with the data of [17], we assume that when there are no neutrons of the first group, $\psi(E, x)dE$ depends on x exponentially. The differential cross section $\frac{d\sigma}{dE}(E)$ for the emission of neutrons with energies of 20-80 MeV for different nuclei is found from the data of [13] for the interaction of protons with aluminum nuclei (it is assumed that the cross section is independent of E'). It should be taken into account that the values of μ_p [18] are determined for the neutron flux hitting perpendicularly to the shielding, while the secondary neutrons have a specified angular distribution [13]. Consequently, we must select the component of the secondary-neutron flux in the direction of the primary flux. If we use the angular distribution of protons with energies of 30-90 MeV, produced when 460 MeV protons interact with aluminum, we can show that this component is equal to 0.6 times the secondary neutron flux. With these assumptions, the solution of (4) will be

$$\psi(E, x) = e^{-\mu_p(E)x} n_0 0.6 \frac{d\sigma}{dE}(E) \int_0^x e^{\mu_p(E)x'} \varphi(x') dx'. \quad (5)$$

The neutron flux is found by integrating (5) with respect to energy from E_{\min} to E_1 :

$$j(x) = \int_{E_{\min}}^{E_1} \psi(E, x) dE. \quad (6)$$

The total flux of neutrons with energies higher than E_{\min} will evidently be the sum of (3) and (6):

$$F(x) = \varphi(x) + j(x). \quad (7)$$

Figure 2 shows how the flux of neutrons produced by bombarding a beryllium target with 660-MeV protons varies as a function of the thickness of steel and cast-iron shielding. The data of Fig. 2 indicate good agreement between the experimental and calculated values of the fluxes for a shielding thickness of more than 20 cm ($\mu x \approx 1$). For individual intervals of shielding thickness the law governing the attenuation may be written in exponential form and we may introduce such a widely used parameter as $\Delta_{\frac{1}{2}}$, the thickness for 50% attenuation. From the slope of the curves of Fig. 2 for a thickness of more than 20 cm, we obtain the following values: $\Delta_{\frac{1}{2}}(\text{exp.}) = 15.9 \pm 0.6$ cm; $\Delta_{\frac{1}{2}}(\text{calculated}) = 16.5 \pm 1.3$ cm.

The table gives the calculated and measured values [1] of the 50% attenuation layers for ordinary concrete ($\rho = 2.35 \text{ g/cm}^3$) for different energies of the neutrons hitting the shielding.

The calculation requires the values of the cross section of inelastic interaction between neutrons and the nuclei of the elements of which the shielding is made; these are taken from [3-11]. For heavy concrete with a specific weight of 3.85 g/cm^3 , the values of $\Delta_{\frac{1}{2}}$ at a shielding depth of 3-4.5 m, calculated by the Monte Carlo method [11] and Eq. (3), are equal to 25.3 ± 2.5 and 24.5 ± 0.07 cm, respectively. The experimental and calculated results, shown in Fig. 2, indicate that for a shielding thickness greater than the relaxation length ($\mu x = 1$) the flux of neutrons with energies above 20 MeV may be described by the following formula:

$$F(x) = 1.3e^{-\mu x} I_0 (2 \sqrt{\eta \mu x (E_0 - E_1)}). \quad (8)$$

For the condition of optimum agreement between the measured and calculated values of $\Delta_{\frac{1}{2}}$ for ordinary concrete and an energy of 660 MeV, the value of the coefficient η was found to be $1.3 \cdot 10^{-3} \text{ MeV}^{-1}$. It is difficult to say whether the value of the coefficient η remains strictly constant for the various elements of which the shielding is made.

Figure 3 shows the energy spectrum of the neutrons at a depth of 460 cm, obtained by means of Eqs. (2) and (5) for the case when a monochromatic flux of 300-MeV neutrons impinges perpendicular to the shielding. It also shows the spectrum of particles (chiefly neutrons) calculated by the Monte Carlo method [11]. The flux of neutrons that did not interact is shown in spectrum 1 by the column. Energy spectrum 2 was normalized by using the condition that the areas under curves 1 and 2 from 100 MeV to 200 MeV were equal. The considerable difference between the spectra in the 250-300 MeV range is apparently due to the fact that the value of the differential cross section for the emission of secondary neutrons in this range is somewhat high in the present study, while it is somewhat low in the study referred to by Lindenbaum [11].

The authors thank V. P. Dzhelepov for his valuable comments and N. A. Chernikov for his evaluation of the methods for solving the kinetic equation.

LITERATURE CITED

1. L. N. Zaitsev, M. M. Komochkov, and B. S. Sychev, *Atomnaya Énergiya*, 12, 525 (1962).
2. O. I. Leipunskii, B. V. Novozhilov, and V. N. Sakharov, *Distribution of Gamma Quanta in Matter* [in Russian], Moscow, Fizmatgiz (1960).
3. B. V. Gavrilovskii and V. I. Moskalev, *Dokl. AN SSSR*, 110, 972 (1956).
4. H. de Carvalho, *Phys. Rev.*, 96, 398 (1954).
5. T. Coor et al., *Phys. Rev.*, 98, 1969 (1955).
6. I. Cassels and I. Lawson, *Proc. Phys. Soc.*, 67A, 125 (1954).
7. G. Millburn et al., *Phys. Rev.*, 95, 1268 (1954).
8. F. Chen, C. Leavitt, and A. Shapiro, *Phys. Rev.*, 99, 857 (1955).
9. V. Nedzel, *Phys. Rev.*, 94, 174 (1954).
10. V. S. Pantuev and M. N. Khachaturyan, *Zh. Éksperim. i teor. fiz.*, 42, 909 (1962).
11. S. Lindenbaum, *Ann. Rev. Nucl. Sci.*, 11, 213 (1961).
12. L. S. Azhgirei et al., *Zh. Éksperim. i teor. fiz.*, 36, 1632 (1959).
13. N. Metropolis et al., *Phys. Rev.*, 110, 185 (1958).
14. V. P. Dzhelepov et al., *Izv. AN SSSR, Ser. fiz.*, 19, 573 (1955).
15. V. S. Kiselev et al., *Zh. Éksperim. i teor. fiz.*, 35, 812 (1958).
16. W. Goodell, H. Loar, R. Durbin, and W. Havens, *Phys. Rev.*, 89, 724 (1953).
17. B. Moyer et al., *AECD-2149* (1947).
18. M. Livingston and J. Blewett, *Particle Accelerators* (1962).

All abbreviations of periodicals in the above bibliography are letter-by-letter transliterations of the abbreviations as given in the original Russian journal. Some or all of this periodical literature may well be available in English translation. A complete list of the cover-to-cover English translations appears at the back of this issue.

THE EFFECT OF REFLECTORS MADE OF VARIOUS MATERIALS
ON THE INCREASE IN THE NUMBER OF NEUTRON CAPTURES
IN THE URANIUM BLANKET OF A FAST REACTOR

V. I. Golubev, A. V. Zvonarev, M. N. Nikolaev,
and M. Yu. Orlov

Translated from Atomnaya Énergiya, Vol. 15, No. 4,
pp. 327-328, October, 1963

Original article submitted March 13, 1963

As was shown in [1], the use of additional reflectors considerably increases the number of neutron captures in a blanket zone consisting of metallic uranium. The purpose of the present study is to investigate the effect of additional reflectors on the increase in the number of captures in a blanket zone made of uranium carbide.

Increase in the Number of Neutron Captures in a Reactor
Blanket

Material of additional reflector	Reflector thickness, mm	B_i	
		Uranium carbide	Metallic uranium
Beryllium	140	0.54 ± 0.08	0.86 ± 0.10
Graphite	600	0.50 ± 0.08	—
Nickel	192	0.47 ± 0.07	0.51 ± 0.10
Iron	184	0.42 ± 0.07	0.28 ± 0.09
Copper	184	0.24 ± 0.06	0.41 ± 0.09
1Kh18N9T steel	160	0.33 ± 0.06	0.40 ± 0.09
Water	144	0.23 ± 0.06	0.49 ± 0.10
Uranium carbide	∞	1.00	—
Uranium	∞	—	1.00

In the present study, as in [1], we investigated the effect of additional reflectors on the asymptotic region of the neutron spectrum [2].

The measurements were made on the BR-1 reactor [2]. The blanket of the reactor was built up from slugs of enriched uranium and graphite 47 mm in diameter and 10 mm high. The slugs were built up in columns (one graphite slug for each two slugs of uranium).

The resulting grid had a uranium-to-carbon nucleus ratio of 1 to 0.884, which is approximately the same as the value found in uranium carbide. The assembled reactor blanket had the shape of a regular hexagon 1100 mm on a side and 700 mm high. Additional reflectors made of beryllium, water, iron, copper, nickel, graphite, or 1Kh18N9T steel were placed against one face of the blanket. The thickness of most of the additional reflectors was selected on the basis of the results found in [1]. We used thicknesses for which it had been found that any further increase in the reflector thickness did not add to the number of neutron captures in the uranium reactor blanket. A number of thicknesses were tried for the iron and graphite reflectors. It was found that for the graphite reflector an increase in thickness beyond 600 mm did not appreciably increase the number of captures in the blanket, while for the iron reflector the value was 184 mm.

In order to verify that the asymptotic spectrum had been established and to determine the number of captures in an infinite uranium carbide blanket, we increased the thickness of the reactor blanket in one direction by 350 mm. It was found that for a blanket of the chosen dimensions, an asymptotic spectrum is established in the region of low energy neutrons, which play the chief role in the $U^{238}(n, \gamma)U^{239}$ reaction.

We measured experimentally the distribution of U^{238} neutron capture density in the reactor blanket both with and without additional reflectors made of the above-mentioned materials. In addition, we plotted a curve of the

neutron capture density distribution in the thickened uranium carbide blanket. The radiative capture of neutrons in the uranium was determined from the β activity of irradiated specimens of powdered uranous-uranic oxide, from which the fission fragments had been chemically removed. Weighed amounts of the powder were placed in flat aluminum containers 47 mm in diameter and 3 mm high (the U_3O_8 layer was about 1 mm thick) and then put between the blanket slugs at the level of the center of the reactor active zone. In order to take account of the inhomogeneity produced in the neutron flux by the slight heterogeneity of the uranium-carbon mixture in the reactor blanket, the specimens were placed both between uranium slugs and between adjacent slugs of uranium and graphite.

To determine the efficiency of the additional reflectors we used the ratio of $B_i = A_i/A_{UC}$, where A_i is the difference between the total number of neutron captures in uranium with and without the i -th additional reflector, and A_{UC} is the same difference for an infinite uranium carbide reflector. The results of the measurements for blankets made of uranium carbide and metallic uranium [1] with various additional reflectors are shown in the table.

It can be seen from the table that the efficiency of the materials that produced considerable softening in the neutron spectrum (water, beryllium) became substantially lower when the uranium blanket was replaced by a uranium carbide blanket, while the efficiency of the heavy materials was only slightly reduced and was even increased in the case of iron, since the effects of the deep interference minima [1] which had been found in the cross section of iron at energies above 25 keV were not noticeable the case of a uranium carbide blanket, owing to the high degree of softening of the neutron spectrum.

In conclusion, the authors thank I. I. Bondarenko for his valuable comments and advice, as well as N. D. Golyaev, P. V. Kindinov, Yu. F. Koleganov, K. I. Nesterov, and E. A. Osipov for their help with the measurements.

LITERATURE CITED

1. V. I. Golubev, A. V. Zvonarev, M. N. Nikolaev, and M. Yu. Orlov, *Atomnaya Énergiya*, 15, 258 (1963).
2. A. I. Leipunskii et al., *Atomnaya Énergiya*, 5, 277 (1958).

CALCULATION OF THE SPECTRAL AND ANGULAR DISTRIBUTION
OF SCATTERED γ -QUANTA FROM A POINT MONODIRECTIONAL
 Cs^{137} SOURCE IN IRON

L. R. Kimel', A. M. Panchenko, and V. P. Terent'ev

Translated from *Atomnaya Energiya*, Vol. 15, No. 4,
pp. 328-331, October, 1963

Original article submitted February 28, 1963

The problem of the spectral and angular distribution of scattered γ -quanta from a point monodirectional source was solved by the Monte Carlo method. The source, located in an infinite iron medium at the point 0 (Fig. 1), emitted γ -quanta with an initial energy $E_0 = 0.661$ MeV in the positive direction of the h axis. The spectral and angular distribution were determined for the scattered energy which passed through rings Δr_j located in planes normal to the beam at distances h_j from the point 0. The spectral and angular distribution of the scattered energy per unit area at distances r_j from the beam were obtained by averaging the results for the distribution within the rings Δr_j .

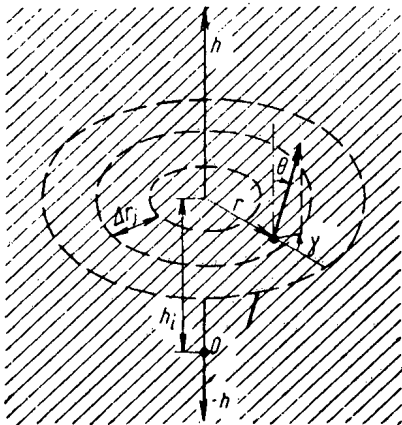


Fig. 1. Geometry used in the computation.

The following values of h_j were selected:

i	-3	-2	-1	0	1	2	3	4	5
h, cm	-4	-2	-0.5	0	2.4	4.8	7.2	9.6	12

Negative values of h corresponded to the reverse half-space, which was beneath the plane passing through the point 0 normal to the beam.

Each plane was subdivided into rings with radii r_j :

j	0	1	2	3	4	5	6
r, cm	0-0.5	0.5-1	1-1.7	1.7-2.7	2.7-4	4-5.5	5.5-8

A study was made of 5420 γ -quanta histories involving the following sequence of events [1]: the γ -quantum path to the first interaction and the type of interaction were determined; in the case of Compton effect, the energy of the scattered quantum and its direction of flight after scattering were calculated. Such a sequence of calculations was repeated until the quantum disappeared as the result of photo-effect or until the quantum fell into the energy region below 10 keV. Upon penetration of a ring by a scattered quantum, the energy of the quantum was recorded along with the angle θ between the quantum velocity vector and the normal to the ring at the point of penetration and also the angle γ between the projection of the quantum velocity vector on the plane normal to the beam and the radius drawn in this plane through the point of penetration (see Fig. 1). The calculations were done on the "Strela-3" electronic data processing machine in the Computing Center of the USSR Academy of Science.

In order to obtain the random numbers needed for the calculations, a special program previously suggested [2, 3], was used in the machine.

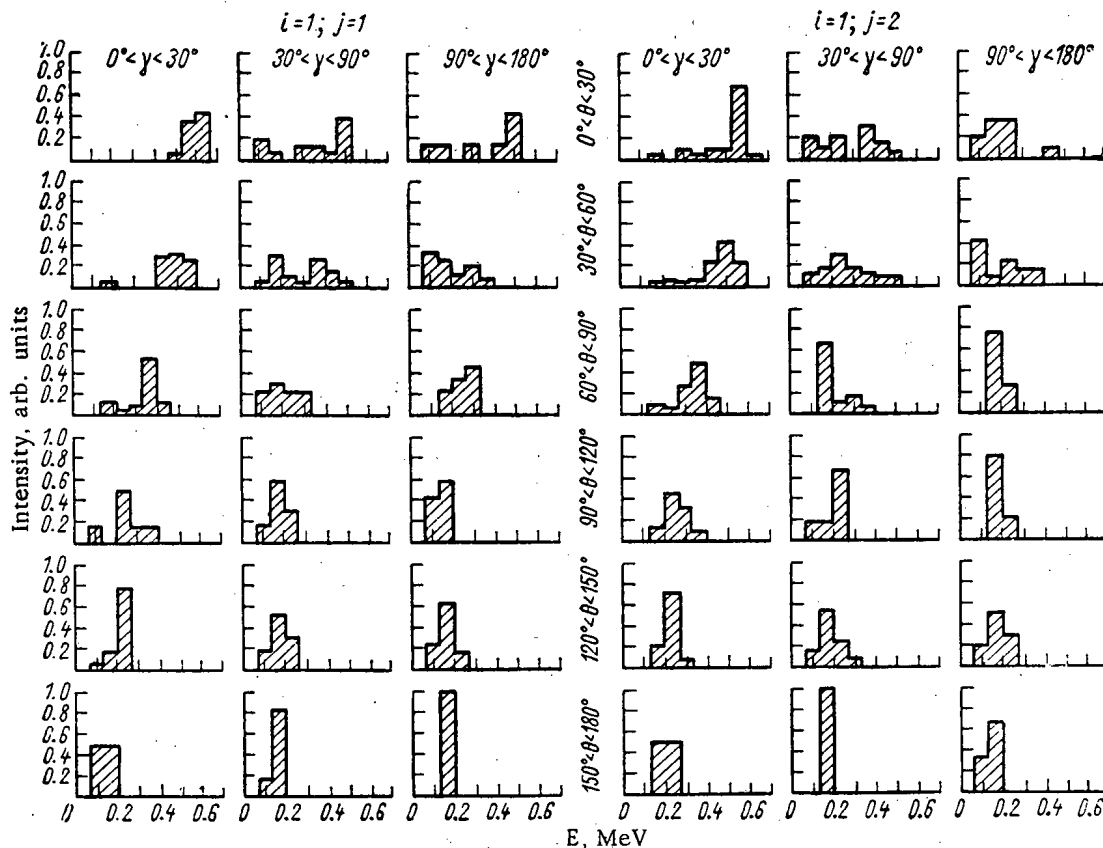


Fig. 2. Spectral and angular distribution for the rings: $i=1; j=1$ ($h=2.4$ cm; $r=0.5-1$ cm) and $i=1; j=2$ ($h=2.4$ cm; $r=1-1.7$ cm).

Figure 2 shows the normalized spectral distribution of the radiation scattered at angles θ and γ from 0 to 180°. The subintervals in the range of θ were each 30°, the subintervals in the range of γ were 0-30°, 30-90°, 90-180° for the first and second rings in the plane $h=2.4$ cm. The figure clearly shows a shift in the spectrum toward lower energies with increasing angle θ , which corresponds to a reduction in energy because of an increase in the number of scatterings or because of large-angle scattering. This same tendency appears less markedly with increasing angle γ .

The scattered radiation spectra integrated over all angles are shown in Fig. 3 for some of the rings Δr_j . In the rings of the zero plane and those of the reverse half-space the γ -quantum energy is mainly limited to the 0.13-0.26 MeV range. In the rings of the forward half-space there is a typical increase with increasing radius in the number of γ -quanta in the low energy region.

Figure 4 shows the radial distribution of scattered energy (histogram) in the planes $h=2.4$ cm and $h=7.2$ cm. For comparison, experimental curves from [4] are shown. The calculated and experimental values were normalized to 1 MeV of incident energy.

On the basis of the results for a point monodirectional source, the energy build-up factor B_E for a plane monodirectional source was computed. Results of the calculations are shown in Fig. 5, where build-up factor curves constructed on the basis of data from [5] are given for comparison.

The authors express their thanks to O. I. Leipunskii for his continuing concern with this work and to V. N. Seleznev for assistance in programming the problem.

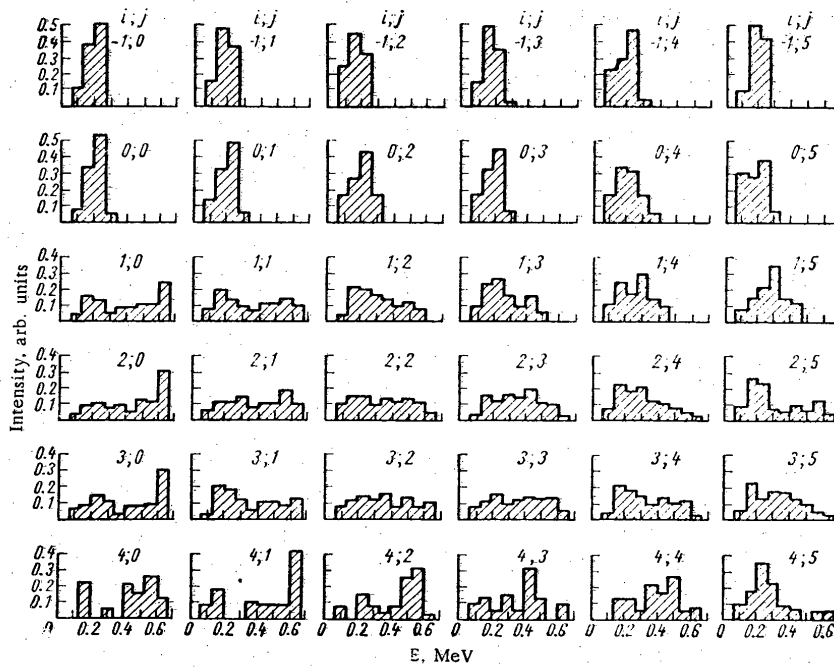


Fig. 3. Integral spectra in the planes of the forward and reverse half-spaces.

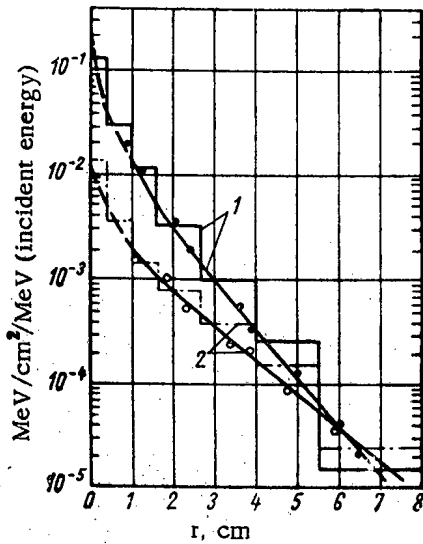


Fig. 4. Radial distribution of scattered energy in the planes $h = 2.4$ cm (1) and $h = 7.2$ cm (2). (Histogram, Monte Carlo calculation; solid curves, experimental data [4].)

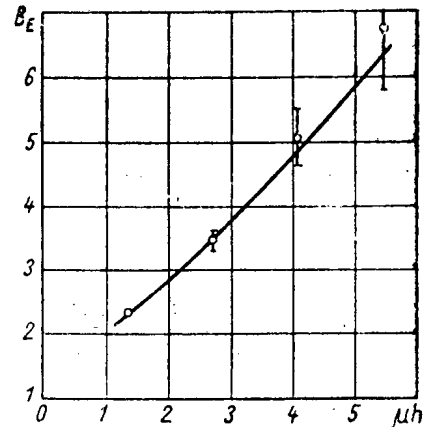


Fig. 5. Energy build-up factor for a plane, monodirectional source: \circ calculated values; — data from [5].

LITERATURE CITED

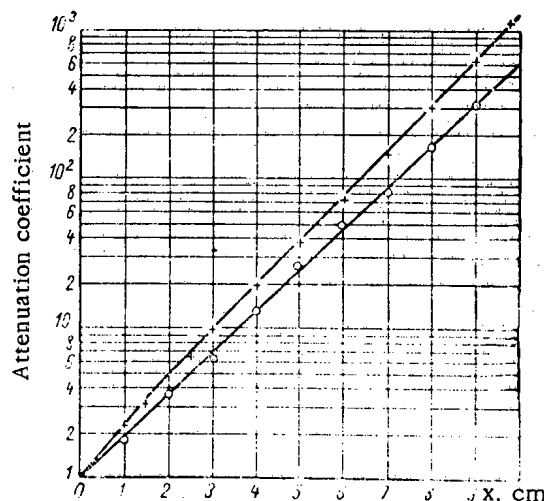
1. O. I. Leipunskii, B. V. Novozhilov, and V. N. Sakharov, The Propagation of Gamma Quanta in Matter [in Russian], Moscow, Fizmatgiz (1960).
2. I. M. Sobol', Teoriya veroyatnostei i ee primeneniya, 3, 205 (1958).
3. D. I. Golenko, Vychislitel'naya matematika, No. 5, 83 (1959).
4. O. I. Leipunskii, L. R. Kimel', and A. M. Panchenko, Atomnaya énergiya, 14, 577 (1963).
5. G. Gol'dshtein, Principles of Reactor Shielding [in Russian], Moscow, Gosatomizdat (1961).

THE EFFECT OF SHIELD SHAPE ON THE ATTENUATION OF γ -RAYS FROM VOLUME SOURCES

D. P. Osanov

Translated from *Atomnaya Énergiya*, Vol. 15, No. 4,
pp. 331-332, October, 1963
Original article submitted January 25, 1963

Plane shielding made of various materials is normally used for protection against radiation. However, shielding of a more complex geometry may be more efficient in some cases. For example, the radiation from volume sources will be attenuated more strongly by a shielding layer whose surface shape resembles the source surface shape. In particular, this applies to a cylindrical shield used as a shadow shield for a cylindrical source. For the same thickness of plane and cylindrical shields, the path of the rays from the surface portion of the source which make the greatest contribution to the dose is always greater in the cylindrical layer than in the plane layer. This difference increases if the shield is brought close to the surface of the source, and reaches a maximum when it becomes a wall of the source.



Comparison of attenuation curves for cylindrical (x) and plane (o) shields.

The calculation of the attenuation of γ -rays from a cylindrical source inside a cylindrically-shaped shield leads to complicated computations. Therefore, quantitative data was obtained experimentally for the differences in attenuation of γ -rays from a volume source by plane and cylindrical shielding. For this purpose, cylindrical shapes were pressed out of lead sheets of thickness $x = 0.5$ cm and with a surface area $S = 100 \times 100$ cm². The radius of curvature increased from one sheet to the next so that they could be set up close to the γ -ray source and to one another. The figure shows one of the experimental curves obtained with a source in the form of a cylindrical container 50 cm in diameter and 100 cm in height. The source was filled with a solution of CoSO_4 containing Co^{60} . In the same figure, an attenuation curve is shown which was obtained under similar conditions with a plane shield. The difference between the curves, amounting to 30% at $x = 2$ cm, increases continuously and reaches 120% at $x = 10$ cm. Thus, if a shield is pressed into cylindrical shape, one can obtain considerable saving in thickness, and, therefore, in shield weight, for volume sources of high specific activity. On the other hand, the experimental data indicates that the differences in attenuation by plane and cylindrical layers for small thicknesses is not large, and, consequently, the attenuation of radiation by the container walls can be determined without taking into account the curvature of the walls.

In conclusion, I wish to thank Yu. P. Kayurin and A. I. Bondar for help in performing the experiment.

MEASUREMENT OF THE FREQUENCY CHARACTERISTICS OF AN IRT-1000 REACTOR BY THE OSCILLATION METHOD

L. V. Konstantinov, A. I. Efanov, and V. V. Postnikov

Translated from *Atomnaya Énergiya*, Vol. 15, No. 4,

pp. 332-334, October, 1963

Original article submitted January 2, 1963

The application of the oscillation method for measurement of the frequency characteristics of various reactors has been described [1-3] in situations where complex electronic equipment was used for recording and analyzing the signals. However, such equipment does not give high precision because of instabilities in the operation of electronic elements.

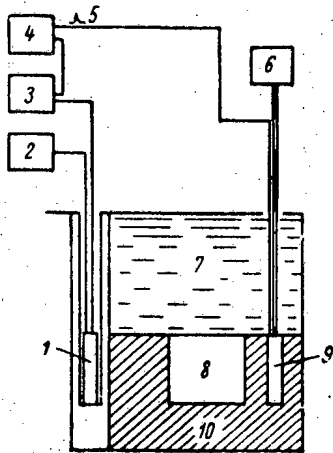
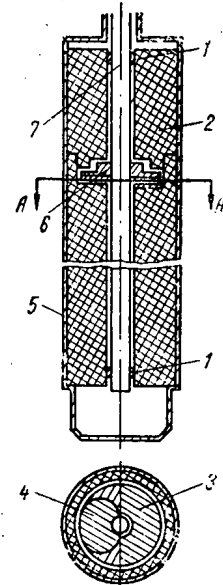


Fig. 1. Block diagram of the apparatus: 1) ionization chamber; 2) high voltage unit; 3) compensation unit; 4) loop oscillograph; 5) reference pulse; 6) direct current motor; 7) water; 8) core; 9) oscillator rod; 10) reflector.



Section through AA'

Fig. 2. General view of oscillator rod: 1) journal bearing; 2) Plexiglas spacer; 3) cadmium stator leaf; 4) cadmium rotor leaf; 5) aluminum shell; 6) duraluminum disc fastened to the shaft; 7) rotating aluminum shaft.

Frequency characteristics may also be determined by the analysis of reactor noise [4]. The chief difficulty in the use of this method arises in the analysis of the results. In the present work, we succeeded in obtaining the frequency characteristics of an IRT-1000 reactor [5] within the frequency range of 0.3-60 cps while using measuring equipment without electronic elements. A block diagram of the apparatus is shown in Fig. 1.

The principle of the measurement of frequency characteristics by the oscillation method consists of the determination of the amplitude and phase of reactor power oscillations for sinusoidal variations in reactivity. If the amplitude of the reactivity oscillations, δk_0 , is small ($\delta k_0 < 3 \cdot 10^{-3}$), then

$$\left(\frac{\bar{n}}{\delta n}\right)^2 = \frac{\beta_{\text{eff}}^2}{\delta k_0^2} (1 - \epsilon_2)^2 + \frac{l^2}{\delta k_0^2} \omega^2 (1 + \epsilon_1)^2, \tag{1}$$

where \bar{n} is the average power level, δn is the amplitude of the power oscillations, l is the average neutron lifetime in the reactor, ω is the reactivity oscillation frequency,

$$\epsilon_1 = \frac{1}{l} \sum_{i=1}^6 \frac{\beta_i}{1 + \omega^2 \tau_i^2}$$

$$\epsilon_2 = \frac{1}{\beta} \sum_{i=1}^6 \frac{\beta_i}{1 + \omega^2 \tau_i^2}$$

(here, β_i is the effective fraction of delayed neutrons in the i -th group, τ_i is the mean lifetime of the delayed neutrons in the i -th group, $\beta_{\text{eff}} = \sum_{i=1}^6 \beta_i$.)

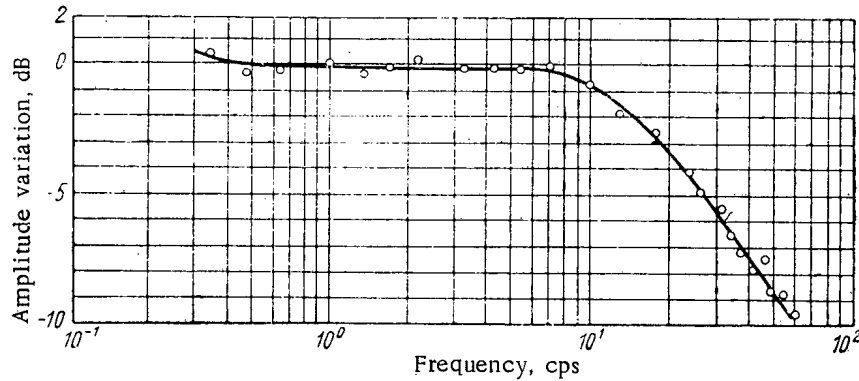


Fig. 3. Amplitude-frequency characteristic of an IRT-1000 reactor: ———) calculated curve; O) experimental points.

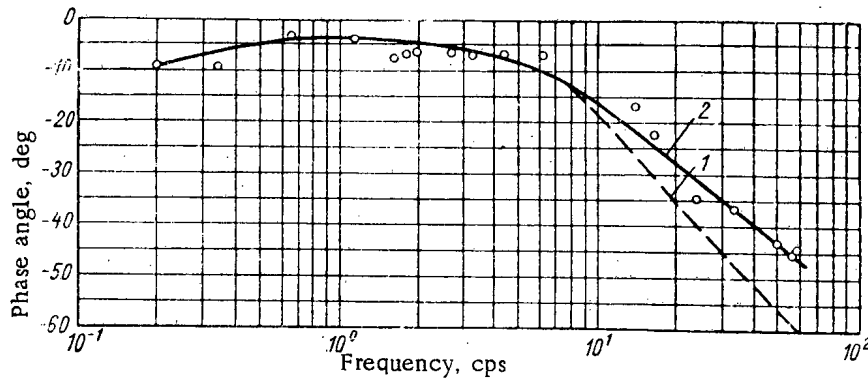


Fig. 4. Phase-frequency characteristic of an IRT-1000 reactor: 1) calculated curve; 2) curve drawn through experimental points.

The correction terms ϵ_1 , ϵ_2 are small in the high-frequency region ($\omega^2 \gg \lambda_6^2$, where λ_6 is the largest decay constant) and in this case

$$\left(\frac{\bar{n}}{\delta n}\right)^2 = \left(\frac{l}{\delta k_0}\right)^2 \omega^2 + \left(\frac{\beta_{\text{eff}}}{\delta k_0}\right)^2. \tag{2}$$

The expression for the phase shift between the oscillations in reactor power and in reactivity has the form

$$\varphi = \arctan \frac{\omega \left(l + \sum_{i=1}^6 \frac{\beta_i \tau_i}{1 + \omega^2 \tau_i^2} \right)}{\sum_{i=1}^6 \frac{\beta_i \omega^2 \tau_i^2}{1 + \omega^2 \tau_i^2}} \quad (3)$$

The oscillator rod (Fig. 2) consists of five cadmium shutters, each of which is composed of a rotor and stator. The rotor is a duraluminum disc with an attached cadmium leaf of varying radius defined by the expression $r = r_0 \sqrt{\sin \theta}$, where θ is the azimuthal angle and $r_0 = 25$ mm. The stator is made of cadmium in the shape of a half-circle 25 mm in radius, and is located beneath the rotor on the same axis. The distance between stator and rotor surfaces is 1 mm. The shutters are separated from one another by Plexiglas spacers 100 mm long. With rotation of the rotor, a sinusoidal variation in cadmium absorbing area takes place which leads to a sinusoidal variation in reactivity. Rotational velocity is varied by means of a reducing gear and by varying the voltage on the rotor of the direct current motor. At the time the measurements were made, the oscillator rod was located in the reactor reflector.

Power oscillations were recorded on a loop oscillograph. The high sensitivity of the galvanometers ($3 \cdot 10^{-7}$ A/mm) made it possible to operate without amplifying the signal from the ionization chamber. Measurements were made with an average reactor power of 1500 W at a reactivity oscillation amplitude $\delta k_0 = 4 \cdot 10^{-4}$.

Figures 3 and 4 give the results of the measurements. The amplitude-frequency characteristic (see Fig. 3) agrees, within the precision of the measurements, with that calculated for a reactor with $l = 7 \cdot 10^{-5}$ sec. The phase-frequency characteristic (see Fig. 4) differs from the calculated at frequencies above 10 cps. Such a deviation can be explained by the presence of a reflector in the reactor [6].

The experimentally obtained ratio $l/\beta_{\text{eff}} = (7.6 \pm 0.3) \cdot 10^{-3}$ sec. For an IRT-1000 reactor $\beta_{\text{eff}} = 1.5$ and $\beta = 9.6 \cdot 10^{-3}$ [7]. Thus, from the measurements it follows that $l = (7.3 \pm 0.3) \cdot 10^{-5}$ sec. This value is in good agreement with the calculated value ($l_{\text{cal}} = 7 \cdot 10^{-5}$ sec). The value of $\delta k/\beta_{\text{eff}}$ obtained by the oscillator method is in good agreement with the value determined by reactor power excursions.

The results of this work make it possible to conclude that one can measure reactor frequency characteristics with sufficient precision by means of the simple apparatus described above. The use of electronic circuits for the harmonic analysis of the signals (multiplication by the functions $\sin \omega t$ and $\cos \omega t$ with subsequent integration after a complete number of cycles) for the measurement of signal amplitude does not give a significant advantage over the method described in this paper, but it assures considerably greater precision in the determination of phase shift.

LITERATURE CITED

1. E. Hellstrand, *Atomics*, 6, 187 (1955).
2. J. Stone, *Commun. and Electronics*, No. 40, 1003 (1959).
3. A. Estrada, *Trans. Nucl. Sci.*, No. 1, 15 (1957).
4. L. Kemeny, *Nucl. Sci. and Engng.*, 6, 208 (1961).
5. V. V. Goncharov et al., *Reports of the Second International Conference on the Peaceful Uses of Atomic Energy [in Russian]*, Dokl. Sov. uchenykh. Vol. 2, Moscow, Atomizdat, p. 273 (1959).
6. C. Cohn, *Nucl. Sci. and Engng.*, 13, 12 (1962).
7. O. Henry, WAPD-141 (1958).

PHOTONEUTRON METHOD FOR BERYLLIUM DETERMINATION
IN THE LABORATORY

V. N. Smirnov and D. V. Tokareva

Translated from *Atomnaya Energiya*, Vol. 15, No. 4,
pp. 334-335, October, 1963
Original article submitted December 25, 1962

The method of quantitative determination of beryllium by means of (γ, n) nuclear reaction has come into increasingly wide use recently in the analysis of beryllium ores and enrichment products and in metallurgical processing.

Under laboratory conditions, the photoneutron analysis is carried out with line sources of radiation and coaxial geometry in the placement of the specimen with respect to the source. As has been shown in many experiments, the use of such geometry is advisable both when the neutron detectors used are boron proportional counters placed around the specimen and when they are disk scintillation detectors.

In the present study we propose some analytic expressions for calculating the number of neutrons formed in the (γ, n) nuclear reaction, depending on the dimensions of the radiation source and the monitored specimen and their position with respect to each other under conditions of coaxial geometry.

The number of interactions N occurring per second per cm^3 may be calculated by the formula

$$N = \sigma J n, \quad (1)$$

where σ is the effective cross section of the reaction in cm^2 , n is the number of beryllium nuclei per cm^3 , and J is the density of the bombardment gamma quanta.

If a line source of length l and total activity A is placed along the axis of a cylinder (the specimen) with inner diameter r_1 , outer diameter r_2 , and height L , then formula (1) in cylindrical coordinates becomes

$$N = \frac{A \sigma n}{4 \pi l} \int_{\varphi=0}^{2\pi} \int_{\rho=r_1}^{\rho=r_2} \int_{Z=a-\frac{L}{2}}^{Z=a+\frac{L}{2}} \left[\arctan \frac{2Z+l}{2\rho} - \arctan \frac{2Z-l}{2\rho} \right] d\rho d\varphi dZ, \quad (2)$$

where ρ and φ are the polar coordinates of the projection of an element of volume of the specimen onto the base plane (XOY), Z is the axial separation, that is, the distance from this element to the base plane, a is the distance between the centers of the specimen and the source along the Z axis.

The integral can be found readily as a combination of elementary functions. However, the expression thus obtained is cumbersome, and it is therefore of practical interest to simplify it. The calculation formula may be simplified considerably if we assume that $a = 0$ (the centers of the source and the specimen are at the same level) and $l = 0$ (the radiation source is considered a point).

Then the expression for the neutron yield becomes

$$N = A \sigma n \left[r_2 \arctan \frac{L}{2r_2} - r_1 \arctan \frac{L}{2r_1} + \frac{L}{4} \ln \frac{L^2 + 4r_2^2}{L^2 + 4r_1^2} \right]. \quad (3)$$

However, the resulting formulas do not take account of the absorption of gamma rays by the specimen. In a cylindrical system of coordinates the expression for the yield of the (γ, n) nuclear reaction from a point source, taking absorption into account, will have the form

TABLE 1. Photoneutron Yields for Different Values of μ

μ , cm^{-1}	0.00	0.035	0.07	0.14
Spec. height L, cm				
1.0	0.454	0.444	0.441	0.425
2.0	0.752	—	0.728	—
4.0	1.048	—	1.008	—
8.0	1.255	1.221	1.195	1.136

TABLE 2. Calculated and Experimental Relative Yields of Photoneutrons

Source length l, cm	Specimen dimensions*, cm		Neutron yield †, relative units		Deviation between calculated and experimental data †, relative units
	r_2	L	calculated data	experimental data	
0	1.50	1	1.74	1.75	+0.01
1	1.50	1	1.73	1.53	-0.20
2	1.50	1	1.41	1.35	-0.06
4	1.50	1	1.00	1.00	0.00
0	1.50	2	1.47	1.46	-0.01
1	1.50	2	1.43	1.30	-0.13
2	1.50	2	1.32	1.26	-0.06
4	1.50	2	1.00	1.00	0.00
0	1.50	4	1.13	1.15	+0.02
1	1.50	4	1.13	1.07	-0.06
2	1.50	4	1.11	1.07	-0.04
4	1.50	4	1.00	1.00	0.00
0	1.50	8	1.01	1.00	-0.01
1	1.50	8	1.01	0.92	-0.09
2	1.50	8	1.01	0.94	-0.07
4	1.50	8	1.00	1.00	0.00
0	0.85	1	2.04	2.05	+0.01
1	0.85	1	1.87	1.85	-0.02
2	0.85	1	1.53	1.52	-0.01
4	0.85	1	1.00	1.00	0.00
0	0.85	2	1.59	1.34	+0.05
1	0.85	2	1.55	1.43	-0.12
2	0.85	2	1.40	1.40	0.00
4	0.85	2	1.00	1.00	0.00
0	0.85	4	1.13	1.18	+0.05
1	0.85	4	1.12	1.08	-0.04
2	0.85	4	1.11	1.10	-0.01
4	0.85	4	1.00	1.00	0.00
0	0.85	8	1.01	1.05	+0.04
1	0.85	8	1.01	0.95	-0.06
2	0.85	8	1.01	0.99	-0.02
4	0.85	8	1.00	1.00	0.00

* $r_1 = 0.55$ cm throughout.

† The neutron yield from a source 4 cm long is taken as unity.

$$N = \frac{A n \sigma}{4\pi} \int_{\varphi} \int_{\rho} \int_{Z} e^{-\mu \frac{\rho-r_1}{\rho} \sqrt{\rho^2+Z^2}} \frac{1}{\rho^2+Z^2} \rho d\rho d\varphi dZ, \quad (4)$$

where μ is the coefficient of absorption in cm^{-1} .

This equation cannot be integrated in terms of elementary functions; we therefore used a method of numerical integration carried out by means of a high-speed electronic computer.

Such calculations were carried out for different specimen dimensions (corresponding to the real dimensions of the photoneutron apparatus) and different values of the absorption coefficient μ .

On the basis of these calculations and of the results obtained from formula (1), we can compare the yields of the (γ, n) reaction found when the absorption of gamma rays in the specimen is taken into account and when it is ignored. The resulting data are shown in Table 1, which indicates that the value of the relative deviation between the yield of the (γ, n) nuclear reaction calculated without taking the absorption into account ($\mu = 0$) and the yield calculated for a real powdered specimen ($\mu = 0.07$) depends on the dimensions of the specimen. For the smallest specimen ($L = 1$ cm, $V = 6.12$ cm^3) the deviation is 3%, and for the largest ($L = 8$ cm, $V = 48.95$ cm^3) it is about 5%.

It is extremely important to determine whether the calculation can be carried out by the simplified formula (3). For this purpose we compared the neutron yields calculated by (2) for different source lengths and different specimen dimensions with the neutron yields calculated by (3) for the same specimen dimensions. The data of our calculations are shown in Table 2.

Without commenting on the question of absolute neutron yield and on the practical advisability of using sources of any particular length, we may point out that if the length of the source is equal to the height of the specimen, then the relative deviation between the yield calculated for a line source and the yield calculated for a point source (for specimens 0.3 and 0.95 cm thick) is 10-13%. As the ratio of specimen height to source length is increased this deviation becomes smaller, and when the ratio is 2 to 1, the values of the neutron yields from a line and a point source are found to be practically the same. For this reason, if $L/l \geq 1$, all analytical calculations of the neutron yield may be made by the simplified formula (3), which corresponds to a point source of radiation.

The data of Table 2 enable us to compare the calculated and experimental values. The average relative deviation between the two is 5%. This deviation is so small (in fact, it may become even smaller when a correction is made for the absorption of gamma rays in the specimen) that the agreement between the experimental and calculated values may be considered satisfactory. By using the formulas so obtained, we can take into account and

evaluate the effect of the difference between the absorption coefficients of the reference standard and the specimen (see Table 1); calculate the sensitivity of the method and its dependence on the dimensions of the specimen and the source and their position relative to each other; estimate the efficiency of the recording apparatus; establish theoretically the dependence of the neutron yield on the height and thickness of the specimen; take exact account of a change in the geometric factors when the analysis is carried out; solve theoretically the problem of choosing the optimum ratio between the height and the thickness of the specimen; estimate the effect of the distance from the radiation source to the specimen; take account of the influence of changes in geometric factors when the analysis is carried out, etc. In solving these problems, one should start from the concrete conditions in each individual case.

As examples of the solution of such problems, we may consider studies on the choice of efficient geometric conditions for the analysis of small specimen weights [formula (1)] and the calculation of corrections for the variation of neutron yield as a function of specimen height in the analysis of enrichment products with no preliminary preparation [formula (2)].

DISPLACEMENT OF URANIUM FROM CHLORIDE MELTS BY ZINC

I. F. Nichkov, S. P. Rasponin, and A. F. Tsarenko

Translated from *Atomnaya Energiya*, Vol. 15, No. 4,
pp. 336-337, October, 1963

Original article submitted December 14, 1962

It is known [1] that a high yield of crystalline uranium trichloride may be obtained by reduction of uranium tetrachloride vapor by zinc metal. In [2] we determined the possibility of reduction of U^{4+} ions during contact of fused uranium-containing halide salts with bismuth metal. As a result of our experiments it was found that the U^{3+} ions formed occur in a compound which is insoluble both in the fused salt system and in bismuth. It was of interest to find whether the uranium tetrachloride in the fused system of alkali metal chlorides would react with zinc metal.

Reaction of U^{4+} Ions and Zinc Metal in a Sodium Chloride-Potassium Chloride Melt with Compound Formation

Temp., °C	Amt. of uranium in elec- trolyte, g	Weight of elec- trolyte, g	Steady-state Zn poten- tial, V*	Uranium content of the electrolyte		Zinc content determined by analysis, g	Zinc con- tent of the compound, g	U/Zn ratio of the compound	U/Zn ratio in the re- action
				Mole %	g				
700	0.348	8.57	1.798	0.082	0.0153	0.0830	0.0677	1.41	1.45
750	0.323	7.68	1.771	0.095	0.0159	0.0755	0.0596	1.49	1.17
800	0.635	8.33	1.729	0.151	0.0290	0.1420	0.1130	1.54	1.23
850	0.344	8.59	1.747	0.070	0.0132	0.0775	0.0643	1.46	1.21

* The zinc electrode potential was recalculated with respect to the chlorine comparison electrode.

For these experiments we used an equimolecular mixture of sodium and potassium chlorides which was fused and a specific amount of uranium tetrachloride added. Before this addition, the melt was thoroughly dewatered and degassed for 2 h in vacuum (residual pressure 1-2 mm Hg). The quartz tube, containing the melt in a crucible, was then filled with pure helium. Uranium tetrachloride was made by chlorinating the dioxide with carbon tetrachloride, followed by purification by sublimation. The purity criterion of the initial components and helium was absence of oxidation and hydrolysis products of carbon tetrachloride in the melts, even after 8 h. A small quartz tube with a lead comparison electrode was placed in the melt. Pure metal was added to the crucible with the uranium-containing melt. Reaction of the latter with zinc was monitored by measurements (with a high-resistance potentiometer) of the zinc potential relative to the lead comparison electrode at 15-20 min intervals. To keep the preset temperature constant (to $\pm 2^\circ\text{C}$), the quartz tube was installed in a metal thermostat unit, heated by an electric resistance furnace. Samples were taken periodically with a quartz pipet to determine the uranium content of the electrolyte. The experiments were ended when the change in zinc potential did not exceed 1 mV in 45-60 min. The cooled electrolyte was dissolved in water and the zinc and uranium contents were determined.

After zinc metal had been added to the U^{4+} -containing melts an insoluble precipitate was formed in all cases and the uranium content of the salt melt fell practically to zero. The precipitate formed as a distinct light-brown layer at the boundary between the cooled electrolyte and zinc. After the melt had been in contact with zinc for a sufficient time, all the uranium was contained in this new phase. The experiments showed that as soon as the reaction of the salt melt with zinc has ended and the electrolyte contains no dissolved uranium the zinc potential remains constant. The change in zinc potential during this reaction is due to displacement of uranium ions by zinc ions, whose concentration in the salt melt determines the zinc electrode potential. We could not separate the precipitate by dissolving the electrolyte in water because it dissolved and was hydrolyzed. To find the zinc content of the precipitate, it was necessary to determine the amount of zinc present in ionic form in the salt melt under these conditions. An investigation of the state of zinc in chloride melts had shown [3] that zinc is present mainly as Zn^{2+} .

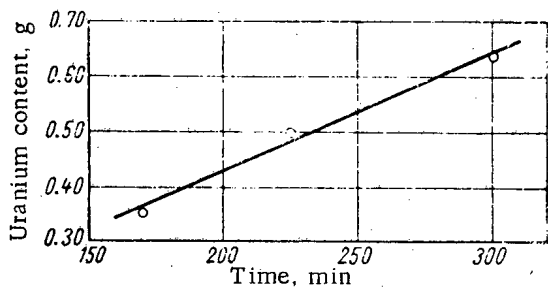


Fig. 1. Relation between the stabilization time of the zinc electrode potential and the amount of uranium at 800°C.

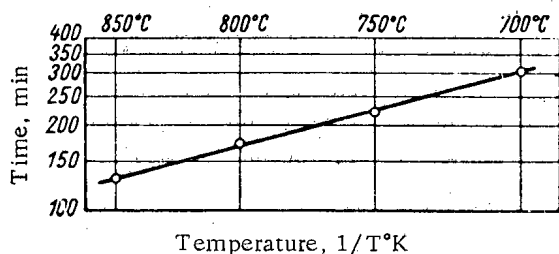
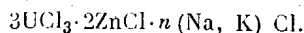
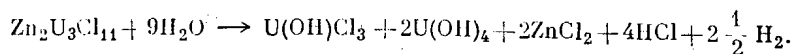


Fig. 2. Variation in the time required for stabilization of the zinc electrode potential in a sodium chloride-potassium chloride melt with 4 wt.% U^{4+} in relation to temperature.

ions (with reduction of U^{4+} ions by uranium metal); one was formed when zinc metal was added to a melt containing U^{3+} and Zn^{2+} ions. It must be admitted that a certain amount of alkali metal chlorides might also form part of the compound. Its composition would then be more complex:



When the electrolyte and the compound were dissolved in water, the latter was decomposed and hydrolysis took place, e.g.,



As a result of instability in aqueous solutions, uranium-zinc chloride of lower valences could not be separated for analysis and further investigation.

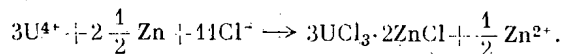
We determined the time necessary for displacement of uranium from fused sodium and potassium chlorides by zinc. Figure 1 shows the relation between the reaction of zinc metal with an equimolecular sodium chloride-potassium chloride mixture to which uranium tetrachloride was added, and time. Stabilization of the zinc potential corresponds to the end of the reaction. It may be assumed that in the investigated concentration range, stabilization of the zinc potential is directly proportional to the uranium content of the melt (for the same area of the zinc surface and at constant temperature, e.g., 800°C). Reduction of uranium to the trivalent state and formation of a compound take place on the zinc metal surface in contact with the electrolyte. It may be assumed that the rate of compound formation will be determined by the rate of transfer of U^{4+} ions to the zinc surface via the diffusion layer of the electrolyte. Therefore, the reaction rate will depend on the diffusion coefficient D of the U^{4+} ions in the sodium chloride-potassium chloride melt.

$D = D_0 \exp\left(-\frac{E}{RT}\right)$, therefore there must be a linear relation between the log of the amount of uranium displaced during the reaction and the reciprocal of the absolute temperature. Figure 2 gives the relation on a semilog scale

ions. The relation between the zinc equilibrium potentials and temperature and the zinc-ion content of the electrolyte had been investigated. Therefore, by measuring the steady-state zinc electrode potential the amount of ionic zinc in the investigated melts could be determined. The difference between the total zinc content, determined by analysis of aqueous solution of the electrolyte, and the zinc content of the electrolyte corresponding to the electrode potential gives the amount of zinc in the precipitate.

The table gives experimental data defining the composition of the compound precipitated from the electrolyte, and the stoichiometric ratios during the reaction of uranium-containing chloride melts and zinc. In all four experiments, stabilization of zinc was obtained and all the uranium passed into the precipitate.

The data of the table show that the ratio of the number of uranium atoms to that of zinc in the compound is ~ 1.5 , and about 1.2 during the reaction (within the limits of possible experimental error). From these ratios we derived the equation for displacement of uranium from chloride melts by zinc with formation of a compound:



The monovalent state of zinc in the compound was confirmed qualitatively. A zinc compound was not formed when zinc chloride was added to a melt containing U^{3+}

between reaction time and temperature under constant experimental conditions. The above linear relation shows that the limiting stage in the reaction is transfer of U^{4+} ions to the surface via the diffusion.

LITERATURE CITED

1. J. Katz and E. Rabinovich, Chemistry of Uranium [Russian translation], Vol. 1, Moscow, Izd-vo inostr. lit., p. 362 (1954).
2. I. F. Nichkov, S. P. Raspopin, and Yu. V. Bazhkov, Zh. prikl. khim., 33, 9, 2136 (1960).
3. I. F. Nichkov, S. P. Raspopin, and A. F. Tsarenko, Izv. vyssh. uchebn. zavedenii, Tsvetnaya metallurgiya, 5 (1962).

All abbreviations of periodicals in the above bibliography are letter-by-letter transliterations of the abbreviations as given in the original Russian journal. Some or all of this periodical literature may well be available in English translation. A complete list of the cover-to-cover English translations appears at the back of this issue.

A NEW TYPE OF POROUS BED MODEL FOR NEUTRON LOGGING

N. K. Kukhareenko, Ya. N. Basin, Yu. P. Bal'vas, and Yu. V. Tyukaev

Translated from *Atomnaya Énergiya*, Vol. 15, No. 4,
pp. 338-339, October, 1963

Original article submitted October 4, 1962

The successful resolution of research problems in neutron logging through the study of geological borehole sections would have been unthinkable without an extensive modeling of porous beds [1]. We shall briefly describe foreign practice in the fabrication of porous-bed models [2]. Blocks of natural rock of a certain lithology and porosity are fashioned in quarries and given a specified shape and size. The rocks are partially dried due to exposure on outcrops, so that they have to be saturated with water or some other fluid prior to fabrication. This technique is highly laborious and even so the resulting models suffer from some important defects: it is difficult, for instance, to find suitably large blocks of rock having adequately preserved porosity throughout their bulk; firm monolithic blocks of rock generally feature low permeability and this hampers fluid saturation; replacement of the fluid filling the pore void of the model (e.g., replacement of water by petroleum) is virtually impossible, and this acts as a severe limiting factor in experimental practice.

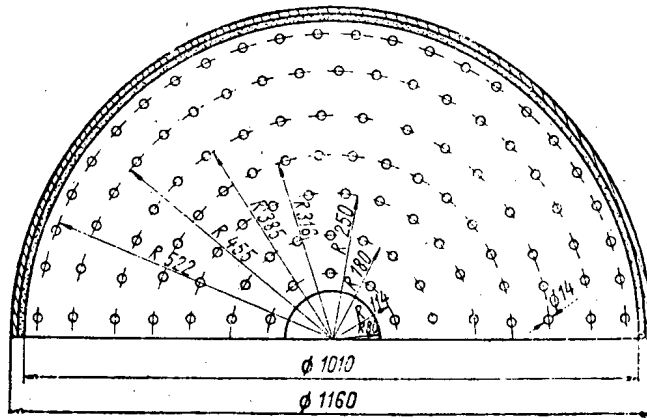
TABLE 1. Hydrogen- and Chlorine-Containing Models

Bed material	Water content, in water equivalents, %				Cl, g/liter (for total bed volume)
	uniform distribution	in horizontal layers	in vertical rods	total	
Sand	4	—	—	4	—
Sand with horizontal celluloid layers	4	2.5	—	6.5	—
Sand with finely divided celluloid evenly distributed throughout the volume	6.5	—	—	6.5	—
Sand with lattice	4	2.5	3.0	9.5	10
Sand with finely divided lattice material	9.5	—	—	9.5	10

A model simulation technique based on the principle of similitude has been proposed in recent years [3]. However, this method likewise suffers from some flaws. First, each new model having a different similitude ratio requires a far-reaching transformation of the borehole instrument; secondly, the design of such models is rendered more difficult by the problem of choosing some substance identical to the fluid filling the borehole and the bed, and replacing that fluid for other measurement conditions.

The authors have developed a new type of model for porous beds, one free from the flaws mentioned.* The outstanding feature of this new line of models is the presence of an artificial pore void. This is brought about by a system of horizontal cavities sandwiched between sheets of dense rock and vertical holes in the sheets. The volume is the same for both. The sheet thickness and the distance between holes (channels) is less than the mean free path length of fast neutrons. The pore void and the borehole model can be filled with ease with any fluid required for the purpose.

* This work was performed at the All-Union Geophysics Research Institute and at the All-Union Research Institute for Nuclear Geophysics and Geochemistry (VNIIG and VNIYaGG).



Arrangement of hydrogen-containing rods in experimental heterogeneous "sand-lattice" model.

TABLE 2. Results of Neutron-Gamma Core Sampling Measurements for Different Hydrogen Distributions in Models (Arbitrary Units)

Bed	50-cm probe		24cm probe
	borehole wall	center	borehole wall
Sand	4.47	3.32	1.51
Sand with horizontal celluloid layers	3.38	2.64	1.61
Sand with finely divided celluloid	3.62	2.96	1.45
Sand with lattice	3.26	2.91	1.38
Sand with finely divided lattice material	3.30	2.97	1.41

An artificial pore void differs substantially from natural bed porosity in size, shape, and distribution throughout the bulk of the rock. This necessitates that the interchangeability of natural and artificial void be justified either theoretically or empirically.

Monte Carlo methods may be used to arrive at results of sufficient accuracy, but no general solution is obtained thereby and, moreover, this approach requires running a program for each variant of the model on a high-speed electronic computer. Beginning steps in this direction have already been taken for a simplified pore-space geometry. At the same time, experiments were conducted on a sand bed model of 40% porosity and 4% moisture content. Sand of this moisture content is roughly equivalent to limestone of 1% moisture content in its moderating properties. Additional water content in the bed (see Table 1) is brought about by a system of horizontal layers of celluloid sheet (2 mm thick in every 50 mm sand), a lattice formed of the same layers and of vertical rods (vinyl chloride tubes of 14/11 mm diameter, paraffin-impregnated, see the figure), pulverized material, evenly mixed with the sand, of the type composing the horizontal layers and the lattice. The celluloid, paraffin, and vinyl chloride material contained, in addition to hydrogen and chlorine, a few other elements. Their effect might be safely ignored on account of their scarcity and their closeness in their neutron properties to oxygen, which is one of the principal components of sand.

In-model experiments were carried out by neutron gamma-logging using probes 50 and 24 cm long in a borehole 15 cm in diameter and filled with fresh water. A VS-14 counter with 0.5-mm thick cadmium lining was used. The results (Table 2) appear in arbitrary units (readings of the appropriate neutron-gamma core sampling probe in fresh water).

We learn from Table 2 that:

1. In the presence of horizontal hydrogen-containing layers, the neutron-gamma log readings were lower for the large probe (50 cm) and higher for the small probe (24 cm) than the readings taken for a homogeneous porous medium of the same hydrogen content. The tabulated hydrogen content in a bed is consequently equivalent to some

hydrogen content larger than the real one (some fictitious water saturation). The differences (derived from comparison to readings for a homogeneous medium) are 7% for the large probe and 11% for the small probe. It is possible to make an approximate estimate of the additional fictitious water saturation from measurements with the 50-cm probe, if we assume the probe readings to be a linear function of the logarithm of water saturation for the range in question. The additional fictitious water saturation will come to roughly 1 abs. %.

2. The neutron-gamma probe readings for both large-probe and small-probe measurements in beds made of sand-with-lattice and the same sand with finely divided lattice material uniformly distributed throughout are almost identical (differing by 1 to 2%). In particular, we see that anisotropy of the bed with respect to hydrogen content brought about by the vertical rods affects the probe readings in just about the same way as anisotropy due to horizontal layers, but with sign reversed. In arriving at this conclusion, we neglected a slight effect exerted by chlorine anisotropy of the sand-with-lattice bed on the probe readings. Tentative calculations demonstrate that this contribution is negligible, however.

The above account confirms the possibility of fabricating artificial porous beds, which we here term heterogeneous porous beds. The new type of model holds great promise and greatly facilitates the solution of research problems in nuclear geophysics. Experimental models of carbonate beds of 11% and 15% porosity for use in neutron core sampling research are now being designed.

LITERATURE CITED

1. O. A. Barsukov et al., Radioactive methods in studies of oil and gas boreholes [in Russian], Moscow, Gostoptekhizdat (1958).
2. I. T. Devan. Symposium on Industrial Geophysics. No. 2 [in Russian], Moscow, Gostoptekhizdat (1960), p. 40.
3. Sh. A. Guberman, Similitude theory and borehole radiometry [in Russian], Moscow, Gostoptekhizdat (1962).

SECONDARY DUST COMPONENT OF RADIOACTIVE CONTAMINATION
IN THE SURFACE LAYER OF THE ATMOSPHERE

B. I. Styro, Ch. A. Garbalyauskas, V. I. Luyanas, V. P. Matulyavichus,
T. N. Nedvetskaite, and I. S. Tomkus

Translated from Atomnaya Energiya, Vol. 15, No. 4,
pp. 339-341, October, 1963

Original article submitted December 8, 1962

A suggestion dating back several years [1] held that a component raised from the ground by the wind in association with finely dispersed dust must be included in the composition of radioactive impurities present in atmospheric air. Subsequently, Reiter [2] discovered, on measuring the concentration of radioactive impurities in both mountain and valley air [2] and taking the ratio of the quantities of long-lived and short-lived components at both such points, that the first ratio was consistently greater than unity, the second consistently less. The explanation offered [1] is as follows. Aerosols settling down from the upper-lying layers of the atmosphere become mixed with radioactive substances accumulated over a long period on the earth's surface and raised by turbulent currents and by the surface air layer. This surface dust contains fallout in which long-lived isotopes predominate.

TABLE 1. Radioactive Fallout in Lithuania, July-August, 1961

Sampling site	Nature of underlying surface	Weight of ashed sample residue, mg	Count of rate sample		Average half-life of sample activity, days
			cpm	cpm · g	
Vil'nius	Sandy ground, overgrown	1992	235	118	36.5
Shilute	Meadowland, thick overgrowth	1553	271	174	57.8
Pile station	Water surface	1823	195	107	57.8
Nida	Running sand covered with sparse flora	4667	522	112	31.5

TABLE 2. Amount of Sr⁹⁰ Present in Radioactive Fallout (July-August, 1961)

Sampling site	Amount of Sr ⁹⁰ precipitated, $\mu\text{C}/\text{km}^2$	Amount of Sr ⁹⁰ precipitated with fallout, $\mu\text{C}/\text{km}^2$	Amount of precipitate, mm	Amount of Sr ⁹⁰ per mm precipitate, $\mu\text{C}/\text{km}^2 \cdot \text{mm}$	Primary component, $\mu\text{C}/\text{km}^2$	Secondary component, $\mu\text{C}/\text{km}^2$	Fraction of secondary component, %
Vil'nius	85.3	76.8	116.0	0.66	31.3	45.5	59
Shilute	127.5	114.7	276.3	0.42	74.6	40.1	35
Pile station	67.8	61.0	226.8	0.27	61.0	0.0	0.0
Nida	61.6	55.4	101.6	0.27	55.4	0.0	0.0

Samplings were made in July and August, 1961 to reveal the secondary component in radioactive fallout and to estimate its quantity. Four sampling points were chosen: the region of the village Nida on the Kursk sand bar (at bar width ~2 km), separated from the mainland by a 12-km bay; at a pile station in the Kursk Bay, 5 km from the sand bar and 7 km from the mainland; in the district of the village Shilute, situated 15 km from the seashore, and in the region of Vil'nius (the Eruzale post at a distance of ~6 km from the city), some 270 km from the shoreline.

Radioactive fallout samples were collected on the surface of distilled water in vessels presenting 3200 cm² surface area, positioned at a height of 0.8 meter above sea level (at a height of ~5 meters above the water level in the case of the pile station). The water was changed once every ten days in the period from July 6 to August 29, 1961, evaporated, and the solid residue was ashed at 500°C.

The activity of the samples collected was measured with an end-window counter, (1.1 mg/cm² thick mica window), following the conventional practice with self-absorption in the sample taken into account. The findings appear in Table 1. Radiochemical isolation of the Sr⁹⁰ from the samples was the next step. In this we were kindly assisted by Prof. V. P. Shvedov, with the analytical work entrusted to N. A. Susorova, to both of whom the authors are deeply indebted.

The relatively large amount of solid residues collected at Nida is accounted for by the existence at that point of fine quartz sand piled up by the strong wind and collected in a cuvette, despite the fact that the terrain is covered by sparse grass. Fine sand grains were carried and deposited by the strong westerly wind even onto the pile station lying 5 km out from the sand bar, and the amount of precipitate collected out there was also comparatively large.

The short effective half-life of the activity of samples collected at Nida and Vil'nius are apparently due to the presence to some components of the naturally radioactive series in the sandy ground.

The minimum of the total activity of the fallout material was discovered at the pile station 7 km off from the mainland, where the possibility of radioactive material and mainland dust impinging is apparently restricted. These data bear evidence of the prominent role played by the dust component blown into the cuvette when turbulent mixing occurs in the ground layer of the atmosphere. The nature of the underlying surface of the restricted region immediately adjacent to the observation point exerts a substantial effect on the activity of the samples collected (see Table 1).

Table 2 lists information on the amount of Sr⁹⁰ precipitated during July and August, 1961. Since the activity of the dry fallout was 10 to 40% of the total activity [3-5], and possibly includes to some extent the secondary dust component, we assume the fraction of the total activity due to dry fallout to be 10%. Assuming this quantity to be 40%, say, the fraction of the secondary component appearing in the last column of Table 2 will agree with the values given to within 1%. After subtracting these 10% from the entries in the second column, we obtain the amount of Sr⁹⁰ precipitated with the fallout. Again, assuming the secondary dust effects above the pile station in the bay to be insignificant, we take 0.27 μC Sr⁹⁰ per km² · mm as the activity contributed by fallout reaching the ground, with no perceptible secondary effects added. This assertion is apparently close to the truth since westerly rains and winds were observed during that period sweeping shoreward air masses into the neighborhood of Nida and the pile station immediately after these air masses passed over the Baltic Sea. The sampling point at Shilute was 15 km away from the shore of the Kursk bay and 20-22 km from the pile station. We may, therefore, assume that the synoptic processes developed above these sampling points were the same during the period of observation, and that the activity swept out of the troposphere by the fallout precipitates was in consequence the same as well. This permits us to assume that 1 mm of fallout precipitate at Shilute also accounts for 0.27 μC Sr⁹⁰ per km² · mm. A similar inference with respect to Vil'nius is less reliable, however.

Making use of the values and fallout data listed, we may calculate the amount of Sr⁹⁰ falling out at Shilute and Vil'nius in rainfall, and the contribution of secondary effects. The data indicate 35% and 59%, and are highly significant. Even though the data for the Vil'nius region may meet with some objection, considering the distance of the pile station sampling post from that city, the data referable to the Shilute area appear to be close to the real values.

If the fraction of the secondary component is about 35%, then this contribution must be taken into account in an estimate of the build-up of fallout activity on the earth's surface. It should be borne in mind that the investigations were conducted during the summer, in a lull in nuclear weapons testing. Values at variance with the ones reported could be obtained at some other time. The numerical values for the fractions of secondary precipitates might be different for other isotopes, and might be different again if this process were studied in areas featuring a different underlying surface and flora.

The authors make no pretension to a high order of accuracy in the values cited for the contribution of the secondary effect. The purpose of this communication is to demonstrate that this effect may be a significant one, and at the same time to draw the attention of the scientific community to the problem of setting up and performing similar investigations, with attendant experimental difficulties.

The authors express their acknowledgements to students R. Minkyavichus and R. Kozhenyauskas of the Vil'nius State University for their invaluable assistance in the work of the sampling expedition.

LITERATURE CITED

1. B. I. Styro, Problems of nuclear meteorology [in Russian], Vil'nius (1959), p. 1.
2. R. Reiter, Naturwissenschaften, 47, 300 (1960).
3. E. Wilkins, Trans. Amer. Geophys. Union, 39, 30 (1958).
4. W. Gerlach and K. Stirstadt, Atomkern Energie, 4, 143 (1959).
5. W. Marquardt, Z. Meteorol., 15, 221 (1961).

NEWS OF SCIENCE AND TECHNOLOGY

CONFERENCE ON ELECTROSTATIC GENERATORS
AND DIRECT-VOLTAGE ACCELERATORS

G. M. Osetinskii

Translated from Atomnaya Énergiya, Vol. 15, No. 4,
pp. 342-343, October, 1963

A workshop attended by member nations of the Dubna Joint Institute for Nuclear Research was held in late March, 1963 at Dubna to discuss the physics and engineering of electrostatic generators and direct-voltage accelerators.

The conference was attended by over 70 specialists from member nations of the Joint Institute, including various institutional representatives from the Soviet Union. Interest in the conference was high, for a vast amount of experimental material has been accumulated in recent years, both on the operation of electrostatic generators and on the design of individual components.

Thirty-three papers were presented to the conference on the design of electrostatic generators, techniques for focusing particle beams, design of ion sources for various electrostatic generators, and various sets of operating conditions. A special session was devoted entirely to the design of polarized sources and direct-voltage accelerators.

A paper presented by V. I. Chetvertkov (NIIÉFA—the D. V. Efrémov Research Institute for Electrophysical Equipment) took up various aspects of the development of high-precision systems for stabilizing accelerating voltages (stabilization to about $\pm 0.01\%$) in proton-accelerating electrostatic generators. The formulas submitted by the author make it possible to estimate the energy variation of accelerated particles when due to instability in the angle of inflection and in the position of the beam as it enters the analyzer magnet, as well as instability of the position of the slit terminal device. This paper also examined for the first time an ion-optics technique for measuring energy fluctuations of charged particles, using beam deflection prior to entry into the magnetic analyzer. This method is distinguished by its high speed and makes it possible to measure the conductor-potential instability even in the presence of a liner. The time-of-flight of negative corona ions in the high-voltage gap of an electrostatic generator was calculated, and an expression was offered for the transient, frequency, and phase response characteristics of the corona spray triode.

A report by M. Čihák (Nuclear Research Institute of the Academy of Sciences of the Czech SSR) was devoted to designs of high-voltage stabilization circuits in electrostatic generators, to an accuracy not inferior to 10^{-4} , and based on the general theory of automatic control.

V. I. Chetvertkov and A. L. Fedulov (NIIÉFA) rendered an account of the performance of an accelerating voltage stabilization network at ~ 150 -200 keV for a neutron generator at currents to 3 mA, designed with transistor and magnetic components. The network stabilizes to within 1-2%, is inexpensive, and is in practice ready for operation immediately after plugging in.

Stabilization of the magnetic field of electromagnetic analyzers by nuclear magnetic resonance was the subject of a paper presented by V. G. Kunstman (NIIÉFA). The author showed that high accuracy in the reproduction of a field distribution, and consequently high accuracy in measuring beam energy of an electrostatic generator requires that the analyzer field follow a specified cycle consistently, otherwise the error in energy measurements will run to 0.5%. If the field is programmed to consistently follow a specified hysteresis loop, at a rate not exceeding 20 Oe/sec, the analyzer may provide an accuracy of about 10^{-4} of relative energy measurements. The error will increase as the rate of change, and the error increase will be less on the downward branch of the hysteresis loop than on the ascendant branch.

P. E. Vorotnikov (I. V. Kurchatov Institute of Atomic Energy) calculated the phase focusing (bunching) of ions emerging from an ion source by a variable longitudinal electric field, to obtain current pulses lasting $\sim 10^{-9}$ sec at a pulse repetition rate 10^6 to 10^7 sec $^{-1}$ from an electrostatic generator. It was shown that a conventional low-current

ion source yields pulses lasting $3 \cdot 10^{-9}$ sec at a pulse current of $\sim 1-1.5$ mA at the accelerator exit when a buncher electrode is added to the ion-optical system. This current is 10 to 30 times larger than currents now achieved. This mode of operating an electrostatic generator has some important practical applications (time-of-flight spectrometry, study of short-lived nuclides, work under high background-level conditions, etc.).

The paper "Remarks on focusing of ion beams in electrostatic generators" submitted by D. Paris (Academy of Sciences of the Hungarian People's Republic) was received with rapt attention. The author presented the operating details of the ion evacuation system using a high-frequency source, and pointed out the intriguing possibility of focusing a beam with a resultant reduction in the amount of gas used up in the source. Attention was directed to the salient features of focusing multicomponent accelerator tubes.

T. Saidl (Institute of Nuclear Research of the Academy of Sciences of the Czech SSR) reported calculations of the principal optical parameters of accelerator tubes (focal length, transverse magnification, ratio of inner and outer beam diameters, etc.).

Papers submitted by G. Ya. Roshal' (NIIÉFA), V. A. Romanov (Power Physics Institute), E. Gurski (Academy of Sciences of the Polish People's Republic), J. Cirak (Academy of Sciences of the Czech SSR), G. Winger (East Germany) presented the results of experience in the design and operation of 2 to 5 MeV electrostatic generators.

Much attention was given to ion sources for dc electrostatic generators.

A report by S. G. Tsepakín et al. (NIIÉFA) told of the development of high-frequency ion sources at currents 300 μ A, 2 mA, 10 mA. A series of duaplasmatron type sources at 20 mA current in the steady state and 0.05, 0.5, and 1.5 A in pulsed operation has been developed. Data on sources using a Penning type discharge and operated in pulsed mode with 15 mA current were presented. Electron sources with currents of 1 and 10 mA in the steady state were also reported on.

A paper submitted by N. F. Ivanov, V. S. Kuznetsov, A. I. Solnyshkov (NIIÉFA) entitled "Shaping of pulsed ion beams with current of the order of hundreds of milliamperes in dc accelerators" presented a procedure for designing the optical system of high-current beams with volume charge taken into account. This method is used for designing the optics of a hydrogen ion injector at 400 mA and 700 keV energy. The results of the measurements, which were in agreement with theoretical prediction, were reported. A beam 15 mm in diameter with 400 mA current and 700 keV beam energy was obtained.

A. N. Serbinov and V. I. Moroko (Power Physics Institute) reported on a pulsed high-frequency source with a honeycomb extraction system. Tests were run on two variants of the extraction system, differing in the size of the cathode-anode space (1.8-2.2 mm). In the first variant an ion current of 21 mA in a pulse lasting 1 μ sec was obtained in acceleration to 270 keV energy. The second variant yielded a current of 220 mA. The gas flowrate of the hydrogen source was 15 cm³/h.

A paper by P. S. Markin (Academy of Sciences of the Ukrainian SSR) cited data on an inexpensive ion source. This ion source is based on an arc discharge in an axial magnetic field with a heated cathode, hollow anode, and insulated anticathode (modeled after the Abel-Meckbach source). The source was studied in steady state and in pulsed operation. Doubly-charged carbon, nitrogen, and oxygen ions are found in the spectrum of the ion source.

A paper by V. I. Man'ko (Institute of Atomic Energy) dealt with parallel feed of ion sources into a double-tube electrostatic generator.

B. P. Ad'yasevich (Institute of Atomic Energy) reported on the fabrication, design, and testing of a source of polarized ions (protons and deuterons) in which polarization of nuclei in an atomic beam is achieved by adiabatic extraction of hydrogen atoms found in the state $m_j = +\frac{1}{2}$ from a strong-field region to a weak-field region, followed by electron collisional ionization. The polarized ion source built by the authors provides a current of ~ 0.1 μ A. Proton polarization reaches 50%, deuteron polarization reaches 33%.

A source designed on the same principle was discussed in a paper by R. P. Slabospitskii et al. (Physics and Technical Institute of the USSR Academy of Sciences).

"Injection system of negative ions for the tandem electrostatic generator PG-5," a paper submitted by A. Ya. Taranov and Yu. Z. Levchenko (Physics and Technical Institute), dealt with the design of a source of negative ions for this electrostatic generator based on the transformation of positive ions to negative ions through a mercury jet target.

The authors obtained intense beams of negative hydrogen and oxygen ions. They studied the injection conditions for a beam of negative ions shot into the tandem accelerator, the conditions for passage of the beam down the accelerator ion duct at various voltages across the duct, etc.

The design of standardized NG-200-Sh neutron generators with neutron flux higher than 10^{10} neutrons/sec was the subject of a paper by V. D. Mikhailov (NIIÉFA).

A report by O. B. Ovchinnikov (NIIÉFA) provided information on the building of a 2.5-MeV accelerator with a balanced multiplication circuit as high-voltage source. The accelerator was designed to produce 25 kW electron or ion beams. The high-voltage part of the accelerator is placed in a compressed-gas tank.

B. I. Al'bertinskii presented a report on the work of a NIIÉFA team developing techniques for calculating the output characteristics of capacitance type voltage-multiplication circuits. The comparison between calculations and results of measurements made on various models of symmetrical cascade generators, presented by G. M. Osetinskii, showed that the method proposed is totally satisfactory for taking into account internal resistance effects in the switching components (transistor components included), internal resistance of the power supplies distributed over protective stages, stray capacitances distributed over compensating inductance stages. Expressions were derived for calculating the simulating factors of various voltage circuits.

Upon the conclusion of the conference, the delegates visited the Nuclear Problems Laboratory, the Nuclear Reactions Laboratory, and the Neutron Physics Laboratory.

INTERNATIONAL CONFERENCE ON SECTOR-FOCUSED CYCLOTRONS
AND MESON FACTORIES*

P. Lapostol

CERN, Geneva

Translated from Atomnaya Énergiya, Vol. 15, No. 4,
pp. 343-346, October, 1963

Sector-focused cyclotrons have been stirring up increasing interest among workers in many laboratories throughout the world during the past few years. In some laboratories, sector-focused cyclotrons are already in operation or are under construction, and many other laboratories have plans for installing such machines. Scientists in universities and laboratories (particularly European ones) engaged in work or studies on sector-focused machines have, therefore, naturally displayed keen interest in any opportunity to exchange their ideas and experiences. At the April 1963 conference sponsored by CERN, 150 scientists from 60 laboratories in Europe (including the Soviet Union) and America were in attendance; a total of 66 papers were read. Since the preceding Los Angeles conference took place rather recently, this conference was devoted either to new advances or new topics which did not find place on the agenda of the preceding conferences covering related matters (e.g., physical experiments which might be carried out with the aid of sector-focused machines, acceleration of polarized particles, etc.).

Experience in the operation of sector-focused cyclotrons. R. Livingston (Oak Ridge), on opening the session, presented a review of the sector-focused machines already in operation, which are listed in the accompanying table. He noted that the difficulties in the way of achieving isochronism have been overcome, the quality of the beam extracted is not inferior to that of other accelerator types, the duty cycle is 4-5, and negative ions have been successfully accelerated, with new vistas opened up for physical experimentation. One serious difficulty, though, is induced radioactivity, but the use of graphite at the low temperatures involved pretty much solves this problem too.

One strong positive feature of sector-focused cyclotrons is their flexibility and reliability; slight energy adjustments can be carried out in a few seconds, the energy may be varied substantially or the type of particle accelerated may be completely changed in a matter of hours, and the machines are capable of stable operation for hours and days on end at the specified operating conditions.

Reports followed on the machines installed at Oak Ridge, Berkely, and elsewhere. The delegates were very much interested in a description of experimental procedure for optimizing the parameters of the r-f voltage and magnetic field in order to attain the optimum isochronism conditions.

In the Karlsruhe cyclotron, the orbits may be run up to the maximum energy (200 turns). Field perturbations with a harmonic of the order of 0.1% were found to result in betatron oscillations of 9-mm amplitude.

The delegates heard a report on the Ann Arbor (Michigan State University) sector-focused machine which was just commissioned. The most sophisticated machine of this type discussed was the Philips firm 130-cm cyclotron. The final assembly of the machine was completed on April 4, 1963, and two days later 400 turns on a radius out to 53 cm (at 14 MeV) were achieved. After some final readjustments, particles of 20 MeV energy were produced on April 12. The deflector was mounted on April 17, and 30% of the particles orbiting were extracted on the following day.

Particle extraction is one of the problems where current progress is most spectacular. Both of the methods used—the now conventional peeler-regenerator method and the resonance method (employing both natural and forced resonance) presented strikingly encouraging results. In the electron analog (Oak Ridge machine), 85% of the particles were extracted when the $\nu_r = 2$ resonance was used. The dependability of this type of extractor is determined not solely by the exact channel design, but also by the careful and thorough examination of the problems connected with high voltage.

* The term "meson factories" in this context means 400-800 MeV accelerators with a proton beam intensity 100 times greater than in present-day synchrocyclotrons.

The Birmingham cyclotron uses an electrostatic peeler and regenerator system to achieve an extracted current of up to 40 μ A at 35-40% efficiency.

Isochronous Cyclotrons Presently Commissioned (as of April 15, 1963)

Location of machine	Year commissioned	Number of sectors	Pole diameter, cm	Maximum internal-beam energy of orbits, MeV	Energy of other beams, MeV	Extracted-beam energy, MeV	Number of orbits
Delft	1958	4	85	12 (p)			>300
Urbana	1958	4	111	15 (p)	4-15 (p)	15 (p)	>100
Dubna	1959	6	120	13 (d)			>1000
Harwell	1959	3	56	3 (p)			
Moscow	1959	3	150	32 (d)	6 (p), 17, 29 (H ²), 35 (He ³)	32(d), 20(H ²)	>160
Los Angeles	1960	4	125	50 (p)	48(H ⁻)	48 (H ⁻)	>1000
Birmingham (UK)	1961	3	102	12 (d)	11 (D ⁻)		>400
Berkeley (Cal.)	1961	3	224	130 (α)	25, 50 (p), 16, 33, 40, 65 (d), 25(He ³), 33, 65, 75, 80 (α)	50 (p), 16-38 (d), 33-75 (α)	>600
Oak Ridge	1962	3	193	90 (α)	8, 12, 32 (p), 40 (d)		>500
Boulder	1962	4	132	24 (p)	80 (α) 16, 19 (p), 8(H ⁻), 17(D ⁻), 30 (α)	8(H ⁻), 16, 19 (p)	>200
Davis	1962	3	56	10 (p)			>100
Ann Arbor	1962	3	229	50 (d)	50 (H ²)		>210
Karlsruhe	1962	3	211	40 (d)	7, 12 (p), 15 (d)	12 (p), 26(d)	>150
Eindhoven	1963	3	142	12 (p)			>400
Oak Ridge (electron analog)	1961	8	79	530keV		430 keV	>2600

The Philips firm has developed a new accessory which they call a regenerator-compressor. The compressor functions to displace a perturbation caused by the regenerator to greater radii, thereby setting the radial focus at the channel entrance and maintaining a wide separation of orbits. This device has been successfully used to extract 15% of the particles from a synchrocyclotron.

Physical experiments using sector-focused cyclotrons and meson factories. On opening this session, A.Zucker (Oak Ridge) made an analysis of the physical problems awaiting investigation on high beam-intensity accelerators in the 20-100 MeV energy range. He stressed the point that one particularly vital feature of sector-focused machines is the possibility of varying the energy and varying the type of particles, combined with the high beam quality and the excellent energy resolution (of the order of 10 keV).

H. Bernadini (Rome, CERN) took note of the value accelerators designed for ~500 MeV have for pion physics. High-intensity proton beams of 800 to 1000 MeV energy are required in some high-precision experiments and studies on rare events. Still higher energy ranges would be interesting in research on higher-lying resonances and even for prying open the K-meson shell, but in the 1 to 12 BeV range there is at present no most preferred energy.

The conference proceeded from these introductory lectures to discuss several special topics:

- acceleration of negative hydrogen ions, now apparently within reach, and promising a most intriguing solution to the extraction problem;

- production and acceleration of polarized particles, which will be a great help in carrying out many novel experiments.

At the present time, satisfactory results have been reported, and it appears to be entirely within the realm of possibility to increase the energy of negative and polarized particles accelerated in sector-focused cyclotrons to 100 MeV by an appropriate engineering of the magnetic field and accelerating system.

Shielding and activation problems which crop up in the design of targets and beam catchers are very serious in the case of high beam-intensity accelerators. These problems are the most serious limitations on meson and pion factories. Many different materials have been studied as potential beam-stop materials, but aside from carbon and

silicon none of them furnish any appreciable decrease in activation. The solution might possibly be found in the choice of geometry for the parts on which the beam impinges, and in the use of heavy materials to shield against induced activity.

One of the reports took up the problem of duty factor, particularly with respect to meson factories. The required low-frequency and high-frequency duty factors may be evaluated in accordance with the requirements of the experiment, the speed of light, and the time required to carry out the experiment.

Advances in the theory and design of sector-focused machines. Many new and interesting developments came to the attention of the conference. Among these we may note a quantitative study of the effect of the spiral angle on the stability region; a program for mapping the magnetic field for an accelerator of up to 800-900 MeV with a specified energy dependence of ν_z ; a new method for calculating the distribution of magnetic field index with variable permeability of the field taken into account.

A report produced by Michigan University showed that the use of a narrow slit at the center in a preacceleration process reduced betatron oscillations and narrowed down the duty cycle. The possibility of employing a double-dee accelerating system operating at various harmonics is under study. More detailed calculations have been performed for various extraction systems. The status of construction and assembly work on various sector-focused cyclotrons (at Milano, Orsay, Grenoble, Michigan State University) was reported. An ingenious technique for studying a cyclotron magnetic field was proposed: direct determination of ν_z with a "floating wire" ("CSF"). A design of the magnetic channel and deflector as a coaxial transmission line with a slit where it would be a comparatively easy matter to shape the field as desired deserves mention here.

A Berkeley team is engaged in the study of problems involving very high deflector voltages: improving the mechanical rigidity of electrodes (to avoid vibrations in response to electrical forces), choice of material (inconel or stainless steel, and tungsten for the anode), and the effect of the beam. For a successful design with a generous safety margin, we may use $VE = 1500 \text{ kV}^2/\text{mm}$.

There was a report on a magnetic beam locator developed at Argonne National Laboratory; the probe is capable of measuring the position of a $0.09 \mu\text{A}$ beam, without introducing distortions, to within $\pm 0.1 \text{ mm}$.

Meson factories. R. Richardson (University of California) made a survey of various types of meson factories. The comparison was based on such parameters as duty cycle, practicability of the beam desired, beam quality with respect to precise energy information, possibility of varying the output energy, possibility of producing several beams simultaneously, induced radioactivity, complexity of design, reliability, and costs. The usual type of sector-focused cyclotron was shown to have acceptable parameters in all respects. A cyclotron built to accelerate negative ions would not be exorbitantly expensive if it were to be doubled in size, and still would feature such advantages as variable energy, good duty factor (if isochronism losses occur immediately prior to stripping), and the possibility of producing several beams simultaneously with different energies. A synchrocyclotron with spiral-ridge focusing may yield appreciably greater intensity than a conventional synchrocyclotron because of the higher repetition rate; the particle extraction efficiency will be enhanced and an added bonus is the possibility of accelerating a variety of particles. A spiral-sector ring synchrocyclotron differing slightly in design from its earlier counterpart had similar beam parameters: intensity to $100 \mu\text{A}$, extraction efficiency of $\sim 30\text{-}40\%$.

A strong-focusing proton synchrotron is much cheaper, but it is impossible to obtain a high intensity with that machine. A separated-orbit cyclotron may feature most of the advantages pointed out, but the cost and complexity of a machine of this type seem too high a price at present.

In linear accelerators, the extraction efficiency is 100%, the beam intensity and energy may be regulated with great ease, and there is no problem in accelerating polarized particles. The disadvantages in this case are the large duty cycle and, possibly, the high cost. Improved duty factors might be attained in the cryogenic linear accelerator. Studies on experimental models have shown that r-f losses may be reduced by a factor of 10^4 when lead and niobium are used. However, the fabrication of full-scale resonators is still an exceedingly difficult engineering feat, and it might take several years before engineering plans for a full-scale accelerator of this type become definitive.

The Zürich group suggested an annular isochronous cyclotron in which the central region would be absent. Particles are to be injected into the racetrack at 70 MeV from a conventional sector-focused machine, and the terminal energy of 500 MeV will be limited by the $\nu_r = 1.5$ resonance. The advantage seen in this annular facility is the potential usage of several extraction systems and greater ease in positioning targets, improvements over the presently

available counterparts. When particles are transferred from the injector cyclotron to the annular one, crossing of resonant lines may be avoided and improved focusing may be attained in the annulus by choosing v_z close to unity. The extraction and injection efficiencies will be less than 100%, of course.

The separated-orbit cyclotron suggested by F. Russell (Oak Ridge) is something of an ingeniously conceived hybrid between linear and cyclic accelerators. It is a cyclic machine, but each revolution (in a total of about 100 revolutions) will have its own independent guide field, and this will make it possible to obviate resonance effects, just as in a linear accelerator. Acceleration will take place in from 5,000 to 10,000 acceleration intervals formed by some 50 to 100 resonators distributed in the meridian planes. Phase stability is the same as in linear accelerators, but the grouping of accelerating gaps in the resonators loosens the r-f field specifications. Energy variation at a given point is impossible, but extraction may be accomplished at 100% efficiency, in theory, from any point on the orbit. The principal defect in this type of accelerator, very similar in construction to a wasps' nest, is the ordinarly high cost and the vast number of engineering problems to be overcome in building suitable magnets, the vacuum system, and the resonators.

The principal limitations imposed on intensity in FM sector-focused cyclotrons were discussed, and it was shown that frequency-modulated sector-focused machines could produce measurably higher intensity than presently existing FM cyclotrons.

Finally, a design of a muon microtron capable of producing high-intensity pure muon beams was described.

The conference clearly revealed that the time when accelerators could be built on the basis of rough cut-and-try calculations or approximations belongs to the past. At present, computer techniques enable designers to begin with a detailed study of not only linear, but also nonlinear, problems.

The experience accumulated in operating machines now in service demonstrates that all of the theoretical work carried out has been exceptionally useful. The machines are operating in accord with theoretical predictions, and are put into operation without mishap, thanks to the accuracy of the engineering calculations, and their performance is dependable, flexible, and versatile. These achievements serve as a stimulus to machine designers, and the development of theory leads to a better understanding of the conventional cyclotrons, synchrocyclotrons, and of extraction problems concerning the successful operation of all existing cyclic accelerators.

Sector-focused cyclotrons pose a host of difficult and fascinating engineering problems before design engineers in connection with the magnetic field, r-f system, and high-voltage techniques. It is quite possible that these machines will excite somewhat lesser interest than accelerators designed for extremely high energies; but they are far more accessible and it is most significant that new advances and new inventions are constantly coming to the fore despite the fact that cyclotron engineering has a rather long history behind it. One might even conjecture that the lack of enthusiasm for acceleration of H^- ions is partially to be accounted for by the relative routineness of this problem, and the fact that it falls short of promising a sufficiently broad field of activity to engage the intense interest of theoreticians and engineers.

Independently of what type of accelerator will be accepted for the task of constructing meson factories, they will all come in handy for a detailed probing into pion and muon physics. It is to be anticipated that 500-800 MeV cyclotrons yielding excellent beams will be built. The energy range up to 12 BeV, where K-mesons and antiprotons come in for intensive study, would obviously be brought within range by machines of other types.

IAEA SYMPOSIUM ON THERMODYNAMICS OF NUCLEAR MATERIALS

V. V. Akhachinkii

Translated from Atomnaya Énergiya, Vol. 15, No. 4,
pp. 346-351, October, 1963

In May, 1962, an international symposium of the thermodynamics of nuclear materials was sponsored by the International Atomic Energy Agency at Vienna. The proceedings appeared subsequently under the title Thermodynamics of Nuclear Materials, IAEA, Vienna, 1962. Forty-six papers delivered at the symposium may be found in this publication. In consideration of the importance of the information contained in those papers, we present here a brief account of the topics covered in them.

The classification as to subtopic was not particularly strict, and there will accordingly be some overlap between the subjects dealt with in different papers mentioned.

General problems of the thermodynamics of the actinides, and applications to theory. E. Westrum and F. Gronfold (USA) presented an information-packed paper on the thermodynamics of oxides, sulfides, selenides, and tellurides of the actinide elements. The reference ran to 135 titles. The major portion of their attention was centered on the thermodynamics and phase relations of the uranium-oxygen system. A method was proposed for estimating the entropies of chalcogenide compounds and values of the standard entropies of oxides of all the actinides and lanthanides were listed, as well as the entropies of the sulfides, selenides, and tellurides of uranium and thorium. For the first time, experimental thermodynamical data were presented (see Table 1) referable to uranium sulfides (at 298°K).

A report by R. Ackerman and R. Thom (USA) used a comparison of the properties of gaseous monoxides and dioxides of the actinide elements to the properties of the counterpart compounds of other elements to explain the duality of the chemical nature of the actinides. The author's view is that this method for shedding light on the nature of the transactinide elements is better than the method used by Cunningham and Haissinsky, who considered ions in aqueous solutions and in solids.

B. Cunningham (USA) reported a wealth of new information on americium and curium: types and parameters of crystal lattices, thermal expansion coefficients, magnetic susceptibilities. The melting point of americium was reported to be $995 \pm 7^\circ\text{C}$, that of curium $1340 \pm 40^\circ\text{C}$.

M. Rand (Great Britain) cited some thermodynamical data for uranium compounds where conflicting reports exist, and suggested several thermodynamics problems for solution.

A report by I. Prigogine and R. Balescu (Belgium) was devoted to the thermodynamics of nonequilibrium states.

G. Reiss (USA) outlined the basic principles of the statistical thermodynamics of fused salts. Some of the characteristics of fused halides of the alkali metals were computed (e.g., heat of mixing, surface tension, compressibility).

S. Takeuchi and K. Suzuki (Japan) reported a statistical-thermodynamical calculation of the pressure of hydrogen in equilibrium with the PuH_2 phase containing a region of homogeneity. The relationship between the number of hydrogen atoms occupying octahedral and tetrahedral vacancies in the plutonium was also computed as a function of composition and temperature.

TABLE 1. Experimental Thermodynamical Data for Uranium Sulfides at 298°K

Compound	C_p , in cal/mole deg	S° , entropy units	ΔF° , kcal/mole
US	12.08	18.63	-87
US ₂	17.84	26.42	-120
U ₂ S ₃	22.85	33.08	-127

A. Searcy and D. Meschi (USA) computed the integrated and the partial thermodynamical functions for the U-H and Zr-H systems from data on dissociation pressure.

A paper submitted by O. Kubashevsky (Britain) contained material on phase diagrams based on thermo-

TABLE 2. Thermodynamical Characteristics of Inter-metallic Compounds of Uranium

Compound	ΔH° , kcal/mole	ΔS° , entropy units
UZn ₁₂	-54.2	-38.2
UCd ₁₁	-27.2	-36.4
UGa ₃	-41.4	-14.5
UIn ₃	-26.3	-13.0
UTh ₃	-43.2	-11.7
USn ₃	-40.8	-13.9
UPb ₃	-20.9	-9.4

dynamical data, as well as a discussion of the solution of the converse problem. Concrete examples were cited of the construction of phase diagrams and prediction of data for binary systems of interest in nuclear power applications (Zr-Hf, U-Zr, Bi-Cd, Bi-Zn, U-W, U-Fe). The author's feeling is that an exact phase diagram might be plotted in some cases exclusively on the basis of thermodynamical data.

E. Rudi (Austria) devoted his report to the thermodynamics of refractory uranium and thorium compounds. Cross sections of ternary phase diagrams of uranium and thorium with carbon and Zr, Hf, Nb, Ta, Mo, W, and

also ternary diagrams of uranium, thorium, and other refractory materials with boron, carbon, and nitrogen were produced.

Experimental procedure and techniques. G. Skinner (Britain) reported on the most recent improvements in methods for determining the heat of formation, the most important of which were, in his view, the rotating calorimetric bomb, combustion in a calorimetric bomb in a fluorine atmosphere, calorimetry of high-temperature reactions, and calorimetry for research on very slow reactions (Tian-Calvet calorimeter).

H. Feder et al. (USA) reported on the application of an oxygen and a fluorine calorimetric bomb, a glass bomb for observing the nature of combustion, a bomb for pyrophoric substances, and several other devices. Experimental procedure and technique was also touched on in most of the other papers.

Alloys. G. Smith (USA) studied the thermodynamics of the formation of binary magnesium compounds with calcium, copper, nickel, and yttrium by measuring vapor pressure by the Knudsen method. Vapor pressure values were reported for magnesium (626-818°K), calcium (844-965°K), and also above certain two-phase systems, as for example, Ca + Mg₂Ca, I + MgI, etc.

G. B. Fedorov and E. A. Smirnov (USSR) used the Knudsen method to measure the vapor pressure of pure zirconium and the partial pressure of zirconium above its alloys with tin.

On the basis of the data obtained, the thermodynamical characteristics of β -zirconium were plotted, as well as thermodynamical activity and changes in partial thermodynamical functions of zirconium and its alloys with tin.

V. V. Akhachinskii, L. M. Kopytin, M. I. Ivanov, and N. S. Podol'skaya (USSR) determined the heats of formation of intermetallic compounds of plutonium with aluminum and iron, and of uranium with iron, from the heats of solution of these compounds and of their constituents, and obtained the following values:

Compound	ΔH° , 298 kcal/mole
PuAl ₂	34.0 \pm 0.8
PuAl ₃	43.2 \pm 0.8
PuAl ₄	43.2 \pm 0.8
PuFe ₂	6.5 \pm 0.4
UFe ₂	7.7 \pm 0.3

In addition, the heats of formation of the compounds PuAl, Pu₃Al, Pu₆Fe, and U₆Fe were estimated at, respectively: -17; -17; -3.3; and -3.9 kcal/mole, with an error not exceeding +30%. I. Johnson and H. Feder (USA) used the electromotive force method to study the thermodynamical properties of binary systems of uranium with Zu, Cd, Ga, In, Tl, Sn, and Pb. Equations for the free energy, heat and entropy of formation of seven compounds were reported over the range from 300 to 950°C. Some of the data referable to the temperature 430°C are reproduced in Table 2.

The optical absorption method was used by P. Rice, G. Balzhiser, and D. Ragone (USA) to determine the thermodynamical activity of bismuth in the uranium-bismuth system over the 1018-1115°K temperature range. The authors calculated the free energy of formation of UBi, U₃Bi₄, and UBi₂ from liquid bismuth and γ -uranium, and obtained the following equations:

$$\begin{aligned} \text{for UBi } \Delta F^\circ &= -12\,320 + 4.40 T \pm 370 \text{ cal/g-atom,} \\ \text{for U}_3\text{Bi}_4 \Delta F^\circ &= -12\,980 + 5.10 T \pm 360 \text{ cal/g-atom,} \\ \text{for UBi}_2 \Delta F^\circ &= -11\,440 \pm 4.90 T \pm 280 \text{ cal/g-atom.} \end{aligned}$$

TABLE 3. Basic Thermodynamical Characteristics of Thorium, Uranium, Plutonium, and Their Oxides

Substance	$\Delta F^\circ (=A+BT)$, cal/mole	$\Delta H^\circ_{\text{subl}}$, kcal/mole	$\Delta S^\circ_{\text{subl}}$, e. u.	Temp. range, °K
Th(g)	131700-27.4T	131.7 ±2.8	27.4 ±1.5	1757-1956
Th(g)	- 40300-14.4T	173.5 ±2.2*	38.4 ±1.0*	2200-3000
ThO ₂ (g)	-137300+11.1T	158.7 ±2.5	35.3 ±1.0	2200-3000
ThO ₂ (s)	-296000-46.4T	—	—	2000-3000
U(g)	106760-26.09T	106.76±0.01	26.09±0.07	1630-1970
UO(g)	(-16800-10.0T)	(151,5)*	(33,4)*	1900-2500
UO ₂ (g)	-121522± 4.24T	137.1 ±1.7	36.4 ±0.9	1600-2400
UO ₃ (g)	-198500±19.0T	92.0 ±2.0 †	41.0 ±2.0 †	1230-1700
UO ₂ (s)	-258650+40.64T	—	—	300-1500
Pu(g)	80500-22.94T	80.50±0.04	22.94±0.6	1392-1793
PuO(g)	- 20600-18.4T	(146)*	(37)*	1700-2000
PuO ₂ (g)	(-122000+ 5.0T)	(131)	(35)	1800
Pu ₂ O ₃ (s)	(-393000+63.0T)	—	—	—
PuO ₂ (s)	-251600+40.25T	—	—	10000-1500

*Corresponds to removal of one mole MeO (g) from MeO₂ (s).
†Corresponds to the hypothetical process UO₃ (s) → UO₃ (g).

The activity coefficient of uranium in a dilute solution with bismuth is $\log \gamma^\circ = 2.670 - 5625/T$ (°K).

The free energy of formation of uranium carbide, $-22,000 \pm 1800$ cal at 1075°K, and $-19,500$ cal at 1275°K per gram-atom of U, was found by determining the concentration of uranium in liquid bismuth existing in equilibrium with uranium carbide UC_x.

D. Wiswall and J. Egan (USA) feel that bismuth has potentialities in reactor engineering. They investigated all the papers published on the thermochemistry of liquid alloys of bismuth with Th, Pa, U, Pu, and fission products, and compared these with their own data.

A. Thorley and K. Teajack (Britain) studied the embrittlement of niobium attacked by the hydrogen-containing alloy Na-K.

Volatilization processes. Processes involving volatilization of refractories play a great role in high-temperature reactors. A discussion of the mechanism underlying volatilization processes shared attention in a paper submitted by P. Gilles (USA) with the techniques of vapor pressure measurement.

D. White, P. Walsh, and L. Ames (USA) presented a review of the thermodynamics of the volatilization of oxides of the rare earths and of yttrium over the 1900-2700°K range. It was found that, aside from a rare exception, stable vapor in equilibrium with oxides consists of gaseous MeO, Me, and monatomic oxygen.

K. Gingerlich and J. Efimenko (USA) carried out a thermodynamical study of thorium phosphides by evaporating them and measuring the activity of the ions in the gaseous phase by means of a mass spectrometer.

E. Keiter, E. Rauh, and R. Thorn (USA) used the effusion technique and mass spectroscopy to find the thermodynamical characteristics of uranium sulfide and uranium oxysulfide.

A. N. Nesmeyanov, Yu. A. Priselkov, and V. V. Karelin (USSR) measured by the Knudsen method the pressure of saturated vapor of 99.5% pure yttrium metal and found that

$$\log P \text{ (mm, Hg)} = 7.8130 - \frac{15803}{T} \text{ (1361-1761° K).}$$

Volatilization and thermodynamics of oxides. N. Voronov, A. Danilin, and I. Kovalev (USSR) determined the rate of evaporation of uranium dioxide in a vacuum over the 1450-2300°C range. The oxide was heated by passing current directly through the specimen under study. The finding was that

$$\log P_{\text{UO}_2} \text{ (mm Hg)} = -\frac{30709}{T} + 10.915.$$

TABLE 4. Vapor Pressure of UO_2 and UO_3

T°, K	$P_{\text{UO}_2}(\text{g}), \text{mm Hg}$	$P_{\text{UO}_3}(\text{g}), \text{mm Hg}$	
		at $P_{\text{O}_2}=10^{-6} \text{ atmos}$	at $P_{\text{O}_2}=10^{-8} \text{ atmos}$
1750	$5.1 \cdot 10^{-7}$	$1.60 \cdot 10^{-3}$	$1.60 \cdot 10^{-4}$
2000	$6.9 \cdot 10^{-5}$	$1.39 \cdot 10^{-2}$	$1.39 \cdot 10^{-3}$
2250	$3.0 \cdot 10^{-3}$	$7.70 \cdot 10^{-2}$	$7.70 \cdot 10^{-3}$
2500	$1.4 \cdot 10^{-2}$	0.309	$3.09 \cdot 10^{-2}$

The rate of evaporation of ZrO_2 and ThO_2 in air was also determined over the 1500-2000°C range. At 1900°C, the rates of evaporation of these two compounds was the same, viz., $\sim 7 \cdot 10^{-8} \text{ g/cm}^2 \cdot \text{sec}$.

R. Ackerman and R. Thorn (USA) devoted their report to a discussion of their own data and data published by others on the volatilization of thorium, uranium, plutonium, and their oxides. The basic thermodynamic characteristics appear in Table 3.

They also derived equations for the vapor pressure of thorium:

$$\log P (\text{atmos}) = (5.991 \pm 0.333) - \frac{(28780 \pm 620)}{T} (1757 - 1956^\circ \text{K}),$$

and of uranium:

$$\log P (\text{atmos}) = (5.701 \pm 0.014) - \frac{(23330 \pm 24)}{T} (1600 - 2000^\circ \text{K}),$$

and of plutonium:

$$\log P (\text{atmos}) = (5.014 \pm 0.047) - \frac{(17587 \pm 73)}{T} (1400 - 1800^\circ \text{K}),$$

and of thorium dioxide:

$$\log P (\text{atmos}) = 7.98 - \frac{34890}{T},$$

and of plutonium dioxide (in vacuo):

$$\log P (\text{atmos}) = 8.129 - \frac{27910}{T},$$

and of plutonium dioxide (in oxygen):

$$\log P (\text{atmos}) = 8.61 - \frac{29500}{T} (1500 - 1700^\circ \text{C}),$$

and finally, of plutonium oxide PuO_x ($1 < x < 2$):

$$\log P (\text{atmos}) = 8.072 - \frac{29240}{T} (2000 - 2400^\circ \text{K}).$$

E. Cordfunke (Netherlands) gave a brief description of the principal techniques used to determine the characteristics of a volatilization process, and discussed the available data on the volatility of oxides of several metals important in nuclear technology, placing special attention on uranium and plutonium oxides. Table 4 cites some data on vapor pressures of UO_2 calculated from the equation

$$\log P_{\text{UO}_2} (\text{mm Hg}) = -\frac{33115}{T} - 4.026 \log T + 25.686,$$

reported by Ackerman et al., from experimentally obtained data, and the vapor pressure of UO_3 , calculated by the author on the basis of known thermodynamical data.

T. Markin, L. Roberts, and A. Walter (Britain) used the emf method to study the thermodynamics of uranium oxides of the compositions from $\text{UO}_{2.01}$ to $\text{UO}_{2.6}$ over the 500-1060°C range. The results were discussed with a view to the available published data and the results of investigations carried out by the authors using the tensimetric method over the 1000-1450°C range. Phase relationships were also surveyed in the uranium-oxygen system and a portion of the phase diagram for compositions from $\text{UO}_{2.00}$ to $\text{UO}_{2.25}$ was reproduced for the 300-1400°C range.

TABLE 5. Thermodynamical Characteristics of Yttrium and Zirconium Hydrides and Deuterides at 298°K

Compound	C_p , cal/mole · deg	S° , entropy units	$(H^\circ - H_0^\circ)$ cal/mole	$-\left(\frac{F^\circ - H_0^\circ}{T}\right)$ cal/mole · deg
ZrH ₂	7.396 ± 0.015	8.374 ± 0.02	1284.1 ± 2	4.067 ± 0.01
ZrD ₂	9.631 ± 0.019	9.168 ± 0.02	1474.4 ± 3	4.223 ± 0.01
YH ₂	8.243 ± 0.016	9.175 ± 0.018	1402.7 ± 2.8	4.470 ± 0.009
YD ₂	10.773 ± 0.022	10.294 ± 0.021	1659.1 ± 3.3	4.729 ± 0.010

E. Aukrust, T. Forland, and K. Hagemark (Norway) measured the equilibrium pressure of oxygen above non-stoichiometric uranium dioxide $UO_2 + x$ at 1100°, 1200°, 1300°, and 1400°C in the range of compositions from UO_2 to U_3O_8 . It was shown that the nonstoichiometric phase of $UO_2 + x$ exists up to the ratio $O/U = 2.245$ at 1300°C and $O/U = 2.255$ at 1400°C. A model was suggested for the defect structure.

T. Mukaibo et al. (Japan) determined the heat of formation of U_3O_7 —an intermediate metastable compound formed in the oxidation of UO_2 to U_3O_8 in air. They used two independent methods: differential thermal analysis and measurement of specific heat. Two values were obtained for $\Delta H_{298}^\circ U_3O_7$, -815.7 ± 2.4 kcal/mole, and -821.1 ± 2.1 kcal/mole. Results were also reported for the measurement of the specific heat of U_3O_7 over the 100-400°C range.

A paper by C. Comareck and M. Silver (USA) presented some experimental data on the determination of thermodynamical characteristics (partial free energies, enthalpy, and entropy) of oxygen dissolved in titanium, zirconium, hafnium in amounts up to 30 at. % and over the 800-1000°C temperature range.

Volatilization and thermodynamics of carbides. E. Huber and C. Holley (USA) systematized existing data on the thermodynamics of the carbides of the actinide elements, and brought forth new data on the heats of formation of ThC, U_2C_3 , $UC_{1.86}$, $PuC_{0.77}$, and Pu_2C_3 , obtained by combustion calorimetry, and found to be -7 ± 6 ; -49 ± 4 ; -18 ± 4 ; 3.7 ± 3.1 ; and -1.7 kcal/mole, respectively.

R. Mulford, G. Ford, and J. Hoffman (USA) employed the Knudsen method to measure the vapor pressure above PuC_2 in equilibrium with graphite over the 2000-2400°K temperature range. The pressure of plutonium above PuC_2 is found from the equation

$$\log P(\text{atmos}) = -\frac{17920 (\pm 250)}{T} + 2.779 (\pm 0.11).$$

The heat of evaporation of Pu from PuC_2 is 95,100 cal/mole. The heat of formation of PuC_2 (ΔH_{298}°), entertaining various pertinent assumptions, is found to range from -7 to -8 kcal/mole. It was shown that probably all plutonium carbides volatilize with some plutonium loss and that there does not exist a solid compound volatilizing congruently.

D. Jackson et al. (USA) applied mass-spectrometric techniques to an investigation of the process and thermodynamics of volatilization of gadolinium and thorium dicarbides. It was found that gadolinium is predominantly present in the gaseous phase above the solid GdC_2 . The amount of gaseous GdC_2 at 2000°K is 1%, and at 2422°K it amounts to 5.8% of the amount of Gd present. Above solid ThC_2 , gaseous Th and ThC_2 are found in commensurate quantities, and their pressure is expressed by the equations

$$\text{for } ThC_2 \log P (\text{atmos}) = -\frac{39364 (\pm 163)}{T} + 7.20 (\pm 0.65) (2400-2600^\circ K),$$

$$\text{for } Th \log P (\text{atmos}) = -\frac{36025 (\pm 144)}{T} + 5.74 (\pm 0.57) (2400-2600^\circ K).$$

The enthalpy of sublimation of $ThC_2(\text{solid})$ from ThC_2 to Th (gas) comes to 213 and 185 kcal/mole, respectively. The calculated heat of formation of ThC_2 (ΔH_{298}°) is -48.6 ± 2.5 kcal/mole.

H. Eick, E. Rauh, and R. Thorn (USA) measured the vapor pressure of uranium above uranium carbide of composition $UC_{1.78 \pm 0.05}$ by the effusion method over the 2060-2820°K temperature range. The amount of U^{235} - and U^{238} -containing uranium volatilized in the process was determined from the α -activity. A mass-spectral analysis revealed that the effusate contained gaseous uranium, monatomic and triatomic carbon, and UC_2 . The ratio of U^+ to UC_2^+ was 4 at 2800°K. The vapor pressure of uranium overlying $UC_{1.80}$ is given by the formula

TABLE 6. Thermodynamical Data on Borides

Compound	C_p , (298°K), cal/mole · deg	S° , 298°, e.u.
BN (cub)	2.95	—
CrB	8.57	8.4±1
MoB	9.42	10.5±1
TaB	11.30	13.1±1
WB	8.01	13.2±1
Mo ₂ B	18.79	22.8±2
W ₂ B	15.36	28.2±2
CrB ₂	12.80	6.6±1
HfB ₂	14.23	11.2±1
MoB ₂	14.45	8.7±1
NbB ₂	11.81	8.6±1
TaB ₂	13.98	11.3±1
TiB ₂	13.02	6.2±1
ZrB ₂	13.12	8.5*
W ₂ B ₅	21.09	21±2

* E. Westrum found the empirical value 8.58.

$$\log P(\text{atmos}) = -\frac{34\,568}{T} + 7.01 \quad (2060 - 2460^\circ \text{K}),$$

$$\log P(\text{atmos}) = -\frac{33\,593}{T} + 7.0 \quad (2540 - 2820^\circ \text{K}).$$

The calculated free energy of formation of UC_{1.80} was -51,400 + 6.02 T cal/mole (at 2060-2460°K).

S. Alcock and P. Greaveson (Britain) used three techniques, all variants of the Knudsen method, to measure the equilibrium vapor pressure above solid systems U-C and U-B, determined uranium activity in these systems, and calculated their thermodynamical characteristics:

$$\begin{aligned} \text{for UC } \Delta F^\circ &= -25\,200 + 3.6 T \text{ kcal/mole} (1450 - 1550^\circ \text{C}), \\ \text{for UC}_2 \Delta F^\circ &= -32\,600 + 3.6 T \text{ kcal/mole} (1700 - 1800^\circ \text{C}), \\ \text{for UB}_2 \Delta F^\circ &= -39\,300 + 3.0 T \text{ kcal/mole} (1450 - 1550^\circ \text{C}), \\ \text{for UB}_4 \Delta F^\circ &= -60\,400 + 4.4 T \text{ kcal/mole} (1730 - 1850^\circ \text{C}), \\ \text{for UB}_{12} \Delta F^\circ &= -106\,000 + 10.5 T \text{ kcal/mole} (1730 - 1850^\circ \text{C}). \end{aligned}$$

The free energies were calculated for the formation of compounds of liquid uranium and solid boron and carbon. Diagrams of the integrated free energy of formation vs. composition were plotted for the systems U-C and U-B at 1450°C. The equation for the pressure of dissociation of uranium above UC₂ was derived as

$$\log P(\text{atmos}) = 6.81 - \frac{31\,170}{T} \quad (1700 - 1800^\circ \text{C}).$$

H. Lonsdale and J. Graves (USA) reported on the results of vapor pressure measurements of the dicarbides of uranium, thorium, and protactinium by the Knudsen method. Protactinium carbide was isolated as a very dilute solid solution in thorium dicarbide by bombarding the latter with neutrons. The vapor pressure of uranium and thorium above their dicarbides in equilibrium with graphite was found to satisfy the equations

$$\begin{aligned} \log P_{\text{U}}(\text{atmos}) &= -\frac{28\,400 (\pm 1\,100)}{T} + 4.76 (\pm 0.47) \quad (2000 - 2900^\circ \text{K}), \\ \log P_{\text{Th}}(\text{atmos}) &= -\frac{37\,600 (\pm 1000)}{T} + 7.39 (\pm 0.39) \quad (2300 - 2900^\circ \text{K}). \end{aligned}$$

The vapor pressure of protactinium above dilute solid solutions of PaC₂ and ThC₂ may be expressed by the formula

$$\begin{aligned} \log P(\text{atmos}) &= -\frac{39\,200 (\pm 1900)}{T} \\ &+ 6.99 (\pm 0.74) + \log \chi_{\text{Pa}} \quad (2300 - 2900^\circ \text{K}), \end{aligned}$$

where χ_{Pa} is the molar fraction of protactinium.

In the temperature region studied, the computed heats of formation of UC₂ and ThC₂ were -25 and -46 kcal/mole, respectively.

W. Deiss, H. Michaud, and G. Pelissier (France) attempted to isolate uranium, UC, and UC₂ of maximum purity by in-vacuum volatilization with electron-bombardment heating of the material. It was found that the condensate arrived at is oxidized when pure uranium is volatilized, while volatilization of carbided uranium yields an oxide-free condensate. The author demonstrated by means of thermodynamical calculations that the formation of carbon monoxide is responsible for the partial pressure of oxygen becoming lowered to such an extent that liquid

and gaseous uranium no longer react with the oxygen, and the probability of any reaction involving the condensate is very slight. UC and UC₂ films are obtained in the process. The authors hold the view that these carbides are stable in the vapor phase.

V. E. Ivanov, A. A. Kruglykh, V. S. Pavlov, G. P. Kovtun, and V. M. Amonenko (USSR) determined the vapor pressure of UC in the 1675-1860°C range, that of UO₂ over the 1650-1930°C range, and that of USn₃ over the 1025-1295°C range from the rate of evaporation from an open crucible. The following equations were derived for the vapor pressure:

$$\text{for UC } \log P \text{ (mm Hg)} = 21.306 - \frac{49\,200}{T},$$

$$\text{for UO}_2 \log P \text{ (mm Hg)} = 12.098 - \frac{32\,150}{T},$$

$$\text{for USn}_3 \log P \text{ (mm Hg)} = 9.067 - \frac{17\,223}{T}.$$

T. Mukaibo et al. (Japan) measured the specific heats of UC and UC₂ in an adiabatic calorimeter over the 100-400°C range:

$$C_p(\text{UC}) = 5.01 + 2.63 \cdot 10^{-2} T - 1.92 \cdot 10^{-5} T^2 \text{ cal/mole,}$$

$$C_p(\text{UC}_2) = 2.93 + 4.33 \cdot 10^{-2} T - 3.17 \cdot 10^{-5} T^2 \text{ cal/mole,}$$

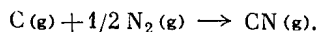
The probable error was estimated at $\pm 3.0\%$ by the authors.

Other thermodynamical data. I. Skidmore and E. Morris (Britain) determined experimentally the equation of state for uranium under a pressure of several kilobars and the specific internal energy at several kilojoules per gram. A knowledge of the properties of uranium under these conditions is required to calculate reactor safety margin. The required states were arrived at by compressing and heating uranium by a shock wave with subsequent adiabatic expansion.

J. Egan, W. McCoy, and J. Bracker (USA) employed the emf method to determine the standard free energies of formation of several chlorides of Mg, Ce, U, and Th over the 400-600°C temperature range. Here are some of the results they reported:

Compound	ΔF° kcal/g·atom at (400° C)
MgCl ₂	-127.80
CeCl ₃	-211.26
ThCl ₄	-232.4
UCl ₃	-168.2

J. Berkowitz (USA) used the nitrogen-graphite reaction in the 2200-2500°K range. The gas effused from a Knudsen cell was ionized by an electron beam, and the positive ions were analyzed in a mass spectrometer. N₂⁺, CN⁺, C₂⁺, and C₃⁺ ions were found to predominate. The author reported the thermodynamical characteristics of the reaction



R. Gross, S. Hayman, and H. Clayton (Britain) determined the heats of formation of UN, U₃Si₂, USi, USi₂ and USi₃ by synthesizing them directly from their constituent elements in a calorimeter. The heats of formation of USi, USi₂, and USi₃ were also determined from the difference in the heats of reaction of these silicides and of their constituent elements and tellurium. The heat of formation of U₂N₃ was determined by measuring the heat of the reaction involving UN and nitrogen. All of the synthesis reactions were carried out at a temperature of the order of 1000°C. The results were reported as:

Compound	ΔH° , kcal/g·atom
USi ₃	7.9 ± 0.03
	7.7 ± 0.2
USi ₂	10.4 ± 0.1
	10.2 ± 0.3
USi	9.6 ± 0.2
	10.4 ± 0.4
U ₂ Si ₃	8.1 ± 0.1
UN	39.8 ± 0.2
U ₂ N ₃	33.7 ± 0.2

The second set of figures was obtained by measuring the heat of the reaction between the silicides and tellurium.

H. Flotow and D. Osborn (USA) measured the specific heats of ZrH_2 , ZrD_2 , YH_2 , and YD_2 in an adiabatic calorimeter over the temperature range 5-350°K, and, on the basis of their results, they compiled a table of several functions: S° , $H^\circ - H_0^\circ$, $\frac{H^\circ - H_0^\circ}{T}$ and $-\left(\frac{F^\circ - H_0^\circ}{T}\right)$. Some of the data referable to the temperature 298°K are reproduced in Table 5. Other thermodynamical data are reported including the heats of formation of ZrH_2 and ZrD_2 , which are -39.3 ± 0.3 and -40.5 ± 0.3 kcal/mole, respectively.

E. Mesaki et al. (USA) studied by the mixing method the enthalpy $H_{T_2} - H_{T_1}$ ($T_1 = 298^\circ\text{K}$, $T_2 = 400$ to 1200°K) of fifteen high-melting borides, computed their specific heats, and estimated the standard entropies. A separate list of data is found in Table 6.

In conclusion, we should like to point out that, in line with the intensified interest in uranium carbide and plutonium carbide, IAEA called a special conference to meet in Vienna in October, 1962 to give experts on the thermodynamics of those carbides an opportunity to discuss their specific field. The conference carried out important work in evaluating and coordinating the available data on the carbides, and passed in recommendations on the most reliable values reported in the literature. A report of the conference will be published along with some new data, particularly the data reported by E. Westrum on the specific heat and entropy of UC and UC_2 .

THE USE OF γ -RAY SOURCES IN NONDESTRUCTIVE TESTING
AT THE CSEPEL METALLURGICAL COMBINE (HUNGARY)

E. Fényvéssy, K. Scserbak, and K. Vara

Translated from *Atomnaya Énergiya*, Vol. 15, No. 4,
pp. 351-353, October, 1963

Research work on applications of γ -ray sources in flaw detection was begun in Hungary in 1953. A radioisotopes laboratory was set up in 1955 at the Csepel metallurgical combine in the central materials testing division. At the present time, γ -ray sources are in systematic use in Hungary in γ -radiographic monitoring of weldments and castings. This work is mainly concentrated at the Csepel metallurgical combine, plants for maintenance work on electric power station equipment, the Lenin metallurgical combine, and the April 4 machine tool factory. Every year, about 40,000-42,000 γ -radiographic plates are taken throughout the country. Co^{60} , Cs^{137} , Ir^{192} are the most commonly used γ -ray sources, and are obtained mostly from Great Britain and the USSR. The training of engineers and technicians specializing in γ -radiographic monitoring work is under the supervision of the Educational Section of the Ministry of Metallurgy and Machinery. Only trained personnel are authorized to perform radiographic work in the plants.

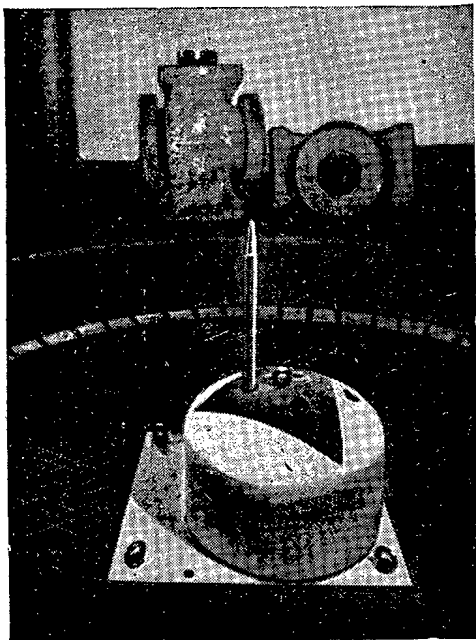


Fig. 1. Radiomonitoring of large parts.

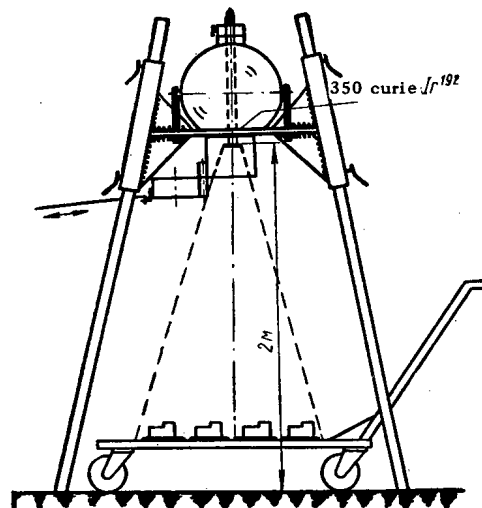


Fig. 2. Apparatus for routine radiography of small castings.

About one-half of all the radiographic work is carried out by the radioisotopes laboratory at the Csepel metallurgical combine. Castings are flaw-monitored in a special room of 100 m² floor area, which has two entrances for admitting parts to be radiographed and a special tunnel for servicing personnel. The doors leading to the monitoring room are interlocked to ensure the automatic withdrawal of the γ -emitting sources into a storage well should any of the doors be accidentally opened during the radiographic work. Large castings are moved about with the aid of an overhead crane. A well 10 meters deep and consisting of three steel tubes nested into one another and filled with concrete is situated in the middle of the asphalt-covered floor. Three different γ -ray sources (60-curie Co^{60} , 26-curie Co^{137} , and 150-curie Ir^{192}) are positioned in that well.

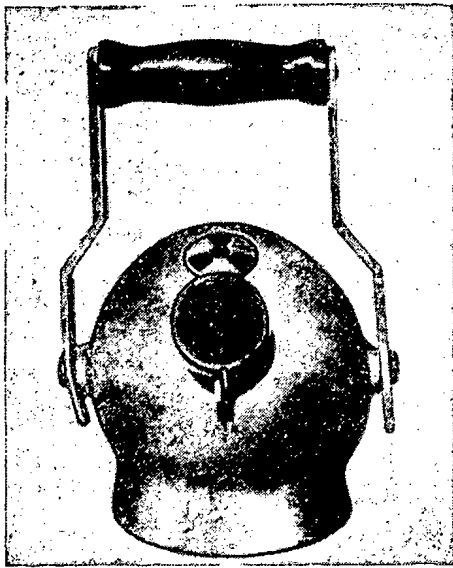


Fig. 3. Portable container weighing ~10 kg.

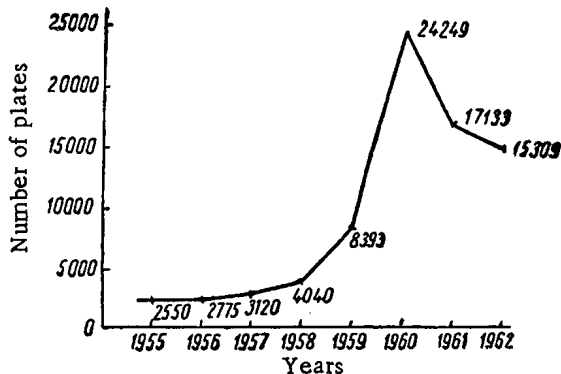


Fig. 4. Number of γ -radiography plates taken by the radioisotope laboratory, year by year.

Large castings to be monitored are positioned around the well and one of the three γ -ray sources is used, the choice being based on the thickness of the specimen (Fig. 1). The radiation sources are moved into the work position by special battery-powered devices. Positioning of the sources is by remote control from a panel mounted in a separate room shielded by 50 cm thick heavy concrete. The height to which the source is raised is monitored by a periscope. Photographic laboratory rooms for developing film and charging plate holders are situated around the control room. The x -radiographic films used most often of the γ -plates are of the brands Agfa, Gevert, Kodak, and Ferramia, as well as 0.15 and 0.45 mm thick intensifying lead foil. DIN-54110 standards are used in interpreting the plates obtained. Depending on film quality, the thickness of the material, and the isotope used, the sensitivity in flaw detection varies from 0.8 to 2.0% of the thickness of the part examined. Small castings (for example, parts of machine tools and sewing machines) are monitored with a special facility consisting of a spherical lead container and a γ -ray source mounted on a tubular framework 2 m high. The container has a collimator shaping the beam in such a way that the semidiameter of the radiation field will be ~1.5 m. A hand cart presenting an area of 1.2 m², on which the parts to be monitored and film holders are wheeled into position, is placed underneath the tubular framework, i.e., in the exposure field. During the exposure, a second hand cart is prepared, and replaces the first after the first exposure is completed. This method of monitoring makes it possible to check out a large number of small castings (Fig. 2). The point of this work is not only to detect existing flaws in the casting, but also to develop, in collaboration with casting technologists, a casting technology which will minimize the amount of scrap produced in routine casting work. The correctness of the method may be evaluated in terms of the eventual savings.

Approximately 75% of the total volume of γ -radiography work consists of monitoring weldments, most of which were fabricated not in the laboratory but in plants throughout the combine or in plants outside the Csepel combine. To meet this need, we designed and built special containers consisting of metallic spheres filled with lead and mounted on rubber-wheeled carts. A special opening in the center of the conveyance accommodates, in an exact fit, a matched tube with a capsule-sealed γ -ray source attached to it. When the plates are being prepared, an aluminum tubular rod ~2 m long is attached to the tube and is used to remove the γ -radiation source from its holder. For monitoring weldments for high-elevation construction cranes, it is a good practice to use a spherical container weighing ~10 kg, moved about by hand and containing an Ir¹⁹² source of 32-curie activity (Fig. 3).

Welded seams of air pressure tanks, cranes, crane rail tracks, railroad cars for transporting butane gas, and other metal structures are monitored systematically in the laboratory. The most useful and interesting of the work projects carried out in the laboratory has been the investigation of illuminating stanchions for the People's Stadium built in 1953, and quality control of weldments for a section of the Druzhba oil pipeline and on the bridge of an intake structure. Monitoring the state and quality of cranes of outmoded design is a routine job at the Csepel metallurgical works.

In several instances in the history of the laboratory, old reinforced-concrete structures were monitored, and this has enabled technicians to successfully determine the spatial arrangement of the iron framework inside the concrete, and thus to check its dimensions against the original blueprints. Useful work was also done in reconditioning

the old Budapest fortress. In answer to the request of a building plant contracted for this work, brick walls ranging from 60 to 120 cm in thickness were radiographed in order to determine the location and nature of voids in the brickwork, and the effect these might have on the load-carrying capacity of the walls. The γ -plates taken allowed for a successful determination and pinpointing of several ventilation holes, and this was an immense aid to the building workers. The number of radiography shots taken in the laboratory's history may be seen in Fig. 4. The largest number is registered for 1960, after which a significant decline may be noted. The reason for this is the fact that an unusually large amount of casting was done at the Csepel works in 1960, and studies were carried out there to determine the location and frequency of appearance of defects, and in order to incorporate into production technology those changes which might eliminate flawed castings.

The use of γ -emitter isotopes in Hungary has advanced far past the initial difficulties encountered, and the technical and cost results have been eminently satisfactory. The use of γ -emitting sources has vastly expanded the arena for monitoring materials. Hungarian specialists reached the conclusion that x-ray facilities and γ -emitter sources, as well as accelerators, are necessary tools in monitoring the quality of commodities and parts produced in today's technology.

BIBLIOGRAPHY

NEW LITERATURE

Translated from *Atomnaya Énergiya*, Vol. 15, No. 4,
pp. 354-358, October, 1963

State Atom Press (Gosatomizdat) Releases

V. F. Turchin: Medlennye neitrony [Slow neutrons]. 1963, 372 pages. 1 ruble, 38 kopeks.

This book takes up interactions between slow neutrons and matter. The first portion deals with the theory of slow neutron scattering on crystals, in gases and liquids, and the theory of magnetic scattering of neutrons, and presents some experiments in scattering research. Sources for producing slow neutrons and means of detecting them are described. Neutron scattering on a single isolated nucleus and on a system of chemically bound atoms are contrasted; the principles of slow-neutron spectrometry are outlined; over-all aspects of the theory of slow-neutron scattering in matter are handled in the spirit of the Van Hove, Placzek, and Wick treatment.

The second portion of the book is devoted to the thermalization and diffusion of neutrons. Here we find questions relating to the spectrum and spatial distribution of slow neutrons in various media.

The appendices list relations between various neutron characteristics, amplitudes and cross sections for scattering on bound atoms, the parameters ϑ , K_{AV} , C_{AV} for the Debye crystal, diffusion characteristics of various substances as measured by pulsed techniques.

The bibliography includes 158 pertinent titles.

Voprosy teorii fiziki plazmy [Advances in the theory of plasma physics]. Edited by M. A. Leontovich. No. 1, 1963, 288 pages. 1 ruble.

This item is the first to appear in a series of symposia devoted to various aspects of plasma theory. This first contribution takes up some over-all problems in the description of a plasma. An article by D. V. Sivukhin outlines the drift theory of motion of a charged particle in electromagnetic fields; a paper by B. A. Trubnikov investigates the simplest kinetic effects brought about by interparticle collisions in a fully ionized homogeneous gas; an article by S. I. Braginskii addresses itself to transport phenomena in a simple and in a multicomponent plasma; an article by A. A. Vedenov discusses plasma statistical thermodynamics as a system of particles undergoing Coulomb interaction.

Teoriya yadernykh reaktorov [Nuclear reactor theory]. Translated from the English, symposium edited by G. Birkhoff and E. Wigner. 1963, 364 pages. 1 ruble, 78 kopeks.

This book, first published by the American Mathematical Society, is the eleventh volume on the proceedings of a symposium on applied mathematics, and deals mostly with mathematical problems encountered in the theory of nuclear reactors. Nineteen papers appear in this volume, and cover the topics: neutron thermalization, resonance absorption, passage of radiation through biological shielding, various aspects of kinetic reactor theory, the concepts of positivity and criticality, diffusion theory, and diffusion models.

M. L. Gol'din. Avtomaticheskii kontrol' urovnya gamma-luchami [Automatic gamma-ray level monitoring]. 1963, 68 pages. 19 kopeks.

This brochure deals with radiation detectors used in a gamma relay switch; a concise exposition of techniques for designing gamma switch shielding with two types of emitters appears; a procedure is cited for designing gamma-emitters and the design of radiation source units is described; examples of technical problems on monitoring and control of levels of free-flowing and liquid media are given; the reader may also find recommendations on the storage, assembly, and servicing of gamma-relay level switches.

Releases by Other Publishers

R. V. Dzhagatspanyan, R. F. Romm, and L. K. Tatochenko. Primenenie radioaktivnykh izotopov dlya kontrolya khimicheskikh protsessov [Radioisotopes in chemical process monitoring]. Moscow, Goskhimizdat (State Chemical Press), 1963, 344 pages. 1 ruble, 25 kopeks.

This book outlines the basic theory underlying radioisotope sensors and gives some standard layouts of industrial instruments in that line; the over-all concept of the origin and properties of nuclear radiations is presented; methods for recording nuclear radiations are described and a discussion appears of the operating principles and characteristics of gas-filled, crystal, and scintillation detectors. A special section is devoted to the application of industrial instruments using radioisotope sensors and to the major problems confronted in safe handling of such instruments; here we find a discussion of automatic process control procedures and level control, density and concentration monitoring and control, automatic production of chlorine and chlorine-derived products, and analysis of the composition of liquid and gases, and some of the rules and regulations mandatory in any work with sources of ionizing radiation.

Literature references are appended to each chapter; the book has a subject index.

M. F. Yudin. Metody i apparatura dlya graduirovki dozimetricheskikh priborov [Techniques and equipment for calibrating dosimetric instrumentation]. Moscow, Standartgiz (Standards Press), 1962, 120 pages. 38 kopeks.

This brochure deals with uniformization of measurements of x-ray and gamma-ray dosage and contains some useful recommendations on the use of various techniques and equipment for calibrating and testing roentgen meters and gamma-emitters. Information presented in a form accessible to a wide readership may be found here on the basic processes involved in the interaction of electromagnetic radiation with matter. The conditions required for uniformity in measurements in the field of dosimetry of ionizing radiations are explained. Techniques and equipment for transmitting the measured roentgen values from standardizing instruments to regularly used devices are described.

The appendices provide tables of linear attenuation coefficients and the albedos of gamma-radiation energy in various media (e.g., air, water, iron, lead), e^{-X} function values, and recommended forms for recording evidence bearing on standard emitters and dosimeters.

Articles from the Periodical LiteratureI. Nuclear Physics

(Nuclear reactions, neutrons, fission of nuclei).
Zhur. éksptl. i teoret. fiz., 44, No. 6 (1963).

N. A. Perfilov et al., 1832-36. Ternary plutonium fission.

L. N. Usachev et al., 1950-52. Determination of fission threshold in experiments on the (d, pf) and (γ, f) reactions.

Pribory i tekhn. éksper., No. 3 (1963).

S. S. Moskalev et al., 58-61. A multifilament neutron detector with nonoverloading preamplifier.

M. P. Sokolov, 66-71. Automatic facility measures radioactivity of wire.

A. B. Ekatorov et al., 72-78. A multidimensional analyzer.

Trudy akad. nauk Litov. SSR. Seriya B, I (1963).

V. Yu. Potsyus and I. S. Tomkus, 29-32. The background of nuclear emulsions used in the study of atmospheric α -activity.

Industries atomiques, 7, Nos. 5-6 (1963).

A. Biette, 123-28. Ultrahigh-vacuum pumps for nuclear research.

Nucl. Physics, 43, No. 2 (1963).

M. Anderson and W. Bond, 330-38. Neutron spectrum of a plutonium-beryllium source.

D. Winterhalter, 339-43. Angular distribution of fast neutrons scattered in aluminum.

Reactor Sci. and Technol., 17, No. 3 (1963).

G. Gierts, 121-24. Fast neutron spectrometry based on the $\text{Li}^6(n, t)\text{He}^4$ reaction.

F. Brown et al., 137-41. Cross section of the $\text{Li}^7(n, t)$ reaction for 3.5 to 15 MeV neutrons.

II. Plasma Physics

Doklady akad. nauk SSSR, 149, No. 5 (1963).

A. E. Bazhanova and V. D. Shfranov, 1049-51. On radiation from a charge moving in a plasma near cyclotron resonance.

L. M. Kovrizhnykh et al., 1052-55. Hydrodynamic oscillations of a low-pressure homogeneous plasma in a magnetic field.

V. K. Mel'nikov, 1056-59. On the lines of force of a magnetic field established by helical currents flowing on the surface of a torus.

Zhur. tekhn. fiz., 33, No. 6 (1963).

E. E. Lovetskii and A. A. Rukhadze, 652-59. Oscillations of a cold inhomogeneous plasma in a gravitational field.

E. E. Lovetskii and A. A. Rukhadze, 660-66. On the convective instability of an inhomogeneous plasma in a gravitational field.

M. V. Samokhin, 667-74. Heat currents and flows in a dual-temperature plasma.

M. V. Samokhin, 675-85. Particle and heat flows in a multicomponent plasma.

Yu. G. Zubov, 686-92. Study of the energy spectrum of electrons and ions escaping through the ends of a magnetic mirror machine.

F. G. Baksht, 693-702. Flight oscillations in an electron-ion stream.

V. P. Demidov and D. A. Frank-Kamenetskii, 703-709. Collisional dissipation on cyclotron overtones in a plasma.

V. V. Matveev et al., 710-14. Investigation of hard plasma radiation in a strong magnetic field.

K. V. Suladze and A. A. Plyutto, 716-18. Some aspects of converging plasma jets in an induction discharge.

Zhur. éksp'tl. i teoret. fiz., 44, No. 6 (1963).

A. A. Galeev, 1920-34. Stability theory of an inhomogeneous rarefied plasma in a strong magnetic field.

L. M. Kovrizhnykh et al., 1953-63. On the oscillations of an inhomogeneous low-pressure plasma.

V. I. Petviashvili, 1993-2000. On anomalous diffusion of a plasma in the presence of oscillations.

L. É. Pargamanik and G. M. Pyatigorskii, 2029-38. Shift and broadening of energy levels of one-electron atoms and ions in a high-temperature plasma.

M. S. Khaikin et al., 2190-93. Standing magnetoplasma waves in bismuth single crystals.

Phys. Fluids, 6, No. 4 (1963).

H. Furth, et al., 459-83. Instability of a planar pinch caused by finite conductivity.

H. Weitzner, 484-89. Green's function for the linearized one-dimensional Crooke's equation.

H. Liemohn and F. Scarf, 490-500. First-order and second-order perturbation of a plasma having a Cauchy equilibrium distribution.

H. Karr et al., 501-507. Resonance interaction of a plasma with a spatially rotating stationary magnetic field.

G. Fejer, 508-12. Reflection and refraction of MHD waves at discontinuities.

L. Talbot et al., 559-65. Comparison between a Langmuir probe and microwave electron density measurements in an arc-heated low-density wind tunnel.

N. Geffen, 566-71. Magnetogas-dynamic flows with shock waves.

L. Taylor, 591-92. Electron temperature in gases situated in radio-frequency fields.

N. D'Angelo, 592-93. Ion waves in an inhomogeneous plasma.

G. Bethke and A. Ruess, 593-94. Dynamical relationship between low-power microwaves and a shock-wave plasma.

G. Bethke et al., 594-96. Dynamical relationship between high-power microwaves and a shock-wave plasma.

K. Uo, 596-97. Adiabatic compression of plasma by a magnetic field of multipole axial cusped geometry.

III. Nuclear Engineering. Nuclear Power

(Neutron Physics. Nuclear reactor theory and calculations. Reactor design. Operation of nuclear reactors and reactor power stations. Nuclear radiation shielding. Disposal of radioactive wastes.)

Izvestiya akad. nauk Lat. SSR, No. 2 (1963).

D. Dobryakov et al., 68-74. Electromagnetic shuttle network at a reactor installation.

Nauka i tekhnika, No. 4 (1963).

K. Shvarts, 7-9. The Salaspils (Latvia) nuclear reactor ready for research work.

Teploenergetika, No. 5 (1963).

L. S. Sterman et al., 35-38. Reactor power station layout with steam superheat in a separate reactor.

Teploenergetika, No. 6 (1963).

V. I. Subbotin et al., 70-74. Measuring temperature fields in turbulent mercury flow through tubes.

Tekhnika kino i televideniya, No. 5 (1963).

N. V. Lapteva and V. S. Polonik, 69-77. Closed-circuit TV in nucleonic and nuclear power applications.

Energia Nucleare, 10, No. 5 (1963).

P. Basso et al., 237-46. Variational technique for computing extrapolation length of some fuel elements, for application in thermal utilization determinations.

Énergie nucléaire, 5, No. 2 (1963).

P. Delattre, 154-67. High-flux-density nuclear reactors.

Industries atomiques, 7, Nos. 5-6 (1963).

M. Barbier, 55-65. Radioactivity induced in materials by high-energy protons, neutron, and photons.

J. Juillard, 73-84. Nuclear power in Japan.

J. Nucl. Materials, 8, No. 1 (1963).

R. Sowden, 81-101. Radiolytic problems in water reactors.

Kemenergie, 6, No. 4 (1963).

H. Heinrich, 146-51. Boundary conditions at the surface of hollow control rods slowing down neutrons in accordance with the three-group method.

Kemenergie, 6, No. 5 (1963).

P. Wenzel, 193-202. Investigations of uranium-plutonium cycles applicable to water-moderated reactors.

F. Krüger and A. Müller, 207-209. Determination of gamma flux inside an extended source.

Nucl. Energy (June, 1963).

A. Thorne, 145-56. Shielding equipment for nuclear deactivation systems.

J. Pearson, 156-64. Internal heat transfer in fuel elements.

Nucl. Engng., 8, No. 86 (1963).

---, 231-36. Glove boxes.

D. Robertson, 236-37. Multiple-purpose shielded cave.

---, 237-38. Design of glove boxes at Aldermaston.

---, 239-41. Brief data on glove boxes available from American, British, and West German manufacturers.

---, 242-44. Shielded cells for handling high-level materials at Windscale.

---, 245-47. Tables of data on shielded caves for handling radioactive high-level materials, country by country.

W. Burton and A. Mills, 248-52. Computer calculations of fuel reprocessing schemes.

Nucl. Sci. and Engng., 15, No. 3 (1963).

C. Wilkins, 229-32. Note on collisional density at epithermal energies.

P. Nichols et al., 233-44. Measurement of lattice constants in gas-cooled reactor.

R. Osborn, 245-58. Discussion of theoretical investigations of probe-induced flux perturbations.

W. Lanning, 259-67. Application of spherical harmonics to gamma flux transport.

P. Tunnicliffe et al., 268-83. Exact determination of relative initial conversion ratio.

E. Bryant et al., 288-95. Loss rates and loss mechanisms of fission products from uranium-graphite fuel.

E. Garelis, 296-304. Time-dependent neutron thermalization for an unreflected multiplying medium.

J. Walker et al., 309-313. Thermal flux perturbations caused by indium foil in water.

G. Hanna, 325-37. Neutron flux perturbations due to absorber foil. Theory compared to experiment.

H. Albers et al., 342-44. Xenon poisoning in a shutdown reactor.

J. Randall and J. Walker, 344-45. Foils which do not cause flux perturbations. Experimental verification.

Nucleonics, 21, No. 6 (1963).

H. Davis, 60-63. How big will power plants get?

R. Creagan and A. Jones, 64-67. How far can we go with PWRs?

W. Oberly and G. Roy, 68-71. How far can we go with BWRs?

L. Koch, 72-75. The future of fast breeders.

M. Edlung and P. Schutt, 76-78. The future of thermal breeders.

D. Stoker et al., 79-84. Wanted: a balanced nuclear economy.

L. Nelson, 88-89. Gamma-ray absorptiometry determines total uranium in flat fuel elements.

A. Humm and S. Protter, 96, 98. Reconditioning the Brookhaven graphite reactor fuel-storage canal.

Nukleonik, 5, No. 4 (1963).

K. Becker, 137-47. Measuring burnup conditions for a flow of boiling water in round vertical channels.

W. Köhler and J. Romanos, 159-63. Neutron flux measurements by fast-neutron fissioning of U^{238} and Th^{232} .

W. Dio et al., 163-70. Experimental determination of the ρ coefficient for reactor lattices for the ARGONAUT reactor.

T. Stribel, 170-73. Neutron lifetime measurements and thermal reactor reactivity measurements by the Rossi α -method.

H. Hejtmanek, 173-78. Elementary solution of the transport equation by means of anisotropic scattering.

A. Belleni-Morante, 183-84. Reactor kinetic equations.

Reactor Sci. and Technol., 17, No. 3 (1963).

H. Meister, 97-114. Subcritical uranium-heavy water lattice experiments using a pulsed neutron source.

Y. Fukai, 115-20. Neutron collision probability in first flight, in a cylindrically shaped moderated fuel system.

E. Axton, 125-35. Absolute in-pile flux density measurement in the GLEEP reactor.

B. Fastrup, 143-44. In-pile epithermal spectrum measured experimentally.

IV. Materials for Atomic Industry

(Geology. Chemistry. Chemical process technology. Metallurgy).

Geokhimiya, No. 4 (1963).

M. M. Botova et al., 361-69. Experience in applying biogeochemical techniques to uranium prospecting in desert areas.

S. M. Manskaya and L. A. Kodina, 370-82. Aromatic monomers of lignin in lignites, and their possible role in the concentration of uranium, germanium, and vanadium.

Doklady akad. nauk SSSR, 149, No. 5 (1963).

A. D. Gel'man et al., 1071-73. Isolation of oxalato-sulfite and sulfite complexes of thorium IV and uranium IV.

Zhur. anal. khim., 18, No. 4 (1963).

A. A. Nemodruk and P. N. Palei, 480-85. Photometric study of the interaction between tetravalent uranium and arsenazo-III.

T. S. Dobrolyubskaya, 486-91. Investigation of the fluorescence of uranyl sulfite and uranyl fluoride solutions, with the aim of enhancing the sensitivity of uranium determinations.

Zhur. struktur. khim., 4, No. 2 (1963).

V. K. Trunov et al., 277-79. On the binary oxides of uranium, tantalum, and tin.

Atompraxis, 9, No. 5 (1963).

H. Getoff and W. Parker, 175-77. Isolation of high-purity I^{131} from Te^{131} by column chromatography.

Energia Nucleare, 10, No. 5 (1963).

Z. Hainski and G. Rossi, 247-58. Application of intensity ratio calculations to impurity determinations in aluminum and SAP alloy.

A. Bassi and G. Camon, 277-79. Chemical polishing of uranium dioxide.

Énergie nucléaire, 5, No. 2 (1963).

R. Taylor, 168-76. Recovery of krypton formed in fissioning of nuclear fuel.

P. Renault and X. Talmont, 177-90. Pulse extraction columns for uranyl nitrate extraction.

Y. Sausselier, 191-94. Evolution of the concept of nuclear grade purity.

J. Inorg. and Nucl. Chem., 25, No. 4 (1963).

- T. Sato, 441-46. Solvent extraction of uranium (VI) from sulfuric acid solutions by tri-n-octylamine.
- S. Adar et al., 447-52. Ion exchange behavior of transuranium elements in LiNO_3 solution.
- W. Jenkins, 463-64. Sulfaminic acid as a plutonium solvent.

J. Inorg. and Nucl. Chem., 25, No. 5 (1963).

- R. Iyer et al., 465-72. Fission of Th^{232} by pile neutrons. Yield curve as a function of mass.
- E. Cordfunke and A. Van der Giessen, 553-55. Pseudomorphological decomposition of UO_4 to UO_3 .
- M. Zangen, 581-94. Note on the synergic effect in solvent extraction. 1. Uranium (VI).

J. Nucl. Materials, 8, No. 1 (1963).

- R. Caillat et al., 1-2. Justification of the choice of the Mg-Zr alloy for fuel-element cladding.
- J. Bernard and B. Bondouresques, 3-11. Mg-Zr alloy as a fuel-cladding material.
- J. Hérenquel, 12-22. Fabrication technology and metallurgical properties of Mg-Zr alloys.
- R. Darras et al., 23-28. Compatibility of Mg-Zr alloys and carbon dioxide under high pressure and at high temperatures.
- M. Salesse, 39-40. A new material for nuclear engineering: sintered magnesium oxide.
- D. Leclercq et al., 41-48. Compatibility of sintered magnesium with carbon dioxide at high pressures and high temperatures.
- J. Hérenquel, 49-59. Processing, transformation, and metallurgical properties of Mg-MgO type compounds.
- L. Popple, 60-76. Oxidation of magnesium alloys under atmospheric conditions in a reactor.
- R. Squires and R. Weiner, 77-80. Grain-boundary denuded zones in magnesium alloy with 0.5 wt. % zirconium.
- J. Berry et al., 102-115. Leakage of gaseous fission products from irradiated sintered uranium oxide.
- A. Lemogne and P. Lacombe, 116-25. Plastic flow and fracture of uranium single crystals under tensile load at 196°C .
- R. Akeret, 126-37. Welding of SAP (sintered aluminum powder).
- P. Poeydomenge et al., 138-42. Uranium decontamination by progressive solidification.
- G. Clottes, 143-47. Uranium recrystallization temperature in zone melting.

J. Nucl. Materials, 8, No. 2 (1963).

- G. Higgins, 153-59. Secondary recrystallization in magnox A1 80 alloy.
- G. Higgins and B. Pickles, 160-68. Hydrogen capture by Zr-55 alloy and its effect on the alloy's mechanical properties.
- R. Doldon, 169-78. Fatigue testing of magnesium-zirconium and magnesium-aluminum cladding materials.
- E. Walker and P. Fisher, 179-86. Design of metallurgically stable magnesium-zirconium alloys.
- S. Marvincovic, 187-97. Formation of a solid solution in the $\text{U}_3\text{O}_8 \rightarrow \text{UO}_2$ transformation.
- R. Kent and T. Wells, 198-206. Creep flow characteristics of the magnesium-zirconium alloy ZA at 400 and 450°C in carbon dioxide.
- D. De Halas and G. Horn, 207-220. Development of changes in the structure of uranium dioxide upon irradiation of fuel rods.
- P. Thrower and W. Reynolds, 221-26. Changes in the microstructure of graphite brought about by neutron irradiation.

- J. Kelly, 227-31. Textured of hot-pressed BeO.
- I. Barwood and B. Butcher, 232-40. α - β -phase transformations in uranium.
- A. Brailsford and K. Major, 241-47. Effects of irradiation on the resistivity and thermal conductivity of α -uranium.
- A. Brailsford, 248-58. Resistivity due to interstices and vacancies in α -uranium.
- N. J. Bailey, 259-62. Oxidation of zirconium thin films.
- K. Mackay and N. Hill, 263-64. Lattice parameter and hardness measurements in high-grade beryllium.
- B. Raz and H. Schmidt, 265-67. Note on the electrical resistivity anomaly of sintered UO_2 .
- M. Salessé et al., 268-70. Accumulation of helium in sintered specimens of neutron-irradiation beryllium oxide.
- I. Amato et al., 271-72. Comment on a case of density loss during sintering of a pair of UO_2 beads.
- A. Carrea 275-77. Sintering of uranium dioxide in an atmosphere of controlled hydrogen content.
- Kernenergie, 6, No. 5 (1963).
- H. Rabold and W. Schimmel, 187-92. Water chemistry problems in water-cooled power reactors.
- R. Münze and O. Hladik, 225-28. Radiochemical investigations of multiple splitting of uranium.
- Kerntechnik, 5, No. 5 (1963).
- W. Ochsenfeld and S. Krawczynski, 218-21. Mixer-settler for experimental research on extraction.
- Nucl. Sci. and Engng., 15, No. 2 (1963).
- M. Silverman et al., 217-18. Radiation damage to Freon-11 (CeF_3).
- L. Baker et al., 218-20. Determination of total emissivity of polished and oxidized surfaces.
- Nukleonik, 5, No. 4 (1963).
- P. Bettzieche et al., 148-53. Changes in the properties of steel irradiated by small doses, depending on irradiation temperature.
- V. Dosimetry and Radiometry. Nuclear Meteorology
- Nauchn. trudy vyssh. ucheb. zaved. Litov. SSR. Geografiya i geologiya, 2 (1962).
- V. Matulyavichene and V. Matulyavichus, 119-26. Some aspects of applications of A-2 type nuclear emulsion in research on atmospheric radioactivity.
- Atompraxis, 9, No. 5 (1963).
- E. Piesch, 179-88. Nuclear emulsions in fast-neutron dosimetry.
- Nucleonics, 21, No. 6 (1963).
- M. Tamers and R. Bibron, 90-94. Benzene method measures tritium in rain without isotope enrichment.
- Nukleonik, 5, No. 4 (1963).
- K. Becker, 154-59. Phosphate film badge for nuclear plant personnel.
- VI. Radioactive and Stable Isotopes
- (Separation, production, applications).
- Vestnik sel'sko-khoz. nauki, No. 4 (1963).
- S. V. Andreev et al., 135-38. Radioisotopes check effectiveness of pesticide spraying of crops.

Izvestiya vyssh. ucheb. zaved. Stroitel'stvo i arkhitektura, No. 3 (1963).

Yu. V. Dezhin and I. I. Borisov, 154-57. How gamma-emitters map boundaries of active zone under an irradiation assembly.

Stroit. i dor. mashiny, No. 4 (1963).

V. I. Postnikov, 22-24. Radioisotopes in the building and building materials industries.

Trudy Volgograd. nauchno-issled. inst. nef. i gaz. prom., No. 2 (1963).

L. A. Korol'kov, 101-102. A radioactive level gage.

Energie nucléaire, 5, No. 3 (1963).

P. Bovard and A. Grauby, 149-53. Soil irradiation experiments in the TRITON pool reactor.

Kerntechnik, 5, No. 5 (1963).

H. J. Marcinowski, 201-204. Accidents in handling radioactive materials.

H. Ramdohr, 204-206. Activation analysis aids in grading copper ore.

W. Kühn, 207-212. Continuous measurement of moisture content in sintered iron by neutron scattering.

Nucleonics, 21, No. 6 (1963).

---, 100-107. Advancing radioisotope applications in engineering and the physical sciences (Gatlinburg, Tenn. April, 1963 conf.).

JÁDERNÁ ENERGIE, No. 9 (1963)

E. Karniková, M. Holinka, and V. Masáryk. Uranium and beryllium compatibility.

J. Truhly and F. Šlandar. Metallographic identification of inclusions in uranium metal.

J. Šimorda. A 2000-curie cobalt gamma facility.

M. Marchol. Ion exchange resins containing phosphor, arsenic, or antimony in their functional groups.

J. Krtil, V. Kourim, and Z. Kolářik. Use of ammonium salts of heteropolyacids in isolation of Cs¹³⁷.

O. Caletka and M. Kirs. Comment on the mechanism underlying sorption of zirconium on silica gel from nitrate solutions.

J. Staroba. Radioactive air ionizers for use in plastics manufacturing.

A. Uncovsky. Thickness measurement of hot-rolled strip in the 1-10 mm range.

L. Šimon. The Alpha RAL-1 scintillation radiometer.

T. Fukatko. New facility measures intensity of beam of accelerated ions.

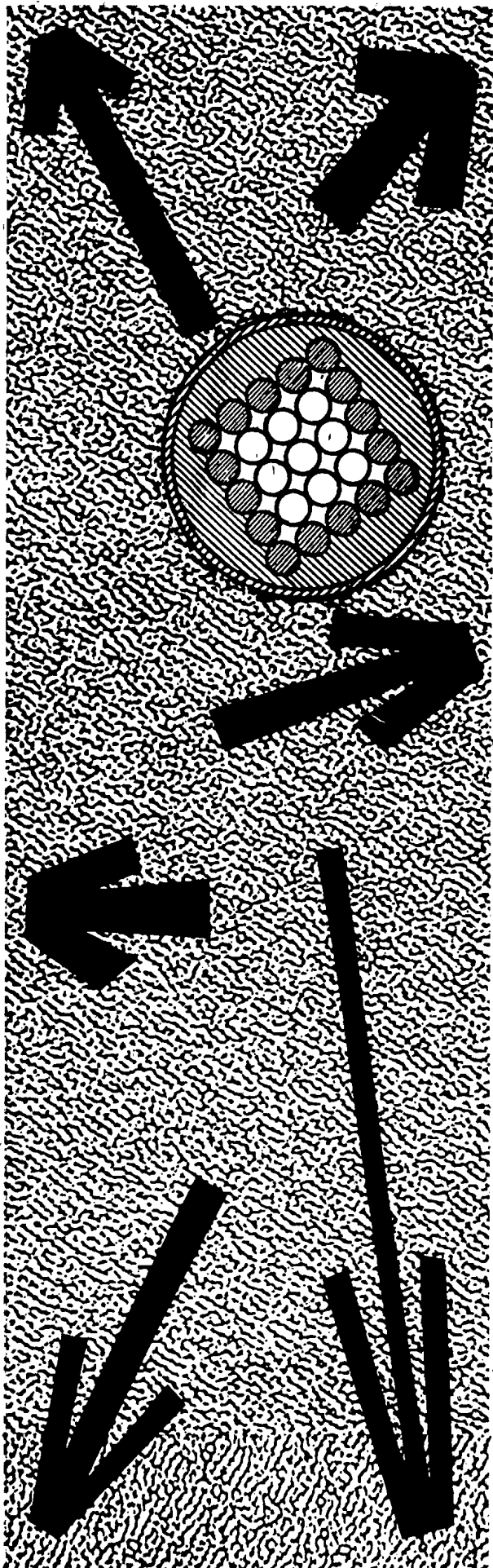
Soviet Journals Available in Cover-to-Cover Translation

ABBREVIATION	RUSSIAN TITLE	TITLE OF TRANSLATION	PUBLISHER	TRANSLATION BEGAN	
				Vol.	Issue Year
AÉ	Atomnaya énergiya	Soviet Journal of Atomic Energy	Consultants Bureau	1	1 1956
Akust. zh.	Akusticheskii zhurnal	Soviet Physics - Acoustics	American Institute of Physics	1	1 1955
Astr(on). zh(urn).	Astronomicheskii zhurnal	Soviet Astronomy - AJ	American Institute of Physics	34	1 1957
Avto(mat). svarka	Avtomaticheskaya svarka	Automatic Welding	Br. Welding Research Assn. (London)	12	1 1959
	Avtomatika i Telemekhanika	Automation and Remote Control	Instrument Society of America	27	1 1956
	Biofizika	Biophysics	National Institutes of Health**	6	1 1961
	Biokhimiya	Biochemistry	Consultants Bureau	21	1 1956
Byull. éksp(erim). biol. (i med.)	Byulleten' éksp(erimental'noi biologii i meditsiny)	Bulletin of Experimental Biology and Medicine	Consultants Bureau	41	1 1959
		Doklady Biological Sciences Sections (includes: Anatomy, biochemistry, biophysics, cytology, ecology, embryology, endocrinology, evolutionary morphology, genetics, histology, hydrobiology, microbiology, morphology, parasitology, physiology, zoology)	National Science Foundation*	112	1 1957
		Doklady Botanical Sciences Sections (includes: Botany, phytopathology, plant anatomy, plant ecology, plant embryology, plant physiology, plant morphology)	National Science Foundation*	112	1 1957
		Proceedings of the Academy of Sciences of the USSR, Section: Chemical Technology	Consultants Bureau	106	1 1956
		Proceedings of the Academy of Sciences of the USSR, Section: Chemistry	Consultants Bureau	106	1 1956
		Proceedings of the Academy of Sciences of the USSR, Section: Physical Chemistry	Consultants Bureau	112	1 1957
DAN (SSSR)	Doklady Akademii Nauk SSSR	Doklady Earth Sciences Sections (includes: Geochemistry, geology, geophysics, hydrogeology, lithology, mineralogy, oceanology, paleontology, permafrost, petrography)	American Geological Institute	124	1 1959
Dok(ady) AN SSSR		Proceedings of the Academy of Sciences of the USSR, Section: Geochemistry	Consultants Bureau	106-123	1 6 1956-1958
		Proceedings of the Academy of Sciences of the USSR, Section: Geology	Consultants Bureau	112-123	1 6 1957-1958
		Soviet Mathematics - Doklady	American Mathematical Society	130	1 1960
		Soviet Physics - Doklady (includes: Aerodynamics, astronomy, crystallography, cybernetics and control theory, electrical engineering, energetics, fluid mechanics, heat engineering, hydraulics, mathematical physics, mechanics, physics, technical physics, theory of elasticity sections)	American Institute of Physics	106	1 1956
		Telecommunications	Am. Inst. of Electrical Engineers	37	1 1957
		Entomological Review	National Science Foundation**	37	1 1958
		Physics of Metals and Metallography	Acta Metallurgica	5	1 1957
		Soviet Physics - Solid State	American Institute of Physics	1	1 1959
		Sechenov Physiological Journal USSR	National Institutes of Health**	47	1 1961
Entom(ol). oboz(r).	Elektrosvyaz'	Plant Physiology	National Science Foundation*	4	1 1957
FMM	Entomologicheskoe obozrenie	Geodesy and Aerophotography	American Geophysical Union	1	1 1956
FTT, Fiz. tv(er)da. tela	Fizika metallov i metallovedenie	Geochimistry	The Geochemical Society	1	1 1956
Fiziol. Zh(urn). SSSR	Fizika tverdogo tela	Petroleum Geology	Petroleum Geology	2	1 1958
	Fiziologicheskii zhurnal imeni I.M. Sechenov	Geomagnetism and Aeronomy	American Geophysical Union	1	1 1961
Fiziol(ogiya) rast.	Fiziologiya rastenii	Artificial Earth Satellites	Consultants Bureau	1	1 1958
	Geodeziya i aerofotosyemka	Measurement Techniques	Instrument Society of America	7	1 1958
	Geokhimiya				
	Geologiya nef'ti i gaza				
Geol. nef'ti i gaza	Geomagnetizm i aeronomiya				
	Iskusstvennyye sputniki zemli				
izmerit. tekhn(ika)	izmeritel'naya tekhnika				

Izv. AN SSSR O(td). Kh(im). N(auk)	Izvestiya Akademii Nauk SSSR: Otdelenie khimicheskikh nauk	Bulletin of the Academy of Sciences of the USSR: Division of Chemical Science	Consultants Bureau	16	1	1952
Izv. AN SSSR O(td). T(ekhn). N(auk): Metall). i top.	(see Met. i top)					
Izv. AN SSSR Ser. fiz(ich).	Izvestiya Akademii Nauk SSSR: Seriya fizicheskaya	Bulletin of the Academy of Sciences of the USSR: Physical Series	Columbia Technical Translations	18	3	1954
Izv. AN SSSR Ser. geofiz.	Izvestiya Akademii Nauk SSSR: Seriya geofizicheskaya	Bulletin of the Academy of Sciences of the USSR: Geophysics Series	American Geophysical Union	7	1	1957
Izv. AN SSSR Ser. geol.	Izvestiya Akademii Nauk SSSR: Seriya geologicheskaya	Bulletin of the Academy of Sciences of the USSR: Geologic Series	American Geological Institute	23	1	1958
Iz. Vyssh. Uch. Zav., Tekh. Tekst. Prom.	Izvestiya Vysshikh Uchebnykh Zavedeni P. Tekhnologiya Tekstil'noi Promyshlennosti	Technology of the Textile Industry, USSR Soviet Rubber Technology	The Textile Institute (Manchester) Palmerston Publishing Company, Inc.	4 18	1 3	1960 1959
Kauch. i rez.	Kauchuk i rezina	Kinetics and Catalysis	Consultants Bureau	1	1	1960
Kolloidn. zh(urn).	Kinetika i kataliz	Coke and Chemistry, USSR	Coal Tar Research Assn. (Leeds, England)	8	8	1959
Metallov. i term.	Kolloidnyi zhurnal	Colloid Journal	Consultants Bureau	14	1	1952
Met. i top.(gorn.)	Kristallografiya	Soviet Physics - Crystallography	American Institute of Physics	2	1	1957
Mikrobiol.	Metallovedenie i termicheskaya obrabotka metallov	Metals Science and Heat Treatment of Metals	Acta Metallurgica	6	1	1958
OS, Opt. i spektr.	Metallurgiya i toplivo (gornoye delo)	Metallurgist	Acta Metallurgica	1	1	1957
Paleontol. Zh(urn)	Mikrobiologiya	Russian Metallurgy and Fuels(mining)	Scientific Information Consultants, Ltd.	1	1	1960
Pribory i tekhn. eks(perimenta)	Ogneupory	Microbiology	National Science Foundation*	26	1	1957
Prikl. matem. i mekh(an).	Optika i spektroskopiya	Refractions	Acta Metallurgica	25	1	1960
PTE	Paleontologicheskii Zhurnal	Optics and Spectroscopy	American Institute of Physics	6	1	1959
Radiotekh.	Ochivovedenie	Journal of Paleontology	American Geological Institute	1	1	1962
Radiotekhn. i elektron(ika)	Poroshkovaya Metallurgiya	Soviet Soil Science	National Science Foundation**	53	1	1958
Stek. i keram.	PriBOROSTROENIE	Soviet Powder Metallurgy and Metal Ceramics	Consultants Bureau	2	1	1962
Svaroch. proiz-vo		Instrument Construction	Taylor and Francis, Ltd. (London)	4	1	1959
Teor. veroyat. i prim.	Pribory i tekhn. eksperimenta	Instruments and Experimental Techniques	Instrument Society of America	3	1	1958
Tsvet. metall	Prikladnaya matematika i mekhanika (see Pribory i tekhn. eks.)	Applied Mathematics and Mechanics	Am. Society of Mechanical Engineers	22	1	1953
JFN	Problemy Severa	Problems of the North	National Research Council of Canada	4	1	1958
UMN	Radiokhimiya	Radiochemistry	Consultants Bureau	4	1	1932
Vest. mashinostroeniya	Radiotekhnika	Radio Engineering	Am. Institute of Electrical Engineers	16	1	1961
Vop. onk(ol).	Radiotekhnika i elektronika	Radio Engineering and Electronic Physics	Am. Institute of Electrical Engineers	6	1	1961
Zav(odsk). lab(oratoriya)	Stal	Stal (in English)	Iron and Steel Institute	19	1	1959
ZhAKh, Zh. anal(it). Khim(ii)	Stanki i instrument	Machines and Tooling	Production Engineering Research Assoc.	30	1	1959
ZhETF	Steklo i keramika	Glass and Ceramics	Consultants Bureau	13	1	1956
Zh. eksperim. i teor. fiz.	Svarochnoe proizvodstvo	Welding Production	Br. Welding Research Assn. (London)	5	4	1959
ZhFKh	Teoriya veroyatnostei i ee primeneniye	Theory of Probability and Its Application	Soc. for Industrial and Applied Math.	1	1	1956
Zh. fiz. khimii	Tsvetnye metall	The Soviet Journal of Nonferrous Metals	Primary Sources	33	1	1960
ZhNKH	Uspekhi fizicheskikh nauk	Soviet Physics - Uspekhi (partial translation)	American Institute of Physics	66	1	1958
Zh. neorg(an). khim.	Uspekhi khimii	Russian Chemical Reviews	Chemical Society (London)	29	1	1960
ZhOKh	Uspekhi matematicheskaya nauk	Russian Mathematical Surveys	Cleaver-Hume Press, Ltd. (London)	15	1	1960
Zh. obshch. khim.	Vestnik mashinostroeniya	Russian Engineering Journal	Production Engineering Research Assoc.	39	4	1959
ZhPKh	Voprosy onkologii	Problems of Oncology	National Institutes of Health**	7	1	1961
Zh. prikl. khim.	Zavodskaya laboratoriya	Industrial Laboratory	Instrument Society of America	24	1	1958
ZhSKh	Zhurnal analiticheskoi khimii	Journal of Analytical Chemistry	Consultants Bureau	7	1	1952
Zh. strukt(urnoi) khim.	Zhurnal eksperimental'noi i teoreticheskoi fiziki	Soviet Physics - JETP	American Institute of Physics	28	1	1955
ZhTF	Zhurnal fizicheskoi khimii	Russian Journal of Physical Chemistry	Chemical Society (London)	33	7	1959
Zh. tekhn. fiz.	Zhurnal neorganicheskoi khimii	Journal of Inorganic Chemistry	Chemical Society (London)	4	1	1959
Zh. vyssh. nervn. deyat. (im. Pavlova)	Zhurnal obshchei khimii	Journal of General Chemistry USSR	Consultants Bureau	19	1	1949
	Zhurnal prikladnoi khimii	Journal of Applied Chemistry USSR	Consultants Bureau	23	1	1950
	Zhurnal strukturnoi khimii	Journal of Structural Chemistry	Consultants Bureau	1	1	1960
	Zhurnal tekhnicheskoi fiziki	Soviet Physics - Technical Physics	American Institute of Physics	26	1	1956
	Zhurnal vychislitel'noi matematika i matematicheskoi fiziki	U.S.S.R. Computational Mathematics and Mathematical Physics	Pergamon Press, Inc.	1	1	1962
	Zhurnal vysshiei nervnoi deyatelnosti (im I. P. Pavlova)	Pavlov Journal of Higher Nervous Activity	National Institutes of Health**	11	1	1961

*Sponsoring organization. Translation published by Consultants Bureau.

**Sponsoring organization. Translation published by Scripta Technica.



CALCULATION OF THERMAL STRESSES IN NUCLEAR REACTORS

by I. I. Gol'denblat
and N. A. Nikolaenko

Translated from Russian

The present book sets forth methods of calculating the temperature stresses in the constructional elements of nuclear reactors — principally stationary type nuclear reactors. Methods are given for calculating the temperature stresses in different shape fuel elements and for designing reactor elements for thermal shock, as well as methods of designing housings and other reactor elements for thermal creep. A particularly large amount of attention is given to calculating the temperature stresses and creep deformations in the concrete biological shield of reactors. Methods of calculating the temperature stresses in special constructional elements of nuclear reactors are also given.

The book takes the view that the *thermoelastic* stresses occurring in reactor elements may be investigated independently of the mechanical stresses produced by external forces, since because of the linearity of the thermoelastic equations the final values for the stresses may be found by simply adding together the temperature and mechanical stresses. The same approach applies to the linear theory of thermal creep, which is used in the book to calculate the stresses and thermal creep deformations in the concrete biological shield of a reactor.

The *thermal plasticity* equations are nonlinear. Accordingly, it is impossible to make a study of the thermoplastic stresses without including the mechanical stresses. This is also true with regard to all the nonlinear thermal creep theories. Therefore, in the present book, the *thermoplastic* stresses (as well as the thermal stresses associated with nonlinear creep) are treated together with the mechanical stresses produced by external force.

The calculations presented in this volume will be of significant interest to engineers concerned with the indices of the maximum permissible dimensions of various constructional elements in reactor technology, and those responsible for their reinforcement.

80 pages

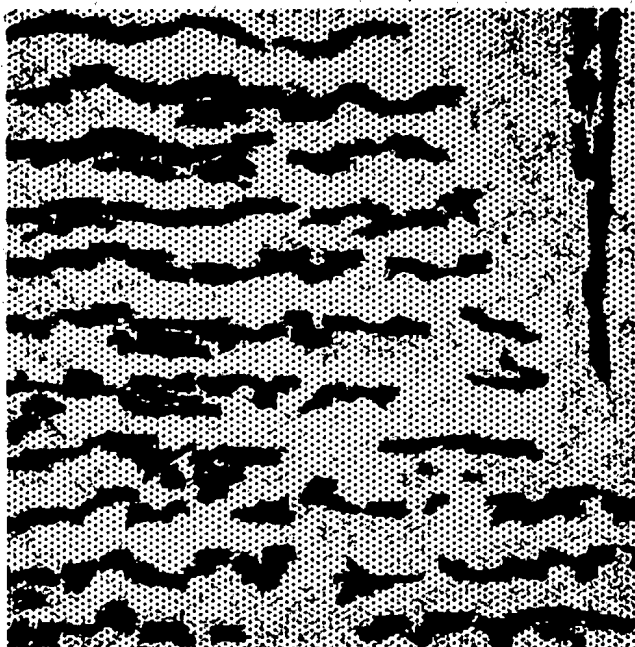
A Special Research Report

\$15.00

Contents on request



CONSULTANTS BUREAU
227 W. 17th St., New York, N.Y. 10011



RESEARCH IN SURFACE FORCES

Edited by B. V. Deryagin

The 29 reports contained in this collection were presented at the conference on surface forces held at the Institute of Physical Sciences of the Academy of Sciences of the USSR. Following an introductory paper, the remaining 28 presentations cover results of investigations (theory and practice) on surface forces in various systems, their properties, and methods of investigations carried out by Soviet scientists. The editor, who has contributed to nearly half the papers in this volume, is an academician of the Academy of Sciences of the USSR, and is also the organizer and permanent Director of the Laboratory of Surface Phenomena at the Institute.

Translated from Russian. A Special Research Report.

190 pages

\$27.50



CONSULTANTS BUREAU 227 W. 17th St., NEW YORK, N. Y. 10011

CONTENTS

Twenty-five Years in the Laboratory of Surface Phenomena of the Institute of Physical Chemistry of the Academy of Sciences of the USSR

GENERAL PROBLEMS IN SURFACE FORCES

Surface Forces and Their Effect on the Properties of Heterogeneous Systems

A Study of the State of Connate Water in Oil Reservoirs

The General Theory of Type II Capillary Effects

Diffusional Surface Forces in the Neighborhood of a Liquid Interface

POLYMER ADHESION

A Luminescence Study of the Adhesion Bonding of Polymers

The Effect of Molecular Weight, Polydispersion and Polarity on the Adhesion of High Polymers to High-Molecular Substrata

The Role of Surface Forces in Mica Crystals

The Double Layer at a Solid Surface Resulting from Acceptor-Donor Bonds

The Application of Infrared Spectroscopy to the Studying of the Interaction of Adhesive and Substrate (Polymer-Glass)

Measurement of the True Density of the Double Electric Layer at a Metal-Dielectric Interface

SURFACE FORCES IN THIN LIQUID FILMS

The Physical Basis of the Fundamental Law of Surface Function

The Properties of Solutions of Organic Acids in Liquid Hydrocarbons at Solid Surfaces

Certain Considerations Concerning the Laws Applying to Type I Friction. New Experimental Data on External Friction

A Cinematographic Study of the Flow of Thin Films of Polymer Solutions

The Effect of Electrolyte Concentration on the Height of the Force Barrier for Adhesion of Platinum Wires

SURFACE EFFECTS IN DISPERSED SYSTEMS

A Radioisotope Study of the Movement of Moisture in Peats

Surface Effects in Soil Mechanics

The Theory of Coagulation of Lyophobic Soils by Mixtures of Electrolytes. Studies on the Filtration of Solutions of Electrolytes Through Highly Dispersed Powders

A Study of Slow Hydrosol Coagulation Using the Continuous Flow Ultramicroscope

An Experimental Study of the Filtration of Air Through Porous Bodies in the Region of Transition Pressures

A Metallic Apparatus for Determining Specific Surfaces of Powders and Porous Bodies

SURFACE FORCES IN AEROSOLS

Diffusional Phoresis of Aerosol Particles

The Behavior of Small Aerosol Particles in a Nonuniformly Heated Gaseous Mixture

A Differential Counter for Condensation Nuclei

A New Method for Obtaining Constant and Uniform Supersaturations. Solution of the Kinetic Equation for Coagulation